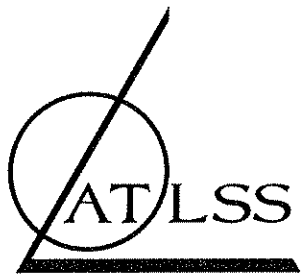

ADVANCED TECHNOLOGY FOR
LARGE
STRUCTURAL SYSTEMS

Lehigh University

EXPERIMENTAL EVALUATION OF THE AXIAL LOAD BEHAVIOR OF TIED HIGH-STRENGTH CONCRETE COLUMNS

by

Wen-Hsiung Lin
Graduate Research Assistant

Stephen Pessiki
Assistant Professor of Civil & Environmental Engineering

ATLSS Report No. 96-06

June 1996

ATLSS Engineering Research Center
Lehigh University
117 ATLSS Dr., Imbt Laboratories
Bethlehem, PA 18015-4729
(610) 758-3525

An NSF Sponsored Engineering Research Center

ACKNOWLEDGMENTS

This research was sponsored by the Portland Cement Association. Any opinions, findings, and conclusions expressed in this report are those of the authors and do not necessarily reflect the views of the sponsor.

TABLE OF CONTENTS

		Page
LIST OF TABLES		vi
LIST OF FIGURES		vii
ABSTRACT		1
CHAPTER 1: INTRODUCTION		2
1.1	INTRODUCTION	2
1.2	OBJECTIVE	2
1.3	SUMMARY OF APPROACH	2
1.4	SCOPE OF REPORT	3
1.5	NOTATION	3
1.6	CONVERSION FACTORS	5
CHAPTER 2: BACKGROUND		6
2.1	INTRODUCTION	6
2.2	STRESS-STRAIN MODELS FOR CONCRETE CONFINED BY RECTANGULAR TIES	6
	2.2.1 Stress-Strain Models for Normal Strength Concrete	7
	2.2.2 Stress-Strain Model for High-Strength Concrete	11
2.3	PREVIOUS EXPERIMENTS ON CONFINED TIED NSC COLUMNS	13
	2.3.1 Influence of Transverse Reinforcement	13
	2.3.2 Influence of Longitudinal Reinforcement	14
	2.3.3 Behavior of Concrete Cover	15
2.4	LARGE-SCALE AXIAL LOAD TESTS OF CONFINED TIED HSC COLUMNS	15
	2.4.1 Influence of Transverse Reinforcement	16
	2.4.2 Influence of Longitudinal Reinforcement	17
	2.4.3 Influence of Concrete Strength	17
	2.4.4 Failure Modes	18
2.5	COMPRESSION TESTS OF HIGH-STRENGTH CONCRETE CYLINDERS AND CORES	18
	2.5.1 Cylinder Compressive Strength	18
	2.5.2 Core Compressive Strength	19

CHAPTER 3: DESCRIPTION OF EXPERIMENTAL PROGRAM 23

3.1 INTRODUCTION 23
3.2 TEST PROGRAM 23
3.2.1 Review of Objective 23
3.2.2 Test Matrix 23
3.3 SPECIMEN DETAILS 24
3.4 INSTRUMENTATION 24
3.4.1 Instrumentation Configuration 24
3.4.2 Instrumentation Protection 24
3.4.3 Data Acquisition System 25
3.5 SPECIMEN FABRICATION DETAILS 25
3.5.1 Construction of Reinforcement Cages 25
3.5.2 Concrete Placement 26
3.5.3 Placement of Columns in the Testing Machine 26
3.6 MATERIAL PROPERTIES OF STEEL REINFORCEMENT 26
3.7 MATERIAL PROPERTIES OF CONCRETE 26
3.8 OBSERVED COMPRESSIVE STRENGTH VARIATIONS AMONG CONCRETE CYLINDERS 28
3.8.1 Cylinder Compressive Strength and Density 29
3.8.2 Comparison between Experimental Test Results and CTL Test Results 29
3.8.3 Final Remarks on Concrete Cylinder Compressive Strengths 30

CHAPTER 4: INDIVIDUAL TEST SUMMARIES 60

4.1 INTRODUCTION 60
4.2 GENERAL LOADING PROCEDURE 60
4.3 INDIVIDUAL TEST SUMMARIES 60
4.3.1 Specimen L1 62
4.3.2 Specimen L2 71
4.3.3 Specimen L3 80
4.3.4 Specimen HA1 90
4.3.5 Specimen HA2 98
4.3.6 Specimen HA3 108
4.3.7 Specimen HB1 118
4.3.8 Specimen HB2 125
4.3.9 Specimen HB3 131

CHAPTER 5: DISCUSSION OF RESULTS 138

5.1 INTRODUCTION 138
5.2 COLUMN AXIAL STRENGTH 138
5.2.1 Predicted Axial Strengths According to the ACI 318 Code Equation 138
5.2.2 Predicted Axial Strengths According to Concrete Confinement Models 139
5.3 COLUMN DUCTILITY 140
5.3.1 Definition of Ductility 140
5.3.2 Influence of Concrete Compressive Strength 142
5.3.3 Influence of the Lateral Reinforcement 142
5.4 INFLUENCE OF THE TIE CONFIGURATION ON THE BEHAVIOR OF THE CORE 143
5.5 SUMMARY AND CONCLUSIONS 144

CHAPTER 6: SUMMARY, CONCLUSION, AND FUTURE RESEARCH 161

6.1 INTRODUCTION 161
6.2 SUMMARY 161
6.3 CONCLUSION 162
6.4 FUTURE RESEARCH 163

REFERENCES 164
APPENDIX A 167
APPENDIX B 177

LIST OF TABLES

Table 3.1 Original test matrix with design concrete compressive strengths.
Table 3.2 Revised test matrix with actual concrete compressive strengths.
Table 3.3 Summary of reinforcement provided in each specimen.
Table 3.4 Mixture proportions of concrete as reported by ready-mix supplier: (a) L-Series specimens; (b) HA-Series specimens; and (c) HB-Series specimens.
Table 3.5 Longitudinal reinforcement properties.
Table 3.6 Transverse reinforcement properties.
Table 3.7 Compressive strength of cored cylinders from tests performed at Lehigh University.
Table 3.8 Average compressive strength of cylinders from tests performed at Lehigh University.
Table 3.9 Specific gravity and density of concrete cylinders from tests performed at Lehigh University: (a) cored cylinders-L-Series; (b) core cylinders-HA-Series; (c) core cylinders-HB-Series; and (d) field-cured cylinders.
Table 3.10 Compressive strength and bulk density (SSD): (a) cored cylinders-L-Series; (b) core cylinders-HA-Series; (c) core cylinders-HB-Series; and (d) field-cured cylinders.
Table 3.11 Test results from CTL.
Table 3.12 Comparison of test results from CTL and Lehigh University.
Table 4.1 Specimen L1-experimentally observed and predicted axial strengths.
Table 4.2 Specimen L2-experimentally observed and predicted axial strengths.
Table 4.3 Specimen L3-experimentally observed and predicted axial strengths.
Table 4.4 Specimen HA1-experimentally observed and predicted axial strengths.
Table 4.5 Specimen HA2-experimentally observed and predicted axial strengths.
Table 4.6 Specimen HA3-experimentally observed and predicted axial strengths.
Table 4.7 Specimen HB1-experimentally observed and predicted axial strengths.
Table 4.8 Specimen HB2-experimentally observed and predicted axial strengths.
Table 4.9 Specimen HB3-experimentally observed and predicted axial strengths.
Table 5.1 Summary of column axial capacity.
Table 5.2 Summary of the predicted axial strengths of the lightly confined HSC columns.
Table 5.3 Observed behavior of the concrete cover.
Table 5.4 Comparison of the axial strengths of the lightly confined HSC columns.
Table 5.5 Comparison of the confinement models developed by Cusson and Paultre (1995) and Mander et al. (1988).
Table 5.6 Observed column axial capacity and ductilities.
Table 5.7 Comparison of column ductility with respect to test variables.
Table 5.8 The effective confinement index (f_{le} / f_{co}).

LIST OF FIGURES

Figure 2.1	Stress-strain model proposed for monotonic loading of confined and unconfined concrete [Mander et al. (1988)].
Figure 2.2	Effectively confined core for rectangular hoop reinforcement [Mander et al. (1988)].
Figure 2.3	confined strength determination from lateral confining stresses for rectangular sections [Mander et al. (1988)].
Figure 2.4	Proposed general stress-strain curve of concrete [(Sheikh and Uzumeri (1982)].
Figure 2.5	Effect of confinement on peak concrete strength [(Cusson and Paultre (1995)].
Figure 3.1	Elevation and section views of column specimens.
Figure 3.2	Schematic of data acquisition system.
Figure 3.3	Computer monitor during testing.
Figure 3.4	Column formwork.
Figure 3.5	Illustration of the different cylindrical specimens used to determine concrete compressive strength.
Figure 3.6	Locations at which cores were extracted.
Figure 3.7	Temperature variations of: (a) L-Series specimens; (b) HA-Series specimens; and (c) HB-Series specimens.
Figure 3.8	Strength versus bulk density (SSD) for L-Series cylinders.
Figure 3.9	Strength versus bulk density (SSD) for HA-Series cylinders.
Figure 3.10	Strength versus bulk density (SSD) for HB-Series cylinders.
Figure 4.1	Specimen L1-axial load versus axial displacement.
Figure 4.2	Specimen L1-axial load versus longitudinal reinforcement strains, gages S1, S2.
Figure 4.3	Specimen L1-series of photographs; (a)-(e).
Figure 4.4	Specimen L2-axial load versus axial displacement.
Figure 4.5	Specimen L2-axial load versus longitudinal reinforcement strains, gages S1, S2.
Figure 4.6	Specimen L2-series of photographs; (a)-(e).
Figure 4.7	Specimen L3-axial load versus axial displacement.
Figure 4.8	Specimen L3-axial load versus longitudinal reinforcement strains, gages S1, S2.
Figure 4.9	Specimen L3-series of photographs; (a)-(f).
Figure 4.10	Specimen HA1-axial load versus axial displacement.
Figure 4.11	Specimen HA1-axial load versus longitudinal reinforcement strains, gages S1, S2.
Figure 4.12	Specimen HA1-series of photographs; (a)-(d).
Figure 4.13	Specimen HA2-axial load versus axial displacement.
Figure 4.14	Specimen HA2-axial load versus longitudinal reinforcement strains, gages S1, S2.
Figure 4.15	Specimen HA2-series of photographs; (a)-(f).
Figure 4.16	Specimen HA1-axial load versus axial displacement.
Figure 4.17	Specimen HA1-axial load versus longitudinal reinforcement strains, gages S1, S2.
Figure 4.18	Specimen HA1-series of photographs; (a)-(f).
Figure 4.19	Specimen HB1-axial load versus axial displacement.
Figure 4.20	Specimen HB1-axial load versus longitudinal reinforcement strains, gages S1, S2.

Figure 4.21 Specimen HB1-series of photographs; (a)-(f).
Figure 4.22 Specimen HB2-axial load versus axial displacement.
Figure 4.23 Specimen HB2-axial load versus longitudinal reinforcement strains, gages S1, S2.
Figure 4.24 Specimen HB2-series of photographs; (a)-(d).
Figure 4.25 Specimen HB3-axial load versus axial displacement.
Figure 4.26 Specimen HB3-axial load versus longitudinal reinforcement strains, gages S1, S2.
Figure 4.27 Specimen HB3-series of photographs; (a)-(e).
Figure 5.1 Determination of displacements to calculate column ductilities.
Figure 5.2 Normalized load and displacement-L1, HA1, and HB1.
Figure 5.3 Normalized load and displacement-L2, HA2, and HB2.
Figure 5.4 Normalized load and displacement-L3, HA3, and HB3.
Figure 5.5 Normalized load and displacement-L1, L2, and L3.
Figure 5.6 Normalized load and displacement-HA1, HA2, and HA3.
Figure 5.7 Normalized load and displacement-HB1, HB1, and HB3.
Figure 5.8 Photographs depicting the behavior of the tie reinforcement; (a)-(b).

ABSTRACT

The objective of this research is to study the axial load behavior of large-scale tied high-strength concrete columns. A total of nine column specimens were made with concrete compressive strengths ranging from approximately 34.5 MPa (5 ksi) to 69 MPa (10 ksi) and tested in concentric axial compression. All nine columns measured 406 mm x 406 mm (16 in x 16 in) in cross-section and 2438 mm (96 in) tall. The influence of concrete compressive strength and the amount of lateral reinforcement on column strength and ductility was evaluated.

In this research, it was found that large differences may exist between the compressive strength values obtained from tests of field-cured cylinders as compared to cored cylinders.

The ACI 318 Code equation for predicting the axial strength of tied columns was found to adequately predict the axial strength of tied high-strength concrete columns, provided that the concrete compressive strength value used in the equation is based on compression tests of cored cylinders. Axial strength predictions for tied high-strength concrete columns that are based on concrete compressive strengths obtained from tests of field-cured cylinders may be unconservative.

The compressive strength of concrete was found to influence column ductility. Columns made with higher strength concrete, in general, exhibited less ductility as compared to columns made with lower strength concrete. The effect of lateral confinement on high-strength concrete column ductility, for the amount of transverse reinforcement treated in this research, was insignificant. Square column ties with 90-degree hooks were used to construct each reinforcement cage. It was observed that this tie configuration was ineffective in providing lateral confining pressure to the core. As a result, column behavior including column strength, ductility, and failure mode was adversely influenced.

CHAPTER 1
INTRODUCTION

1.1 INTRODUCTION

The use of high-strength concrete which permits smaller cross sections, reduced dead loads, and longer spans has been getting more popular in tall buildings during the last decade. Concrete strengths of up to 131 MPa (19 ksi) have been used successfully in high-rise buildings (ENR 1/18/90 pp. 58). Unfortunately, research on high-strength concrete members has lagged behind the use of this material in practice, and much remains unknown about the structural behavior of these members.

Many current building codes have fallen behind prevailing practice in terms of the implementation of high-strength concrete. One particular area of concern is the use of high-strength concrete in compressive members such as columns. In current codes such as ACI 318 Building Code Requirements for Structural Concrete (ACI 318-95) and Commentary (ACI 318R-95) (hereafter referred to as the ACI 318 Code), the requirements for lateral reinforcement in compression members are based largely on the results of tests performed on reinforced concrete members with concrete compressive strengths lower than 41.4 MPa (6 ksi). This is a concern in part because it is generally accepted that higher strength concretes exhibit more brittle material behavior relative to lower strength concretes. Therefore, applicability of current code requirements needs to be evaluated for high-strength concrete columns.

1.2 OBJECTIVE

The objective of this research is to study the behavior of large-scale, tied high-strength concrete columns subjected to concentric axial load. The experimental program was developed to specifically evaluate the role of concrete compressive strength and the amount of lateral reinforcement on column strength and ductility. The specific objectives of this research are as follows:

1. Evaluate the influence of concrete compressive strength on the axial strength and ductility of tied concrete columns.

2. Evaluate the influence of the amount of lateral reinforcement on the axial strength and ductility of tied high-strength concrete columns.

3. Evaluate the effectiveness of existing empirical models for predicting the axial strength of confined tied high-strength concrete columns. The models evaluated in this report are based on the research performed by Mander et al. (1988) and Cusson and Paultre (1995), and are presented in Chapter 2.

1.3 SUMMARY OF APPROACH

A total of nine large-scale tied concrete columns were tested in concentric axial compression. The tests were performed in a 22.2 MN (5000 kip) capacity universal testing machine. All nine specimens measured 406 mm x 406 mm (16 in x 16 in) in cross-section and 2438 mm (96 in) tall. The concrete

compressive strengths treated ranged from approximately 34.5 MPa (5 ksi) to 69 MPa (10 ksi). Three different lateral reinforcement spacings were also treated in the experimental program. The experimental results were compared to evaluate the role of concrete strength and amount of transverse reinforcement on column strength and ductility. The experimental results were also compared with existing empirical models to predict column strength to assess the appropriateness of these models for tied high-strength concrete columns.

1.4 SCOPE OF REPORT

Chapter 2 presents the background information relevant to this research. Much of the literature reviewed in this chapter is related to tied concrete columns subjected to concentric axial load.

Chapter 3 explains the experimental program. This includes a description of the test matrix, specimen fabrication details, instrumentation, and the results of tests made to determine the concrete and steel material properties.

Chapter 4 describes the general loading procedure used to test each specimen along with a summary of observations made during the test of each specimen.

Chapter 5 discusses the results of the tests performed on the nine columns. This includes a discussion of the influence of concrete compressive strength and the amount of transverse reinforcement on column strength and ductility. The conclusions from the research are also presented.

Chapter 6 summarizes the findings and conclusions from this study and outlines areas for future research.

1.5 NOTATION

The following notation is used in this report:

A_c	=	net concrete area of the column, mm^2 (in^2);
A_{cc}	=	concrete core area enclosed by the centerlines of the perimeter hoops, mm^2 (in^2);.
A_{core}	=	effective area of the core, mm^2 (in^2);
A_{cover}	=	area of the cover, mm^2 (in^2);
A_e	=	the area of effectively confined concrete core at midway between the levels of the ties, mm^2 (in^2);
A_i	=	total area of ineffectively confined concrete core at the level of the tie, mm^2 (in^2);
A_s	=	total area of longitudinal reinforcement, mm^2 (in^2);
A_{sx}	=	total area of transverse reinforcement in x-direction, mm^2 (in^2);
A_{sy}	=	total area of transverse reinforcement in y-direction, mm^2 (in^2);
b_c, d_c	=	core dimensions to centerlines of perimeter hoop in x and y directions, respectively, where $b_c \geq d_c$, mm (in);
E_c	=	tangent modulus of elasticity of the concrete, MPa (ksi);

E_{sec} = secant modulus of elasticity of the concrete, MPa (ksi);
f_c = longitudinal compressive concrete stress, MPa (ksi);
$f_{c\text{-}28}$ = compressive strength of the 28-day, wet-cured prepared cylinders, MPa (ksi);
$f_{c\text{-}field}$ = compressive strength of the field-cured prepared cylinders, MPa (ksi);
$f_{c\text{-}core}$ = compressive strength of the cored cylinders, MPa (ksi);
f_c' = concrete compressive strength determined from concrete cylinders, MPa (ksi);
$f_{c\,102}'$ = concrete compressive strength determined from 102 mm x 203 mm (4 in x 8 in) HSC concrete cylinders, MPa (ksi);
$f_{c\,152}'$ = concrete compressive strength determined from 152 mm x 305 mm (6 in x 12 in) HSC concrete cylinders, MPa (ksi);
f_{cc} = compressive strength of confined concrete, MPa (ksi);
f_{co} = compressive strength of unconfined concrete, MPa (ksi);
f_{hcc} = computed stress in the tie, MPa (ksi);
f_l = lateral fluid pressure, MPa (ksi);
f_{le} = effective lateral confining pressure, MPa (ksi);
f_{lex} = effective lateral confining pressure in x-direction, MPa (ksi);
f_{ley} = effective lateral confining pressure in y-direction, MPa (ksi);
f_{lx} = lateral confining pressure in x-direction, MPa (ksi);
f_{ly} = lateral confining pressure in y-direction, MPa (ksi);
f_{yh} = yield strength of transverse reinforcement, MPa (ksi);
f_{yl} = yield strength of longitudinal reinforcement, MPa (ksi);
k_e = effective confinement coefficient;
k_1 = coefficient related to concrete strength enhancement due to confinement;
k_2 = coefficient related to concrete strain enhancement due to confinement;
P_c = predicted confined column axial capacity (Equation 5.1), MN (kips);
P_{ccore} = predicted confined column capacity based on cored cylinder concrete compressive strength and Equation 5.1, MN (kips);
P_{cfield} = predicted confined column capacity based on field-cured cylinder concrete compressive strength and Equation 5.1, MN (kips);
P_{max} = maximum load sustained by the column, MN (kips);
P_{ocore} = predicted column capacity based on cored cylinder concrete compressive strength and Equation 4.2, MN (kips);
P_{ofield} = predicted column capacity based on field-cured cylinder concrete compressive strength and Equation 4.1, MN (kips);
r = parameter used in computing f_c and equal to the ratio of $E_c/(E_c\text{-}E_{sec})$;
R_c = strength ratio of P_{max} / P_{core};
R_f = strength ratio of P_{max} / P_{field};
R_F = ratio of column ductilities defined at column failure;
R_P = ratio of column ductilities defined at the maximum sustained load;
s = tie spacing, mm (in);
s' = clear tie spacing, mm (in);
S1 = strain gage no. 1 located at the midheight of the column;
S2 = strain gage no. 2 located at the 3/4 height of the column;

x	=	parameter used in computing f_c and equal to the ratio of ϵ_c/ϵ_{cc};
w_i	=	i^{th} clear distance between adjacent longitudinal bars, mm (in);
Δ_1	=	extrapolated elastic axial displacement computed as the maximum load sustained by the column divided by the initial slope of the column load-deflection plot in the linear elastic range of response, mm (in);
Δ_F	=	column axial displacement at failure, mm (in);
Δ_P	=	column axial displacement at the maximum sustained load, mm (in);
ϵ_c	=	longitudinal compressive concrete strain;
ϵ_{cc}	=	concrete strain corresponding to f_{cc};
ϵ_{co}	=	concrete strain corresponding to f_{co};
ϵ_{hcc}	=	computed strain in the tie;
μ_P	=	ductility of the column at the maximum sustained load, computed as the ratio of the axial displacement at the maximum sustained load to the extrapolated elastic axial displacement;
μ_F	=	ductility of the column at failure, computed as the ratio of the axial displacement at column failure to the extrapolated elastic axial displacement;
ρ_x	=	transverse reinforcement ratio in x-direction;
ρ_y	=	transverse reinforcement ratio in y-direction.

1.6 CONVERSION FACTORS

The following conversion factors are used in this report:

1 in	=	25.4 mm;
1 in^2	=	645 mm^2;
1 ft^3	=	0.02837 m^3;
1 yd^3	=	0.765 m^3;
1 gal	=	0.003785 m^3;
1 kip	=	4.448 kN;
1 ksi	=	6.895 MPa;
1 lb/ft^3	=	16.02 kg/m^3;
1 lb/yd^3	=	0.5933 kg/m^3;
1 oz/yd^3	=	0.02189 kg/m^3.

CHAPTER 2
BACKGROUND

2.1 INTRODUCTION

This chapter provides background information relevant to this study. Much of the literature reviewed in this chapter is related to tied concrete columns subjected to concentric axial load. Stress-strain models for confined tied concrete columns are presented in Section 2.2. Section 2.3 summarizes the previous research and findings on tied normal-strength concrete columns, and Section 2.4 summarizes the previous research and findings on large-scale, tied high-strength concrete columns. Section 2.5 and Section 2.6 discuss the cylinder compressive strength and the core compressive strength of the high-strength concrete, respectively.

In this report the following definitions are adopted: low- to normal-strength concretes (NSC) have compressive strengths less than 41.4 MPa (6 ksi); medium strength concretes (MSC) have compressive strengths that range from 41.4 to 55.2 MPa (6 to 8 ksi); and, high-strength concretes (HSC) have compressive strengths that exceed 55.2 MPa (8 ksi).

2.2 STRESS-STRAIN MODELS FOR CONCRETE CONFINED BY RECTANGULAR TIES

The concept of confining concrete by transverse reinforcement to enhance its strength and ductility has existed for many years. First introduced by Considere in 1899, the idea was explored by many engineers around the turn of the century. Early investigators showed that the maximum strength and the corresponding longitudinal strain of concrete confined by an active hydrostatic fluid pressure can be represented by the following simple relationships:

$$f_{cc} = f_{co} + k_1 f_l \tag{2.1}$$

$$\varepsilon_{cc} = \varepsilon_{co}\left(1 + k_2 \frac{f_l}{f_{co}}\right) \tag{2.2}$$

In Equations 2.1 and 2.2, f_{cc} and ϵ_{cc} are the maximum concrete stress and the corresponding strain, respectively, under the lateral fluid pressure f_l; f_{co} and ϵ_{co} are the unconfined concrete strength and corresponding strain, respectively; and k_1 and k_2 are the coefficients that are functions of the concrete mix and the lateral pressure. Mander et al. (1988) summarized the average values of k_1 and k_2 found by early researchers including Richart et al. (1928), Balmer (1949), and Richart et al. (1929). The average values of k_1 and k_2 determined by Richart et al. (1928) were 4.1 and 5, respectively. Balmer (1949) reported the value of k_1 varied between 4.5 and 7.0 with an average value of 5.6, the higher values occurring at the lower lateral pressure. Also, Richart et al. (1929) found that the enhancement of concrete strength by active fluid pressure was approximately the same as by the passive

confinement pressure from closely spaced circular steel spirals causing an equivalent lateral pressure. This concept was widely used in later experiments on full-sized specimens to develop the stress-strain models of confined concrete.

The stress-strain behavior of normal-strength concrete columns confined by tie reinforcement has been extensively studied in recent years. Mander et al. (1988) developed a stress-strain model for confined normal-strength concrete applicable to both circular and rectangular shaped transverse reinforcement with monotonic loading at a slow strain rate. Sheikh and Uzumeri (1982) developed an model for the confinement mechanisms in tied columns. Mohamed et al. (1989) developed a general approach for nonlinear analysis of reinforced-concrete columns based on finite element studies. A detailed description of the stress-strain models developed by Mander et al. for normal strength concrete tied columns is presented later in Section 2.2.1.

Stress-strain models developed based on test results from normal-strength concrete columns may be inadequate for high-strength concrete columns which possess a less ductile stress-strain behavior. An overview of existing confinement models presented by Cusson and Paultre (1993) for both NSC and HSC columns pointed out the need for the development of a confinement model for HSC columns. Cusson and Paultre (1995) developed a stress-strain model for confined high-strength concrete and calibrated it against the test results from 50 large-scale, tied HSC columns tested under concentric loading. 30 of those 50 axial compression tests on tied HSC columns with dimensions of 235 mm x 235 mm x 1400 mm (9.3 in x 9.3 in x 55 in) were performed by Cusson and Paultre (1994) and the remaining 20 tests on tied HSC columns with dimensions of 225 mm x 225 mm x 715 mm (9 in x 9 in x 28 in) were performed by Nagashima et al. (1992). A detailed discussion of this stress-strain model for tied HSC columns is presented in Section 2.2.2.

2.2.1 Stress-Strain Models for Normal Strength Concrete

This section discusses of the stress-strain models developed for NSC tied columns by Mander et al. (1988), and briefly discusses the works done by Sheikh and Uzumeri (1982), and Mohamed et al. (1989).

Mander et al.

The stress-strain model developed by Mander et al. (1988) is illustrated in Figure 2.1 and is based on an equation suggested by Popovics (1973). For a slow (quasi-static) strain rate and monotonic loading, the longitudinal compressive concrete stress f_c and strain ϵ_c are related by Equation 2.3:

$$f_c = \frac{f_{cc}\, xr}{r - 1 + x^r} \tag{2.3}$$

where f_{cc} is the compressive strength of confined concrete, and

$$x = \frac{\varepsilon_c}{\varepsilon_{cc}} \tag{2.4}$$

where ϵ_c is the longitudinal compressive concrete strain. The concrete compressive strain corresponding to the maximum stress is given by Equation 2.5 which was based on the value of k_2 of 5 as suggested by Richart et al. (1928):

$$\varepsilon_{cc} = \varepsilon_{co}[\ 1 + 5(\frac{f_{cc}}{f_{co}} - 1)] \tag{2.5}$$

where f_{co} and ϵ_{co} are the unconfined concrete strength and the corresponding strain, respectively (generally $\epsilon_{co} = 0.002$ can be assumed for normal strength concrete). The parameter 'r' in the preceding equation is determined as

$$r = \frac{E_c}{E_c - E_{sec}} \tag{2.6}$$

where E_c and E_{sec} are the tangent and secant moduli of elasticity of the concrete, respectively.

$$E_{sec} = \frac{f_{cc}}{\varepsilon_{cc}} \tag{2.7}$$

A constitutive model involving a specific ultimate strength surface for multiaxial compressive stresses was incorporated in Mander's model to compute the compressive strength of confined concrete f_{cc}. Mander's model was based on the confinement effectiveness for rectangular concrete section confined by rectangular hoops with or without cross ties. Figure 2.2 displays the effectively confined core for rectangular hoop reinforcement. The arching action which defines the region of effectively confined concrete as shown in Figure 2.2 is assumed to act in the form of a second-degree parabola with an initial tangent slope of 45°. Arching occurs vertically between layers of transverse hoop bars and horizontally between longitudinal bars. The effectively confined area of concrete at hoop level is found by subtracting the area of the parabolas containing the ineffectively confined concrete. For one parabola, the ineffective area is $(w_i)^2/6$, where w_i is the i^{th} clear distance between adjacent longitudinal bars as shown in Figure 2.2. Thus the total plan area of ineffectively confined core concrete at the level of the hoops when there are n longitudinal bars is given by Equation 2.8:

$$A_i = \sum_{i=1}^{n} \frac{(w_i)^2}{6} \tag{2.8}$$

Incorporating the influence of the ineffective areas in the elevation, the area of effectively confined concrete core at midway between the levels of transverse hoop reinforcement is given by Equation 2.9:

$$A_e = (b_c d_c - A_i)(1 - \frac{s'}{2b_c})(1 - \frac{s'}{2d_c}) \quad (2.9)$$

where b_c and d_c are core dimensions to centerlines of perimeter hoop in x and y directions, respectively, where $b_c \geq d_c$. The concrete core area (A_{cc}) enclosed by the center lines of the perimeter hoops is given by Equation 2.10, and the effective confinement coefficient (k_e) for rectangular hoops is given by Equation 2.11 as follows:

$$A_{cc} = b_c d_c - A_s \quad (2.10)$$

$$k_e = \frac{A_e}{A_{cc}} \quad (2.11)$$

It is possible for rectangular reinforced concrete members to have different quantities of transverse confining steel in the x and y directions. These may be expressed as follows in Equation 2.12 and Equation 2.13, respectively:

$$\rho_x = \frac{A_{sx}}{sd_c} \quad (2.12)$$

$$\rho_y = \frac{A_{sy}}{sd_c} \quad (2.13)$$

where A_{sx} and A_{sy} are the total areas of transverse bars running in the x and y directions, respectively, as shown in Figure 2.2.

The lateral confining stress, assuming the transverse steel yields at peak resistance, on the concrete (total transverse bar force divided by vertical area of confined concrete) is given in the x direction by Equation 2.14 and in the y direction by Equation 2.15.

$$f_{lx} = \frac{f_{yh} A_{sx}}{S d_c} = \rho_x f_{yh} \quad (2.14)$$

$$f_{ly} = \frac{f_{yh} A_{sy}}{S b_c} = \rho_y f_{yh} \quad (2.15)$$

Thus, the effective lateral confining stresses in the x and y directions can be computed using Equation 2.16 and Equation 2.17, respectively.

$$f_{lex} = k_e f_{lx} \tag{2.16}$$

$$f_{ley} = k_e f_{ly} \tag{2.17}$$

Figure 2.3 presents a general graphical solution for the compressive strength of confined concrete f_{cc} of the multiaxial failure criterion in terms of the two lateral confining stresses.

Sheikh and Uzumeri

A model for the stress-strain behavior of concrete columns confined by tie reinforcement has been developed by Sheikh and Uzumeri (1982) based on previous research on small-scale NSC tied columns. Test results of over five-hundred small-scale NSC specimens confined by simple tie configurations were incorporated in the development of this analytical model. One important feature of all specimens was the ratio of the area of the core to the gross area of the column which was relatively small for each specimen. Therefore, despite any possible strength enhancement of the confined concrete, the total capacity of the specimen, after the cover had spalled off, would not exceed the capacity of the unconfined specimen. This, as suggested by Sheikh and Uzumeri, might be the main reason for the disagreement among researchers about the beneficial effects of the rectilinear ties on the strength of the confined concrete. A few models were developed based on these test results before Sheikh and Uzumeri (1982) had published their model, however, it was concluded that none of the available models predicted the behavior of confined concrete in a satisfactory manner after an attempt to predict the results of the tests conducted at the University of Toronto. None of the previously proposed equations took into account the distribution of longitudinal and lateral reinforcement in the specimen. Therefore, all the models underestimated the strength and ductility of the confined concrete in columns with well-distributed steel. Other variables, such as tie spacing, amount of lateral and longitudinal reinforcement, and characteristics of steel, were also not considered appropriately in any of the available models prior to the work done by Sheikh and Uzumeri in 1982. In developing their model Sheikh and Uzumeri took into account the effects of the above variables on the strength and ductility of confined concrete tied columns.

Figure 2.4 presents the complete stress-strain curve for confined concrete used in the model developed by Sheikh and Uzumeri (1982). The concept used in this model is similar to Mander's model. The strength of confined concrete was calculated by using the concept of the effectively confined concrete area within the nominal concrete core. The area of the effectively confined concrete was determined by the tie spacing, the distribution of longitudinal steel around the core perimeter and the resulting tie configuration.

Mohamed et al.

Mohamed et al. (1989) developed a general approach for nonlinear analysis of reinforced-concrete columns based on the finite element method and using Cedolin, Crutzen, and Deipoli's material model

for concrete (Cedolin et al. 1977). This approach accounted for concrete cracking with tension stiffening effect, multiaxial behavior and strength properties of concrete under a generalized stress condition, nonlinear stress-strain characteristics of the steel, and the shear stiffness in a cracked element due to aggregate interlock and dowel action. The numerical results obtained by this approach were compared to the test results of eight specimens with the same dimensions of 457 mm x 457 mm x 1219 mm (18 in x 18 in x 48 in). One of the eight specimens contained 8 longitudinal bars and square ties, while the other seven specimens contained 12 longitudinal bars and both rectangular and octagonal ties. The volumetric ratio of the lateral ties was varied by adjusting either the spacing or the size of these ties. Thus, the influences of longitudinal reinforcement, lateral reinforcement, and the resulting tie configuration on concrete strength and ductility were determined from the comparisons among these specimens which will be discussed in Section 2.3. Based on the agreement between the theoretical and the experimental results, Mohamed et al. concluded that the finite element method can be used to study the confinement action in NSC columns confined by tie reinforcement.

2.2.2 Stress-Strain Model for High-Strength Concrete

It is presently well-known that high-strength concrete exhibits more brittle stress-strain behavior than normal-strength concrete. Present models for NSC stress-strain behavior may not be adequate to predict the strength and ductility enhancement in HSC confined by transverse reinforcement (Cusson and Paultre 1994). A new confinement model was developed by Cusson and Paultre (1995) based on their test results and the test results from Nagashima et al. (1992) to predict the behavior of HSC tied columns. As previously stated, Cusson and Paultre (1994) tested 30 tied HSC columns with the same dimensions of 235 mm x 235 mm x 1400 mm (9.3 in x 9.3 in x 55 in), and Nagashima et al. (1992) tested 20 tied HSC columns with the same dimensions of 225 mm x 225 mm x 715 mm (9 in x 9 in x 28 in).

Cusson and Paultre (1995) recognized that the use of the confinement index $\rho_h f_{yh}/f_c'$ as an indicator of the confinement efficiency of reinforced concrete columns often overestimated the real degree of confinement in HSC columns. The actual stress in the transverse steel at the maximum load is less than its yield strength in lightly confined high-strength concrete which leads to an overestimation of the degree of confinement. Cusson and Paultre proposed a more accurate indicator of confinement efficiency, the *effective* confinement index, which was defined as the ratio of the effective confinement pressure (f_{le}) to the unconfined concrete strength (f_{co}). This makes an allowance for the arching action occurring in the concrete core, and for the actual stress in the transverse reinforcement at peak strength of confined concrete. A comparative study of the response of the 30 HSC tied columns tested by Cusson and Paultre (1994) allowed them to separate the columns into three classes according to their effective confinement index: (1) Low confinement: $0 < f_{le}/f_{co} < 5\%$; (2) medium confinement: $5\% < f_{le}/f_{co} < 20\%$; and (3) high confinement: $f_{le}/f_{co} > 20\%$. They concluded based on their test results that lightly confined concrete specimens of class 1 produce no strength gain and little ductility. Concrete specimens with medium confinement of class 2 produce moderate strength gains and ductile post-peak behavior. Highly-confined concrete specimens offer significant strength gains as well as very ductile post-peak behavior.

The relationship between the strength gains of confined concrete, f_{cc}/f_{co}, and the effective confinement index, f_{le}/f_{co} was proposed in their model as shown in Figure 2.5 and as given by Equation 2.22 as follows:

$$\frac{f_{cc}}{f_{co}} = 1.0 + 2.1\left(\frac{f_{le}}{f_{co}}\right)^{0.7} \tag{2.22}$$

where f_{le} for a square section is given by Equation 2.16 or 2.17 with f_{hcc} equal to the actual transverse steel stress at the peak strength of confined concrete column. An iterative procedure was suggested to compute the strain (ϵ_{hcc}) in transverse reinforcement at the peak strength of confined concrete using the proposed equation for ϵ_{hcc} given by Equation 2.23:

$$\varepsilon_{hcc} = 0.5\varepsilon_{cc}\left(1 - \frac{f_{le}}{f_{cc}}\right) \tag{2.23}$$

and the stress (f_{hcc}) in transverse reinforcement is equal to ϵ_{hcc} multiplied by E_s, and the equation of ϵ_{cc} proposed by Cusson and Paultre is given by Equation 2.24 as a function of the effective confinement index:

$$\varepsilon_{cc} = \varepsilon_{co} + 0.21\left(\frac{f_{le}}{f_{co}}\right)^{1.7} \tag{2.24}$$

The suggested iterative procedure to compute the actual stress and strain in the transverse steel at the peak strength of confined concrete is summarized as follow:

Step 1. Compute the effective confinement pressure, f_{le}, with $f_{hcc} = f_{yh}$.
Step 2. Estimate f_{cc} and ϵ_{cc} based on Equations 2.22 and 2.24.
Step 3. Compute ϵ_{hcc} with Equation 2.23.
Step 4. Calculate f_{hcc}.
Step 5. Re-evaluate f_{le} with f_{hcc} from step 4 for $f_{hcc} < f_{yh}$.
Step 6. Repeat steps 2 to 5 until convergence.

Once the actual stress and strain in the transverse steel at the peak strength of confined concrete are calculated, the degree of confinement and the strength and ductility enhancement of confined concrete can be computed. A computer program was developed based on the above iterative procedure to compute the actual stress and strain in the transverse steel at the peak confined concrete strength as well as the degree of confinement and the strength enhancement. The computer program is listed in Appendix A.

The stress-strain model developed by Cusson and Paultre (1995) may be thought as a modified version of Mander's model. In Mander's model the transverse reinforcement is assumed yielded because a confined NSC column often produces large deformation at its peak strength. However, high-strength concrete is less ductile and the tests by Cusson and Paultre (1993) indicated that lightly confined HSC column did not produce yielding in the transverse reinforcement at its peak strength. As a result, Mander's model tends to overestimate the actual degree of confinement and the strength and ductility enhancement in confined high-strength concrete. Comparisons of the predicted axial strength of each specimen in this research based on both confinement models will be presented in Chapter 5.

2.3 PREVIOUS EXPERIMENTS ON CONFINED TIED NSC COLUMNS

This section of the report summarizes previous research on the axial load behavior of NSC columns confined by tie reinforcement. The summary focusses primarily on the effect of lateral reinforcement and longitudinal reinforcement on column strength and ductility and the behavior of the cover. The behavior of confined NSC tied columns has been extensively studied in recent years. Based on an extensive review of the literature, Sakai and Sheikh (1989) presented a summary on the confinement in reinforced concrete columns. Their research provided a critical review of previous work and code provisions on concrete confinement. The objectives of the research were divided into four categories: (1) characteristics of materials; (2) characteristics of cross section; (3) behavior of reinforced concrete columns; and (4) other mechanical characteristics and design constraints, such as structural detailing, and the code provisions considered included ACI Building Code (ACI 318-83) and the New Zealand (NZS 3101:1982) Code. Their primary focus was, in general, on the influence of confinement on the behavior of reinforced concrete columns in comparison to the existing code provisions. Thus, this paper provided a good reference to the effect of confinement, but it is not very useful in explaining the effect of lateral and longitudinal reinforcement on column behavior individually. Therefore, the summary presented in this chapter is based primarily on the research performed by Sheikh and Uzumeri (1980) and Mohamed et al. (1989).

Sheikh and Uzumeri tested 24 short tied columns under monotonic axial compression to failure. The columns were 305 mm (12 in) square and 1960 mm (77 in) high. Primary experimental variables included distribution of longitudinal steel, amount and the characteristics of transverse steel, and tie configuration and spacing. Mohamed et al. (1989) performed numerical analyses of eight confined concrete tied columns using the finite element method. Each column was 406 mm (16 in) square and 1219 mm (48 in) high and contained either 8 or 12 longitudinal bars. For each column, the numerical results obtained by the finite element method were compared to the experimental results. The effects of the test variables including the volumetric ratio of lateral reinforcement and the distribution of the longitudinal steel and the resulting tie configuration on the confinement action were evaluated from these comparisons. Results and conclusions from the experiments are summarized in the following sections. Included are discussions of the influence of transverse reinforcement, the influence longitudinal reinforcement, and the behavior of concrete cover.

2.3.1 Influence of Transverse Reinforcement

The effect of the volumetric ratio of lateral reinforcement, tie spacing, and the characteristics of lateral reinforcement such as hook configurations on the behavior of the confined NSC core is well-understood. Based on their test results, Sheikh and Uzumeri (1980) concluded that the amount of lateral reinforcement has a very significant effect on the behavior of the confined core. An increase in lateral reinforcement content results in an increase in both the strength and ductility of the confined core.

Sheikh and Uzumeri recognized that the effect of tie spacing is a very important parameter in determining the behavior of the confined core. An increase in tie spacing, even with the same volumetric ratio of tie reinforcement, results in a reduction in the strength gain of the concrete core. The ductility is also adversely affected. The strength gain of the confined core as well as its ductility is affected by tie spacing in two ways: (1) area of effectively confined concrete; and (2) buckling of longitudinal bars. Larger tie spacing leads to a smaller effectively confined core and may also result in premature buckling of the longitudinal bars. Both effects decrease the capacity of the column.

Tie configuration has also been shown to have an influence on column ductility. According to Sakai and Sheikh's summary, numerous experiments have shown that the rectangular ties with 90-degree hooks were not capable of providing as effective a support to the longitudinal bars as the ties with 135-degree hooks in the column subjected to high axial loads and cyclic flexure. Poor tie anchorage, in general, decreased the actual degree of confinement and, consequently, the strength and ductility enhancement of the column. Experiments on confined tied NSC columns subjected to concentric axial loads also have shown similar results as reported by Sheikh et al. (1990). In their report, ties with 135 degree hooks plus an extension of at least 6 bar-diameter embedded in the core are recommended.

In their numerical studies, Mohamed et al. (1989) considered the effect of the volumetric ratio of transverse reinforcement in their model. Seven columns of different lateral reinforcement ratios were analyzed, and the effects of the volumetric ratio of lateral reinforcement and the tie spacing were evaluated. They concluded that an increase in the volumetric ratio of lateral reinforcement results in a greater increase in the strength of confined columns as well as in the ductility capacity. This could be attributed to: (1) spacing of ties: as spacing decreases, the effectively confined concrete increases; and (2) the size of the tie bar: as the tie bar gets larger, the flexural rigidity of the tie increases, producing better confinement.

It was found that the stress-strain characteristics of lateral reinforcement determine the state of the confining pressure at any level of the applied load (Sheikh and Uzumeri 1980). On the other hand, the yield strength of lateral reinforcement determines the upper limit of the confining pressure. Sheikh and Uzumeri examined this parameter in their experiments by comparing two identical columns except that in one column the tie reinforcement was heat treated to lower its yield stress and delay the onset of strain hardening, and in the other column it was not. They concluded that the reintroduction of flat yield plateau results in a reduction of the gain in concrete strength, due to the reduction in steel strength, and due to elimination of strain hardening regions at lower strain; but the change in the gain in concrete strength is less than proportional to the change in steel stress.

2.3.2 Influence of Longitudinal Reinforcement

Sheikh and Uzumeri found that, within the range of the amounts of longitudinal reinforcement tested in their program, longitudinal reinforcement showed insignificant influence on the behavior of the confined core. However, it was postulated and, then, confirmed from their test results that, confining concrete with well distributed longitudinal steel, fully supported by ties, exhibits a very significant strength gain, as well as increased ductility. Well distributed longitudinal steel and the resulting tie configuration, and tie spacing determine the area of effectively confined concrete. Thus, a closely knit cage both in longitudinal and lateral directions increases the efficiency of confinement. A similar conclusion was made by Mohamed et al. (1989) based on their numerical studies. They stated that better concrete confinement can be obtained by using a larger number of smaller-diameter longitudinal bars to make up the required area of longitudinal reinforcement.

2.3.3 Behavior of Concrete Cover

Sheikh and Uzumeri presented a discussion of the behavior of an effectively confined concrete core and its cover. They observed the confined core and its cover exhibit different mechanical properties. During the initial loading of a column, the longitudinal strains in both the cover and the core, as well as the lateral expansion due to Poisson's ratio effect, are small. As a result, the effect of lateral confinement may be negligible and the cover and the core behave in a similar manner. As the axial load increases, the longitudinal strain and the Poisson's ratio effect of concrete, thus the lateral strain of concrete, also increase. The concrete in the core is restrained from expansion by transverse reinforcement, resulting in the confinement of the core and the separation of the cover from the core. At this stage, the core and the cover begin to follow different stress paths. The test results showed the corresponding longitudinal strain values at this stage were about 0.0015-0.0020. Beyond this point the load carrying capacity of the core is primarily a function of the confinement, and can be expected to be higher than that of plain concrete. On the other hand, the cover, whose behavior is similar to a thin plate, shows poorer behavior due to its slenderness. Its load carrying capacity can be expected to be lower than that of plain concrete. At higher strains the confined core can still carry further loads while the cover starts to unload, and, at one point its contribution to the load carrying capacity of the column becomes negligible. This corresponding strain is hard to measure. However, the test results from Sheikh and Uzumeri (1980) suggested its value varies between 0.0040 and 0.0050. Sheikh et al. (1990) observed the cover crushed at the strain value of 0.00375 from their tests. At approximately this strain level, the cover concrete may be assumed ineffective in resisting the applied axial load.

2.4 LARGE-SCALE AXIAL LOAD TESTS OF CONFINED TIED HSC COLUMNS

The work reviewed in Section 2.3 was limited to experiments of confined tied normal-strength concrete columns. This section of the report summarizes previous research on the axial load behavior of large-scale, confined, tied high-strength concrete columns. This summary focusses primarily on the research performed by Cusson and Paultre (1994), Razvi and Saatcioglu (1993), Sheikh et al. (1994), Itakura and Yagenji (1992), Galeota, Giammatteo, and Marino (1992), and a summary of the strength and deformability of confined HSC columns based on the test results of up to 250 HSC columns presented by Razvi and Saatcioglu (1994). Cusson and Paultre (1994) presented an experimental study of the behavior of large-scale HSC columns confined by rectangular ties tested under concentric

loading. Twenty-seven large-scale columns (235 x 235 x 1400 mm (9.3 in x 9.3 in x 55 in)) with the concrete strength ranging from 60 MPa (8.7 ksi) to 120 MPa (17.4 ksi) were tested and the results were evaluated in their research program. Razvi and Saatcioglu (1993) tested 12 large-scale confined HSC columns (254 mm x 254 mm x 1524 mm (10 in x 10 in x 60 in)) with the concrete strength ranging from 81 MPa (11.7 ksi) to 124 MPa (18 ksi) and presented an experimental evaluation of the behavior of confined HSC columns. Sheikh et al. (1994) tested 4 large-scale confined HSC columns with the concrete strength of about 55 MPa (8 ksi) under combined axial load and cyclic flexural load. The cross section of all specimens were 305 mm (12 in) square. The height of one specimen was 2438 mm (96 in), and 1475 mm (58 in) for the remaining three specimens. Itakura and Yagenji (1992) tested 24 columns with the concrete strength of 74 MPa (10.7 ksi) under concentric compression. The columns had 18 mm (8.6 in) square cross-sections, and were either 508 mm (20 in) or 762 mm (30 in) height. Galeota et al. (1992) performed axial tests on 40 HSC specimens measuring 152 mm x 152 mm x 457 mm (6 in x 6 in x 18 in) with the concrete strength of about 60 MPa (8.7 ksi). Three loading histories involving monotonic, gradually increasing strain cyclic, and constant strain cyclic were used during the compressive tests. Razvi and Saatcioglu (1994) presented a summary of the strength and deformability of confined HSC columns after reviewing the test results of up to 250 specimens.

In the following sections, topics discussed based on these research reports cited above are the influence of transverse reinforcement, the influence of longitudinal reinforcement, the influence of concrete strength, and the observed failure modes.

2.4.1 Influence of Transverse Reinforcement

The lateral confining pressure imposed on the concrete core is directly related to the amount of lateral reinforcement. Thus, a better confinement efficiency can be achieved by increasing the amount of lateral reinforcement. Cusson and Paultre compared four different pairs of specimens, and within each matched pair, two specimens were different only in their ratio of lateral reinforcement. They found that the specimens with a higher lateral reinforcement ratio exhibited a very significant gain in both the strength and the toughness of the specimens as compared to the specimens with less lateral reinforcement. Sheikh et al. (1993) compared their test results and found that the specimens with an increased lateral reinforcement ratio performed better and showed significant improvements in both strength and ductility. They increased the lateral reinforcement ratio by reducing tie spacing. However, the increase in the amount of tie steel is believed to have had the major effect. An overview by Razvi and Saatcioglu (1994) indicated that the influence of lateral confinement on the strength and ductility for high-strength concrete columns is, in general, the same as for normal-strength concrete columns. However, larger lateral confinement pressure is needed to provide the same degree of strength and ductility enhancement in HSC columns relative to NSC columns due to the brittle behavior exhibited by high-strength concrete.

The influences of tie spacing and tie configuration on confined HSC columns were also found to be the same as for confined NSC columns. Razvi and Saatcioglu (1994) concluded that the reduction in tie spacing improves both strength and ductility of confined HSC columns. Similar conclusions were also made by other researchers. As mentioned in Section 2.3.1, the rectangular ties with 90-

degree hooks were not capable of providing as effective a support to the longitudinal bars as the ties with 135-degree hooks, thus resulting in reduced ductility of the section. Itakura and Yagenji recommended the use of rectangular ties with 135-degree hooks with an extension of at least 10 bar-diameters embedded into the core for high-strength concrete columns, as opposed to 6 bar-diameters for normal-strength concrete columns.

Cusson and Paultre (1994) found that, for HSC columns confined with high-strength lateral steel, that the tie yield strength was developed at the peak strength of confined concrete only for well-confined concrete specimens. Steel stress lower than the tie yield strength, measured at the maximum strength of confined concrete, was observed for less confined concrete columns. Thus, Cusson and Paultre concluded that an increase of the tie yield strength results in an enhancement of the strength and toughness gains only for well-confined HSC specimens with large ratios of lateral reinforcement. Razvi and Saatcioglu (1993) also suggested the same conclusion based on their test results.

2.4.2 Influence of Longitudinal Reinforcement

Experiments on high-strength concrete columns have shown that the influence of the amount and distribution of longitudinal reinforcement on the axial load behavior of confined tied HSC columns was the same as of confined NSC tied columns discussed in Section 2.3.2. Cusson and Paultre (1994) found good enhancements in both the strength and toughness of the specimens with a larger amount of longitudinal reinforcement and a higher ratio of transverse reinforcement. The increased amount of longitudinal reinforcement was provided by a larger bar diameter in which the premature buckling of longitudinal bars was prevented. Razvi and Saatcioglu (1994) suggested that the spacing of laterally supported longitudinal reinforcement may play an important role in column confinement. Columns with 12-bar arrangement, where each reinforcement is supported by the corner of a tie, require significantly lower volumetric ratio of confinement steel than those with 4-bar arrangements.

2.4.3 Influence of Concrete Strength

The influence of concrete strength on the behavior of the confined core was examined by several researchers. Previous tests (Razvi and Saatcioglu (1993), Galeota et al. (1992)) have shown that an increase in lateral confinement enhanced the concrete compressive strength, strain at maximum stress, and the ductility. These tests also showed the amount of these enhancements is less for high-strength concrete than for normal-strength concrete.

Razvi and Saatcioglu (1993) compared test results of tied columns made with concrete strengths that ranged from 81 to 124 MPa (11.7 to 18 ksi) and with the same amount of lateral and longitudinal reinforcement. They found that specimens with higher strength concrete showed more brittle behavior than specimens with lower strength concrete. Although these tests showed that there is an improvement in the deformability of the column, it is not proportional to the increase in the volumetric ratio of lateral reinforcement; a significantly higher volumetric ratio is required for high-strength concrete columns in order to achieve deformations usually expected from normal-strength columns. Cusson and Paultre also observed greater strength and toughness gains for specimens made with lower-strength concrete.

Galeota et al. (1992) found that an increase in the compressive strength and ductility of the confined core as the degree of confinement increased. However, the increase in compressive strength and ductility in high-strength concrete was less than for lower strength concrete with same confinement.

2.4.4 Failure Modes

Cusson and Paultre (1994) reported the experimental observed failure of confined tied high-strength concrete columns was characterized by the formation of an inclined "shear" failure plane, separating the concrete core into two wedges. The angle of the inclined failure plane measured from the vertical axis varied from 25° for lightly confined columns to 45° for well-confined columns.

2.5 COMPRESSION TESTS OF HIGH-STRENGTH CONCRETE CYLINDERS AND CORES

Section 2.5.1 discusses the cylinder compressive strength of HSC concrete. The primary variables that influenced the compressive strength of HSC concrete cylinders include specimen size, method of curing, compression test bearing block, and the preparation of specimen ends. Section 2.5.2 evaluates core compressive strength and the variables which affected its compressive strength include the drilling location of the core, temperature variations of the core, and length-to-diameter ratio of the core.

2.5.1 Cylinder Compressive Strength

Lessard, Chaallal, and Aitcin (1993) studied the variables influencing the cylinder compressive strength of high-strength concrete based on 378 compression tests on 152 x 305-mm (6 x 12-in) and 102 x 203-mm (4 x 8-in) specimens made of a total of 14 different batches of concrete in which 5 batches of concrete were made in the laboratory and 9 batches of concrete were made in the field. The study showed that the compressive strength of HSC decreases as the specimen size increases. Comparisons between compressive tests of 152 x 305-mm (6 x 12-in) HSC specimens ($f'_{c\,152}$) and 102 x 203-mm (4 x 8-in) HSC specimens ($f'_{c\,102}$) within the same batch of concrete indicated an average ratio of strengths $f'_{c\,102}/f'_{c\,152}$ of 1.05. Compressive test results also showed the strength of different size HSC specimens varied with the size of the bearing block of testing machine. Thus, the size of bearing block used in the compression test has to be adequate for the size of the specimen. It was recommended to use a bearing block with a diameter which exceeds the diameter of the test specimen by 2 mm (0.08 in). Tests were also performed to evaluate the compressive strengths of specimens with different end preparations and capped with different capping compounds. It was suggested, when using a high-quality capping compound testing 50 to 60 MPa (7.3 to 8.7 ksi) on 50-mm (2-in) cubes, grinding of cylinder ends is necessary only if high accuracy is required for concrete below 130 MPa (18.9 ksi) or if the cylinders have a compressive strength above 130 MPa (18.9 ksi). When capping is required, a very thin layer of a very high-quality capping compound should be used. However, Lessard et al. (1993) recommended all specimens that may exceed 100 MPa (14.5 ksi) should be ground. The effect of eccentric loading on specimen compressive strength was also examined in this study. It found that the measure of compressive strength is not affected by eccentricity with respect to the vertical axis of the testing machine provided this eccentricity is kept below 6 mm (0.24 in) for NSC and below 4 mm (0.16 in) for HSC.

Aitcin et al. (1994) investigated the effect of cylinder size and curing on cylinder compressive strength of normal and high-strength concrete. Specimens were made with design compressive strengths of 35 MPa (5 ksi), 90 MPa (13 ksi), and 120 MPa (17.4 ksi), and compression tests were performed on 102-, 152-, and 203-mm diameter (4-, 6-, and 8-in diameter) cylinders. The different curing conditions studied included air-cured, seal-cured, and water-cured. Compression test results of different size HSC cylinders suggested that smaller HSC cylinders exhibited higher compressive strengths, and larger cylinders possessed a larger coefficient of variation on the compressive strength. The effect of curing was evaluated by comparing test results of specimens prepared with different curing. As expected, Aitcin et al. found the maximum compressive strength was developed in water-cured cylinders. Sealed cylinder strengths were less than water-cured cylinders, but higher than air-cured cylinder. The air-cured cylinders had compressive strengths of about 80 percent of the compressive strengths of companion cylinders cured in lime-saturated water, and had compressive strengths about 16 percent lower than companion sealed cylinders. Aitcin et al. suggested that the difference in compressive strengths between cylinders that were sealed versus those that were air-cured gives an indication of the influence of drying on compressive strength.

2.5.2 Core Compressive Strength

Yuan et al. (1991) tested high-strength concrete cores drilled from two 1.8 m x 1.8 m x 1.8 m (72 in x 72 in x 72 in), unreinforced concrete mock columns and 96 standard 152 x 305 mm (6 x 12 in) cylinders. The two unreinforced concrete mock columns were cast at different temperatures to study the influence of temperature variation on core strengths. Column I was cast at a concrete placement temperature of 33° C (91° F), and Column II was cast at 39° C (102° F). Based on their test results, Yuan et al. found that there was no significant difference among the compressive strength of cores extracted, at any given age, from the upper and lower portions of the concrete mass. Therefore, it was concluded that the coring location has little or no effect on core strength. The in-situ strength in the vertical direction appears to be more uniform in high-strength concrete than in normal-strength concrete. However, tests also have shown the core strength at the center is significantly lower than that near the surface for a HSC column with a large cross-sectional area. It was also found that, at any given age, core strength is about 75 percent of moist-air cured cylinder strength and about 85 percent of field-cured cylinder strength. The field-cured cylinder strength is approximately 90 percent of the moist-air cured cylinder strength. In addition, the compression test results of HSC cylinders and cores extracted from Column I and Column II indicated that the placement temperature had little or no effect on the strength gain of concrete cylinders and cores.

Bartlett and MacGregor (1994) studied the effect of core length-to-diameter ratio on concrete core strength. They proposed a length-to-diameter correction factor for concrete cores with compressive strength of less than 96.5 MPa (14 ksi). The proposed equation (Equation 3.1) is discussed in Section 3.7 in which a correction factor of less than 1.0 is applied to concrete core strength with a length-to-diameter ratio between 1.0 and 2.0. Based on the analyzed data, Bartlett and MacGregor concluded the required strength correction is significantly reduced for high-strength concrete. As the concrete strength increases, correction factors closer to 1.0 are appropriate.

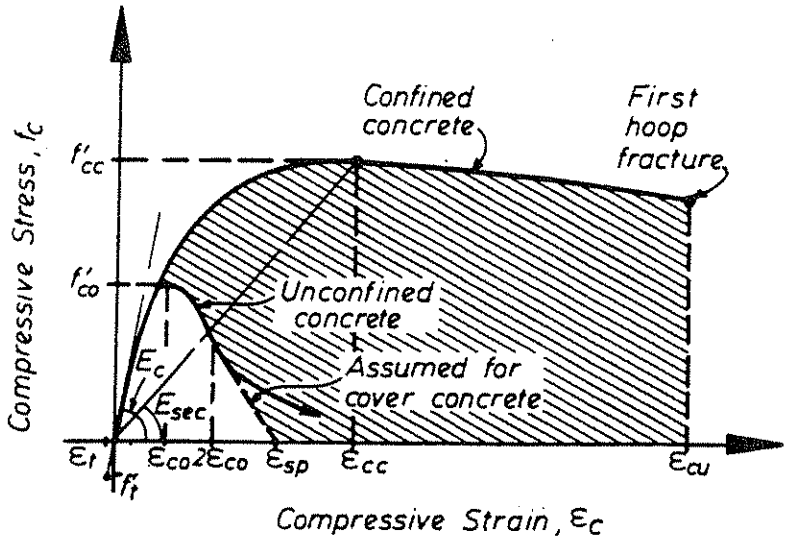

Figure 2.1 Stress-strain model proposed for monotonic loading of confined and unconfined concrete [Mander et al. (1988)].

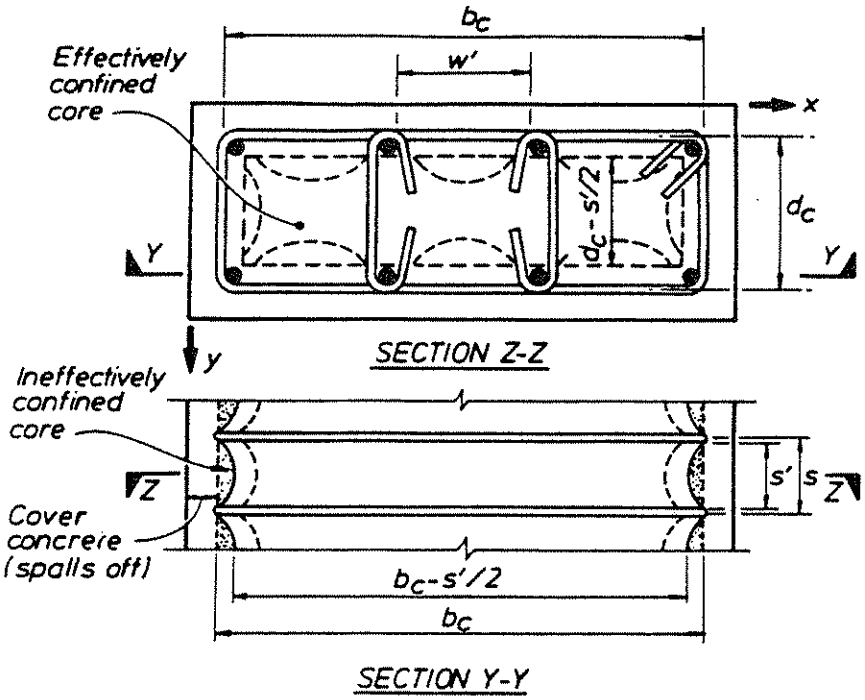

Figure 2.2 Effectively confined core for rectangular hoop reinforcement [Mander et al. (1988)].

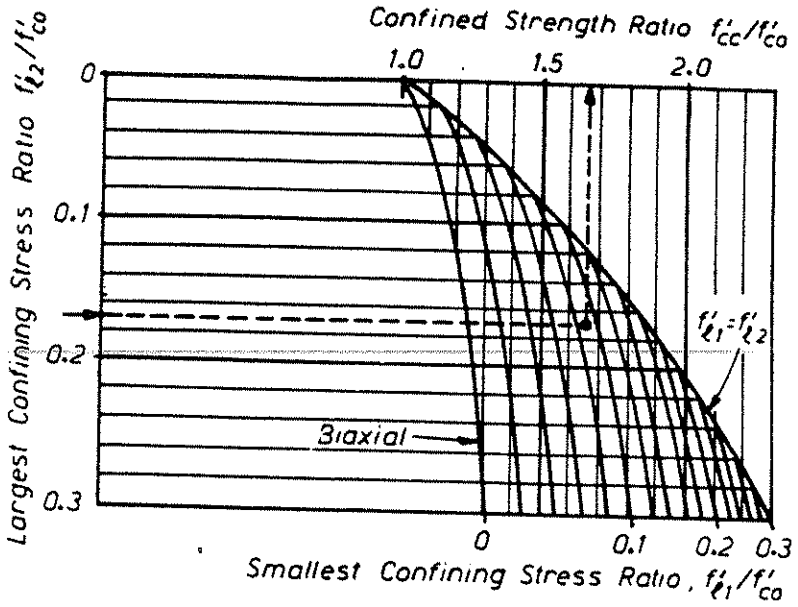

Figure 2.3 Confined strength determination from lateral confining stresses for rectangular sections [Mander et al. (1988)].

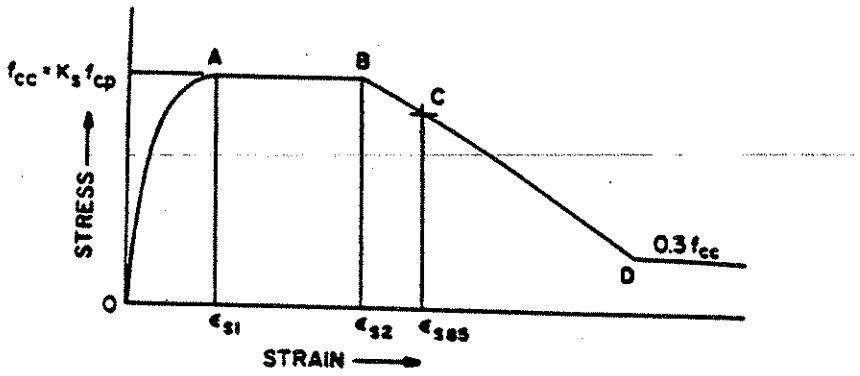

Figure 2.4 Proposed general stress-strain curve of concrete [Sheikh and Uzumeri (1982)].

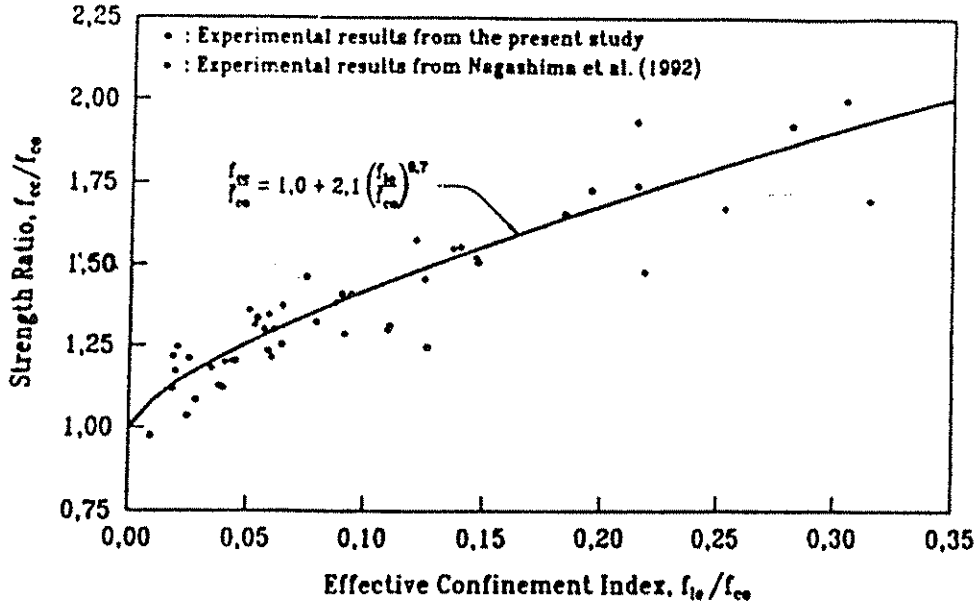

Figure 2.5 Effect of confinement on peak concrete strength [Cusson and Paultre (1995)].

CHAPTER 3
DESCRIPTION OF EXPERIMENTAL PROGRAM

3.1 INTRODUCTION

This chapter provides a detailed description of the experimental program. Section 3.2 reviews the research objective and presents the experimental test matrix. Section 3.3 describes the specimen details, and Section 3.4 discusses the instrumentation used to evaluate the behavior of the columns. Section 3.5 presents specimen fabrication details. Section 3.6 and Section 3.7 summarize the material properties of reinforcement steel and concrete used to construct the specimens, respectively. Finally, Section 3.8 discusses the variations in the concrete compressive strengths that were observed between the prepared concrete cylinders and the cored concrete cylinders.

3.2 TEST PROGRAM

3.2.1 Review of Objective

As stated in Chapter 1, the objective of this research is to study the behavior of large-scale, tied high-strength concrete columns subjected to concentric axial load. The experimental program was developed to specifically evaluate the role of concrete compressive strength and the amount of lateral reinforcement on column strength and ductility. The specific objectives of this research are as follows:

1. Evaluate the influence of concrete compressive strength on the axial strength and ductility of tied concrete columns.

2. Evaluate the influence of the amount of lateral reinforcement on the axial strength and ductility of tied high-strength concrete columns.

3. Evaluate the effectiveness of the existing empirical models for predicting the axial strength of confined tied high-strength concrete columns. The models evaluated in this report are based on the research performed by Mander et al. (1988) and Cusson and Paultre (1995), and are presented in Chapter 2.

3.2.2 Test Matrix

The test matrix is presented in Table 3.1. This test matrix was established in collaboration with the research sponsor, the Portland Cement Association (PCA). A total of nine columns were tested in this research. The primary variables treated are concrete compressive strength and the amount of lateral reinforcement. All columns had the same overall dimensions measuring 2.44 m (8 ft) tall and 406 mm x 406 mm (16 in x 16 in) in cross-section. All columns were reinforced with 8-#8 grade 60 longitudinal bars to provide a longitudinal steel ratio of 2.45%. As shown in Table 3.1, three series of columns made with three different design concrete compressive strengths were included in the test matrix, 34.5 MPa (5 ksi), 67 MPa (10 ksi), and 103.4 MPa (15 ksi). All columns were reinforced with #3 grade 60 ties. As shown in Table 3.1, 3 different tie spacings along the height of each column were treated, 406 mm (16 in), 203 mm (8 in), and 102 mm (4 in). Unfortunately, the third series of specimens did not achieve the intended design compressive strength of 103.4 MPa (15 ksi). Instead,

the actual compressive strength of these specimens was similar to the compressive strength of the second series of specimens. Thus, the third series of specimens essentially represents a replica of the second series of specimens. This leads to the revised test matrix shown in Table 3.2. For the purposes of this report, the following shorthand notations are used to denote the three series of specimens: L-Series denotes the three column specimens, L1, L2, and L3, made with "low" strength concrete and tie spacings of 406 mm (16 in), 203 mm (8 in), and 102 mm (4 in), respectively; HA-Series denotes three specimens, HA1, HA2, and HA3, made with "high" strength concrete and tie spacings of 406 mm (16 in), 203 mm (8 in), and 102 mm (4 in), respectively; HB-Series denotes three specimens HB1, HB2, and HB3 also made with "high" strength concrete and tie spacings of 406 mm (16 in), 203 mm (8 in), and 102 mm (4 in), respectively.

The test matrix was arranged to evaluate the influence of concrete compressive strength and the amount of lateral reinforcement upon the strength and ductility of high-strength concrete columns. Two major comparisons can be made:

1. The influence of concrete strength can be evaluated by comparing the specimens with a similar volumetric ratio of lateral reinforcement, i.e., by comparing the results of specimens in any one column in Table 3.2.

2. The influence of the amount of lateral reinforcement for a given concrete compressive strength f_c' can be evaluated by comparing the results of specimens in any one row in Table 3.2.

3.3 SPECIMEN DETAILS

Table 3.3 summarizes the longitudinal and transverse reinforcement provided in each column specimen, and Figure 3.1 presents elevation and section drawings of the specimens.

3.4 INSTRUMENTATION

3.4.1 Instrumentation Configuration

All nine specimens were tested with the same instrumentation configuration. The columns were instrumented with two electrical resistance strain gages and a linear variable differential transformer (LVDT) displacement transducer. Two strain gages were used to monitor the strains in the longitudinal reinforcement. Both strain gages were located on the same midface longitudinal bar located on the west face of each column. One gage was located at the mid-height of the column, and the second gage was located at the three quarters of the height of the column. These gages were labeled S1 and S2, respectively. One LVDT displacement transducer was used to measure travel of the testing machine head. This displacement is taken as the axial shortening of the column.

3.4.2 Instrumentation Protection

Several measures were taken to protect the strain gages from damage during concrete placement. The protection system applied to the strain gages prior to concrete placement was as follows. After the gages were bonded to the reinforcement and the lead wires were attached, the gages were coated with poly-urethane. Next, a coat of liquid rubber was applied generously over the entire gage area,

then mastic tape was placed over the gage and lead wires. A strip of foil tape was then placed around the mastic tape and reinforcing bar. This foil tape was then sealed at the end with an epoxy.

The LVDT used to measure column axial shortening was located at the corner of the testing machine head to prevent possible damage from falling concrete debris during testing.

3.4.3 Data Acquisition System

A schematic drawing of the data acquisition system is presented in Figure 3.2. In addition to the strain gages and displacement transducer, the data acquisition system consisted of power supplies, strain gage signal conditioners, analog-to-digital (A/D) converter, computer, and monitor. The output signals from the signal conditioners and the displacement transducer were wired to a high speed programmable data acquisition board which translated the information from an analog signal to a digital signal. Each channel's reading was an average of 20 high speed samples. The information was then processed by a computer program and displayed to the monitor so that column strain and shortening behavior could be observed during testing. Specimen information displayed to the computer monitor was updated every three seconds.

A computer program written in BASIC programming language by Pieroni (1995) was modified and used to acquire, process, display, and save data during testing. The modified computer program allowed the user to balance channels, save data to the hard drive at specified time intervals or on command, and change the time interval at which data was saved. A photograph of the computer monitor during testing is presented in Figure 3.3.

3.5 SPECIMEN FABRICATION DETAILS

3.5.1 Construction of Reinforcement Cages

Each reinforcement cage consisted of 8-#8 bars 2.44 m (8 ft) in length and square ties as the transverse reinforcement. Each square tie had an outside-to-outside dimension of 330 mm x 330 mm (13 in x 13 in) which defined the area of the core and provided a concrete cover of 38 mm (1.5 in) thick around the core of the column. Each square tie had a 90 degree-bent corner with the extensions of at least 95 mm (3.8 in) (10 tie-diameters). In completing the cages, ties were wire tied to the appropriate longitudinal bar as described in ACI 318 Code. As shown in Figure 3.1, tie spacing was reduced to 51 mm (2 in) and extra diamond-shaped ties were added over a length of 406 mm (16 in) at each end of the cage to provide extra confinement to prevent premature failure in the end regions.

Each cage was attached to a 864 mm x 864 mm x 19 mm (34 in x 34 in x 3/4 in) steel base plate to provide stability to the column during handling and concrete placement. To accomplish this, three 305 mm (12 in) long #8 bars were welded to each base plate. A column cage was then wire tied to the three bars to attach the cages to the plates prior to concrete placement.

Wood formwork was used to construct the columns. After the base plate and cage construction was complete, formwork was oiled and assembled and held in-place by threaded rods. During the assembly of the formwork, the lead wires to the strain gages were carefully pulled through the pre-drilled holes in the formwork. Then, 38 mm (1.5 in) long plastic sheaths were slipped over the strain

gage lead wires and fitted inside the drilled holes. These sheaths were used to protect the lead wires during testing, as the wires were able to slip through the sheath as the concrete cover spalled from the column. Figure 3.4 shows the column formwork set up prior to concrete placement.

3.5.2 Concrete Placement

All columns were oriented in a vertical position during casting, and concrete was placed in the columns in approximately 3 or 4 lifts. The concrete was placed with a bucket and consolidated with an electrically powered internal submersion vibrator at each of the lifts.

Three separate concrete batches were placed, one each for the L-, HA-, and HB-Series specimens. Ready-mixed concrete was used for all three series. Table 3.4 summarizes the mixture proportions provided by the ready-mix supplier.

The L-Series columns were cured in the formwork for 7 days after casting, during which time the tops of the columns were covered with wet burlap and plastic sheeting. After this time period the formwork was removed. The HA- and HB-Series columns were cured in a similar manner except that the formwork remained in place for 21 and 28 days, respectively, after casting.

3.5.3 Placement of Columns in the Testing Machine

All the columns were tested in concentric compression in a 22.2 MN (5000 kip) capacity universal testing machine. The steel base plate of each specimen rested against the steel base in the testing machine. The tops of the columns were grouted in place with a thin layer of hydrostone with one day strength of 76 MPa (11 ksi). A plastic sheet was placed between the hydrostone and machine head to protect the steel machine head from moisture from the hydrostone before the machine head was lowered against the specimen.

3.6 MATERIAL PROPERTIES OF STEEL REINFORCEMENT

Table 3.5 and Table 3.6 summarize the material properties of the longitudinal and transverse reinforcement, respectively. Tension tests were performed according to ASTM A615-87 on both longitudinal and transverse reinforcement to determine yield and ultimate strengths of the steel. In each test, reinforcement bars with a clear distance between machine grips of approximately 30.5 mm (12 in) were loaded to failure. The yield and ultimate strengths of each of the deformed bars were read directly from the testing machine according to the procedure stated in ASTM A615-87. The results from tension tests agreed reasonably well with the mill test reports from the reinforcement supplier.

3.7 MATERIAL PROPERTIES OF CONCRETE

Concrete compressive strengths were determined by performing compression tests on 3 different types of cylindrical specimens: (1) wet-cured prepared cylinders ($f_{c\text{-}28}$); (2) field-cured prepared cylinders ($f_{c\text{-}field}$); and (3) cores ($f_{c\text{-}core}$), as illustrated in Figure 3.5. The wet-cured prepared cylinders were used to determine the 28-day compressive strengths of the different concrete mixtures. The field-cured cylinders and cores were intended to be more representative of the actual concrete in the columns.

The wet-cured and field-cured cylinders measured 152 mm (6 in) in diameter and 305 mm (12 in) high and were made according to ASTM C-31 procedures. These cylinders were cast in plastic cylinder molds and covered with wet burlap and plastic sheeting for the first 24 hours after casting. The wet-cured cylinders were stripped from their molds after about 24 hours after casting and placed in lime-saturated curing baths. The field-cured cylinders were stripped from their molds at the same time the columns were stripped from their forms, and were tested at approximately the same age as the columns were tested. The L-Series columns and cylinders were tested over a three day period at an age of about 130 days. The HA-Series columns and cylinders were tested over a three day period at an age of approximately 110 days, and the HB-Series columns and cylinders were tested over a three day period at an age of approximately 150 days.

The core specimens were extracted from a plain concrete column that was cast along with each set of reinforced columns (see Figure 3.5). Procedures as outlined by ASTM C-42 were approximately followed to extract these cores. The cores were extracted from the column with an electric coring machine, and the ends of the cores were then saw cut to obtain smooth and parallel ends. Figure 3.6 shows the locations at which the cores were extracted from the columns. The cores were extracted and tested at approximately the same age as the columns were tested. The cores of the L- and HA-Series measured about 145 mm (5.70 in) in diameter and about 292 mm (11.5 in) high with a length-to-diameter ratio of about 2.02. The cores of the HB-Series, however, were extracted using a coring bit with the resulting averaged diameter of about 152 mm (6 in) and the height of about 267 mm (10.5 in). The length-to-diameter ratio was 1.75, and a strength correction factor was applied to these cores as discussed later in this section.

It is thought that of the three types of concrete strength specimens (wet-cured, field-cured, and cored cylinders), the cored cylinders best represent the concrete in the columns, because they represent the actual consolidation, moisture, and temperature histories experienced by the columns. As shown schematically in Figure 3.5, a thermocouple was placed in the plain columns and a field-cured cylinder to monitor temperatures early in the curing process for each concrete pour. Figure 3.7 shows temperatures reached in the column and cylinders in each concrete pour.

All the cylinders except the L-series wet-cured cylinders were tested in compression in a 3584 kN (800 kip) displacement-controlled testing machine at a displacement rate of 1.4 mm/min (0.055 in/min), which is approximately equal to the ASTM prescribed rate of 1.3 mm/min (0.05 in/min). The L-series, wet-cured cylinders were tested in compression in a 1344 kN (300 kip) load-controlled testing machine at a load rate approximately equal to 283 kPa/sec (41 psi/sec) which is within the range of 138-345 KPa/sec (20-50 psi/sec) as specified in ASTM C-39. All cylinders were capped with a sulfur mortar compound according to ASTM C-617 specifications and tested according to ASTM C-39.

In reporting the concrete compressive strengths, a length-to-diameter correction factor was applied to the cored cylinders. The correction factor for the normal-strength cored cylinders was based on ASTM C-42 provisions. These provisions are only good for concrete strengths less than or equal to 41.4 MPa (6.0 ksi). The correction factor for the higher strength concretes was based on a study by

Bartlett and MacGregor (1994). Equation 3.1 was found to accurately predict the length to diameter correction factor for concrete compressive strengths up to 96.5 MPa (14 ksi):

$$CF = 1+(-0.144+0.027Z_{WD}+0.003\frac{f_{c-NS}}{1000})(2-\frac{l}{d})^2 \quad (3.1)$$

where Z_{WD} = indicator variable for core moisture condition, = 0 for air dried, = 1 for soaked, = 0.5 for sealed (cores were air dried).

f_{c-NS} = average strength of concrete core specimens with constant length to diameter ratio between 1 and 2.

l = length of cored specimen.

d = diameter of cored specimen.

The compressive strengths of the cored cylinders with the corresponding correction factors are tabulated separately in Table 3.7. The average concrete compressive strengths of the wet-cured, field-cured, and cored cylinders are presented in Table 3.8. Observations were made on the compressive strength variations among these three types of cylinders and are discussed in the next section.

3.8 OBSERVED COMPRESSIVE STRENGTH VARIATIONS AMONG CONCRETE CYLINDERS

As noted earlier, the field-cured cylinders and cores were intended to be more representative of the actual concrete in the column, and the wet-cured prepared cylinders were used as a mean of assessing the relative potential strength of each concrete mixture.

In this experiment, some unexpected results were obtained from the compression tests of the cylindrical test specimens. The average concrete compressive strengths of the wet-cured, field-cured, and cored cylinders are presented in Table 3.8. Some observations are as follows. In the L-Series concrete specimens, the field-cured cylinders exhibited a lower strength than the cored cylinders. The opposite situation obtained in the HA-Series cylinders, where the field-cured cylinders exhibited a significantly higher strength than the cored cylinders. Finally, for the HB-Series specimens, the field-cured cylinders and cored cylinders exhibited similar compressive strengths, with the field-cured cylinders exhibiting slightly higher strengths than the cored cylinders.

It is also noted in Table 3.8 that the 28-day wet-cured cylinders of both the HA- and HB-Series exhibited about the same compressive strength. Based on discussions with the ready-mix concrete supplier and other materials suppliers, it is thought that the compressive strengths of these concrete mixtures may have been limited by the strength of the limestone coarse aggregate used in these

mixtures. Future attempts to produce concrete with a compressive strength in excess of 69 MPa (10 ksi) with locally-available materials should evaluate the use of a different coarse aggregate.

Unfortunately, with the limited data obtained from this experiment, it is difficult to provide a conclusive explanation for the cause of the observed strength relationships discussed above. Two additional tests were performed in an attempt to understand the cause of these strength variations. First, density tests were performed on the cylindrical specimens in an attempt to identify any influence of the differences in consolidation among the specimens that may have influenced their compressive strengths. Section 3.8.1 discusses the density test results and the observed relationship between concrete density and compressive strength. Second, the validity of concrete compressive strengths obtained from tests at Lehigh University was verified through tests of additional cylinders at the Construction Technology Laboratories (CTL) in Illinois. Section 3.8.2 presents the test results from CTL and compares those results with the results obtained from the Lehigh University tests.

3.8.1 Cylinder Compressive Strength and Density

The specific gravities of the field-cured cylinders and the cores were obtained in accordance with the procedure outlined in ASTM C642-81. The corresponding concrete density was then computed by multiplying each specific gravity value by the unit weight of water at room temperature (997.5 kg/m^3 or 62.27 lb/ft^3). Appendix B presents the sample concrete specific gravity and density calculation, and Table 3.9 presents concrete specific gravity and density test results.

In the L- and HA-Series concrete mixtures, the saturated, surface dry (SSD) bulk density of the cored cylinders exhibited little variation along the height of the column as shown in Table 3.10, and the average density of the field-cured cylinders agreed reasonably well with the cores. Figure 3.8 and Figure 3.9 show the strength variations with respect to the density of both the field-cured cylinders and the cores of the L- and HA-Series concrete mixtures, respectively. As shown in these figures, the densities of cores were comparable to the weighted average densities of field-cured cylinders. The weighted average densities of field-cured cylinders in all three concrete series were calculated by averaging all specimens' densities proportioned to their weights as described in ASTM C127-81.

Figure 3.10 shows the strength variations with respect to the density of both the field-cured and cored cylinders of the HB-Series concrete mixture. The density of cored cylinders varied randomly and significantly along the height of the column, but the compressive strength remained about constant. The weighted average density of the field-cured cylinders fell within the range of the density variations of the cores.

The results presented in Table 3.10 and Figures 3.8, 3.9, and 3.10 suggest the observed differences in compressive strengths between the field-cured cylinders and cores were not attributable to differences in consolidation which could be identified by differences in densities.

3.8.2 Comparison between Experimental Test Results and CTL Test Results

The compressive strengths of the concrete cylinders tested by CTL were determined in accordance with ASTM C42. Table 3.11 summarizes the CTL test results of the cylinders. Table 3.12 presents

the comparisons between CTL test results and the test results from this experimental program. In most specimens, the average compressive strengths of the cylinders in different concrete mixtures obtained by CTL were higher than from the Lehigh University tests. However, a part of the increased strength is due to the effects of specimen size and age. CTL tested cylindrical specimens that measured 102 mm x 203 mm (4 in. x 8 in.) at a concrete age of approximately one year. In general, test results from CTL agreed reasonably well with the test results from the Lehigh University tests. It is therefore concluded that the Lehigh University test results are valid and therefore the Lehigh University results are used to interpret the results of the experimental program.

3.8.3 Final Remarks on Concrete Cylinder Compressive Strengths

The differences observed between the compressive strengths of the field-cured cylinders and cored cylinders may be explained by examining the possible role of temperature on the amount of water in each specimen as the concrete was gaining strength. Specifically, the higher temperatures experienced by the columns as compared to the cylinders may have had the effect of driving off moisture from the columns. The temperatures reached during curing in the columns and cylinders in each concrete series are plotted in Figure 3.7. These temperature plots show that: (1) the columns of each series reached higher temperatures as compared to the field-cured cylinders; and, (2) the HA- and HB-Series columns and cylinders reached higher early temperatures than the L-Series columns and cylinders. The consequence of the role of early temperatures and resulting moisture contents was not specifically studied in this research. However, it is conceivable that these factors may have had a role in determining the relative strength values of the field-cured cylinders and cores.

For the HA- and HB-Series columns, a loss of water caused by evaporation at a high early temperature may have resulted in insufficient water for continued hydration at some point early in the curing of these columns. This would have limited the strength gain of the concrete in the columns and contributed to the low strength values obtained for the cores. The field-cured cylinders, by contrast, did not reach as high a temperature as the columns, and as a consequence may not have lost as much water to evaporation prior to form removal, and thus were able to continue to gain strength with age for a longer period of time as compared to the columns.

The high early column temperature may not have had a significant influence of the strength gain of the L-Series specimens, since even with some water loss due to evaporation, these specimens (with a higher initial water-to-cement ratio) would likely still have had adequate water for continued hydration. Thus the L-Series columns may have been able to continue to gain strength with age more so than the HA- and HB-Series columns. Evidence to support this is that the L-Series cored cylinders exhibited a considerable strength gain over the L-Series 28-day wet-cured cylinders. It is also noted that the field-cured cylinders exhibited lower strengths than the cores for the L-Series specimens. This is not readily understood from the discussion above since the field-cured cylinders, being at an even lower temperature than the columns, would be expected to have lost even less moisture than the columns prior to formwork removal. It may be that once the cylinders and columns were stripped from the forms (at an age of 7 days), the small volume of the field-cured cylinders may have dried out more quickly (and thus ceased appreciable strength gain) as compared to the larger volume of the columns, and thus the field-cured cylinders exhibited a lower compressive strength than the cores.

The above discussion is speculative in nature and is intended to provoke thought on additional measures that may be taken in future studies (to understand the observed differences between compressive strengths of the various types of concrete strength test specimens). Again, as noted above, the role of temperature and moisture on the strength gain of the specimens was not specifically studied in this research so no definitive conclusions can be made here.

Table 3.1 Original test matrix with design concrete compressive strengths.

Concrete Strength	Transverse Reinforcement		
	#3 @ 406 mm (16 in)	#3 @ 203 mm (8 in)	#3 @ 102 mm (4 in)
Series 1 $f_c' =$ 34.5 MPa (5 ksi)	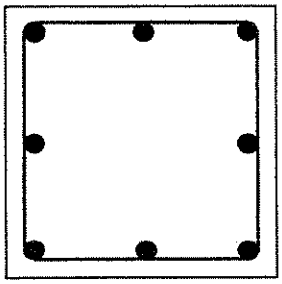	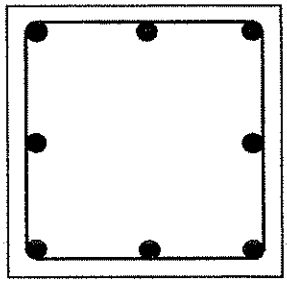	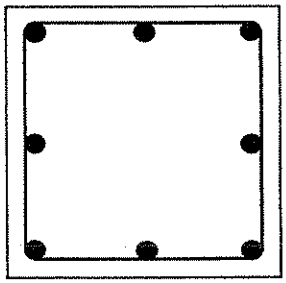
Series 2 $f_c' =$ 69 MPa (10 ksi)	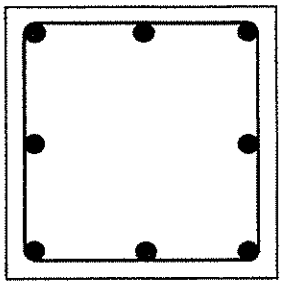	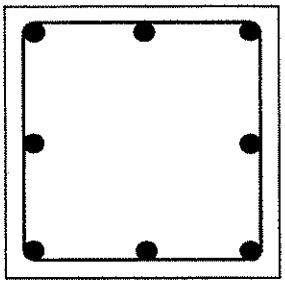	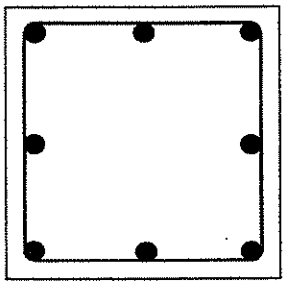
Series 3 $f_c' =$ 103.4 MPa (15 ksi)	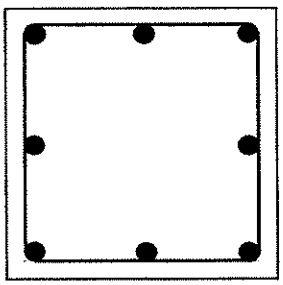	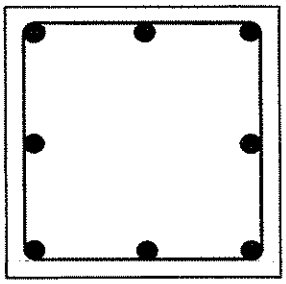	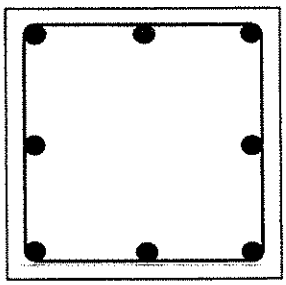

Table 3.2 Revised test matrix with actual[1] concrete compressive strengths.

Concrete Strength	Transverse Reinforcement		
	#3 @ 406 mm (16 in)	#3 @ 203 mm (8 in)	#3 @ 102 mm (4 in)
L-Series $f_c' =$ 35.4 MPa[1] (5.14 ksi)	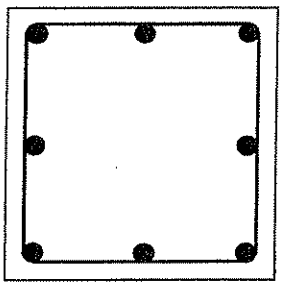 L1	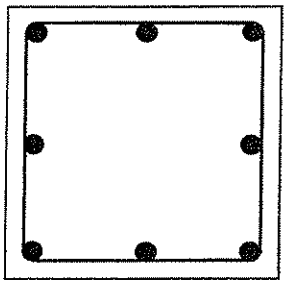 L2	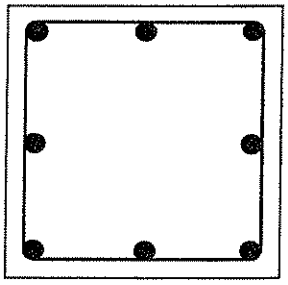 L3
HA-Series $f_c' =$ 60.7 MPa[1] (8.82 ksi)	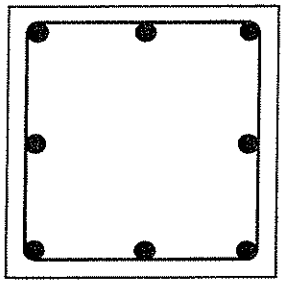 HA1	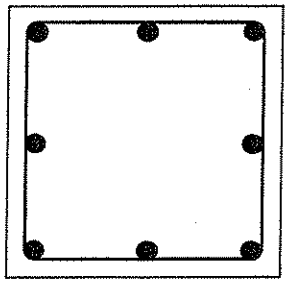 HA2	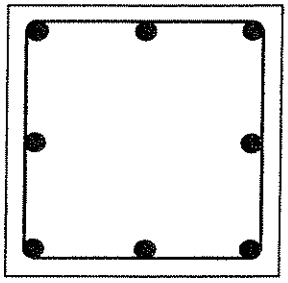 HA3
HB-Series $f_c' =$ 65.9 MPa[1] (9.56 ksi)	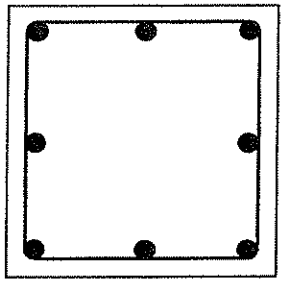 HB1	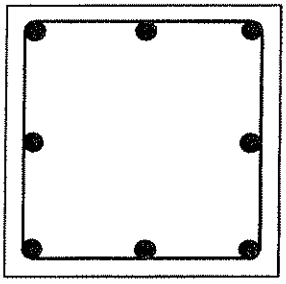 HB2	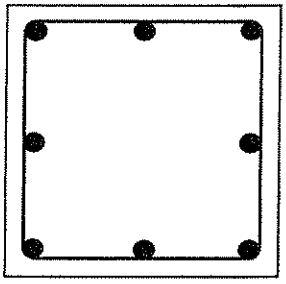 HB3

[1] compressive strength reported here is from tests of cored cylinders

Table 3.3 Summary of reinforcement provided in each specimen.

Specimen	Steel Reinforcement							
	Longitudinal				Transverse			
	bar size	no. of bars	Area mm^2 (in^2)	ρ (%)	bar size	Area mm^2 (in^2)	s mm (in)	ρ (%)
L1	#8	8	4050 (6.28)	2.45	#3	71 (0.11)	406 (16)	0.21
L2	"	"	"	"	"	"	203 (8)	0.42
L3	"	"	"	"	"	"	102 (4)	0.85
HA1	"	"	"	"	"	"	406 (16)	0.21
HA2	"	"	"	"	"	"	203 (8)	0.42
HA3	"	"	"	"	"	"	102 (4)	0.85
HB1	"	"	"	"	"	"	406 (16)	0.21
HB2	"	"	"	"	"	"	203 (8)	0.42
HB3	#8	8	4050 (6.28)	2.45	#3	71 (0.11)	102 (4)	0.85

Table 3.4 Mixture proportions of concrete as reported by ready-mix supplier: (a) L-Series specimens; (b) HA-Series specimens.

Ingredient	Remark	Amount
Cement	bin-2	582 lb/yd^3
Flyash		112 lb/yd^3
Coarse Aggregate	1/2 in. stone (0.5% moisture content)	1793 lb/yd^3
Fine Aggregate	litt gap (3.5% moisture content)	1213 lb/yd^3
Admixture	MDVR	7.7 oz/yd^3
Admixture	Polyheen	17.3 oz/yd^3
Water	1 gal. water = 8.31 lbs.	23.7 gal/yd^3

(a)

Ingredient	Remark	Amount
Cement	bin-2	902 lb/yd^3
Coarse Aggregate	1/2 in. stone (0.5% moisture content)	1620 lb/yd^3
Fine Aggregate	litt gap (3.5% moisture content)	1333 lb/yd^3
Admixture	100-XR	49.7 oz/yd^3
Admixture	RHEO1000	250 oz/yd^3
Water	1 gal. water = 8.31 lbs.	22.7 gal/yd^3

(b)

Table 3.4 Mixture proportions of concrete as reported by ready-mix supplier: (c) HB-Series specimens.

Ingredient	Remark	Amount
Cement	Hercules Cement	660 lb/yd^3
Blast Furnace Slag Cement	New Cement	330 lb/yd^3
Coarse Aggregate[1]	#57 Eastern Industries	1800 lb/yd^3
Fine Aggregate[1]	Eastern Industries	1200 lb/yd^3
Admixture	Microsilica Force 10,000 - W.R. Grace	100 lb/yd^3
Admixture	Daracem 100 - High Range Water Reducer	142 oz/yd^3
Admixture	Daratard (retarder)	3.3 oz/yd^3
Water	1 gal. water = 8.31 lbs.	29.6 gal/yd^3
Air Content		1.0 +/- 1.0 %

(c)

[1] aggregate weights reported are saturated, surface dry (SSD)

Table 3.5 Longitudinal reinforcement properties.

Specimen Series	Bar Size	Bar Area mm^2 (in^2)	Yield Load kN (kip)	Ultimate Load kN (kip)	Yield Stress MPa (ksi)	Ultimate Stress MPa (ksi)
L, HA, HB	#8[1]	510 (0.79)	234 (52.6)	340 (76.4)	459 (66.6)	667 (96.7)

[1] loads and stresses reported for these bars are an average of 3 tests

Table 3.6 Transverse reinforcement properties.

Specimen Series	Tie Size	Tie Area mm^2 (in^2)	Yield Load kN (kip)	Ultimate Load kN (kip)	Yield Stress MPa (ksi)	Ultimate Stress MPa (ksi)
L, HA, HB	#3[1]	71 (0.11)	32 (7.2)	52 (11.7)	451 (65.4)	732 (106)

[1] loads and stresses reported for these bars are an average of 3 tests

Table 3.7 Compressive strength of cored cylinders from tests performed at Lehigh University.

Concrete Strength	Core Designation	L/D	$f_{c\text{-}core}$ MPa (ksi)	Correction[1] Factor	$f_{c\text{-}core}$[2] MPa (ksi)
L-Series	L-c1	2.0	N/A[3]	1.0	N/A
	L-c2	"	34.2 (4.97)	"	34.2 (4.97)
	L-c3	"	35.0 (5.07)	"	35.0 (5.07)
	L-c4	"	36.2 (5.24)	"	36.2 (5.24)
	L-c5	"	37.0 (5.37)	"	37.0 (5.37)
	L-c6	"	34.9 (5.06)	"	34.9 (5.06)
	L-c7	"	N/A	"	N/A
HA-Series	HA-c1	2.0	59.7 (8.66)	1.0	59.7 (8.66)
	HA-c2	"	60.4 (8.76)	"	60.4 (8.76)
	HA-c3	"	62.9 (9.12)	"	62.9 (9.12)
	HA-c4	"	58.1 (8.43)	"	58.1 (8.43)
	HA-c5	"	61.5 (8.92)	"	61.5 (8.92)
	HA-c6	"	61.2 (8.88)	"	61.2 (8.88)
	HA-c7	2.0	61.6 (8.93)	1.0	61.6 (8.93)
HB-Series	HB-c1	1.67	67.9 (9.85)	0.987	67.0 (9.72)
	HB-c2	"	N/A	"	N/A
	HB-c3	"	65.2 (9.46)	"	64.4 (9.34)
	HB-c4	"	64.6 (9.37)	"	63.8 (9.25)
	HB-c5	1.67	69.1 (10.0)	0.987	68.2 (9.89)

[1] Bartlett and MacGregor (1994) correction factor for HA- and HB-Series specimens
[2] core strength computed with the corresponding correction factor
[3] cores were damaged prior to testing

Table 3.8 Average compressive strength of cylinders from tests performed at Lehigh University.

Series	$f_{c\text{-}28}$[1] MPa (ksi)	$f_{c\text{-}field}$[2] MPa (ksi)	$f_{c\text{-}core}$[3] MPa (ksi)
L	26.5 (3.84)	24.0 (3.48)	35.5 (5.14)
HA	69.6 (10.1)	85.3 (12.4)	60.8 (8.82)
HB	73.5 (10.7)	72.1 (10.5)	65.9 (9.56)

[1] average of 4 cylinders
[2] average of 6 cylinders
[3] average of 6, 7, and 4 cylinders for L-, HA-, and HB-Series, respectively

Table 3.9 Specific gravity and density of concrete cylinders from tests performed at Lehigh University: (a) cored cylinders-L-Series.

Specimen	Bulk sp. gr. (dry)	Bulk sp. gr. (SSD)	Apparent sp. gr.	Bulk Density[1] (dry) kg/m^3 (lb/ft^3)	Bulk Density (SSD) kg/m^3 (lb/ft^3)	Apparent Density kg/m^3 (lb/ft^3)
L-c1	2.13	2.25	2.41	2127 (132.8)	2244 (140.1)	2409 (150.4)
L-c2	2.14	2.26	2.44	2133 (133.1)	2254 (140.7)	2429 (151.6)
L-c3	2.15	2.27	2.45	2145 (133.9)	2265 (141.4)	2439 (152.3)
L-c4	2.11	2.25	2.44	2109 (131.7)	2241 (139.9)	2430 (151.7)
L-c5	2.14	2.27	2.47	2131 (133.0)	2266 (141.4)	2464 (153.8)
L-c6	2.16	2.29	2.48	2154 (134.5)	2283 (142.5)	2473 (154.4)
L-c7	2.19	2.31	2.48	2185 (136.4)	2302 (143.7)	2474 (154.4)

(a)

[1] the density equals to the product of specific gravity and the unit weight of water at room temperature (997.5 kg/m^3 or 62.27 lb/ft^3)

Table 3.9 Specific gravity and density of concrete cylinders from tests performed at Lehigh University: (b) cored cylinders-HA-Series.

Specimen	Bulk sp. gr. (dry)	Bulk sp. gr. (SSD)	Apparent sp. gr.	Bulk Density[1] (dry) kg/m^3 (lb/ft^3)	Bulk Density (SSD) kg/m^3 (lb/ft^3)	Apparent Density kg/m^3 (lb/ft^3)
HA-c1	2.27	2.42	2.66	2263 (141.3)	2411 (150.5)	2656 (165.8)
HA-c2	2.27	2.41	2.64	2260 (141.1)	2403 (150.0)	2638 (164.7)
HA-c3	2.27	2.41	2.64	2267 (141.5)	2407 (150.2)	2636 (164.6)
HA-c4	2.30	2.44	2.68	2292 (143.1)	2436 (152.1)	2678 (167.2)
HA-c5	2.27	2.41	2.65	2267 (141.5)	2408 (150.3)	2641 (164.9)
HA-c6	2.27	2.42	2.65	2268 (141.6)	2411 (150.5)	2648 (165.3)
HA-c7	2.29	2.43	2.68	2285 (142.6)	2429 (151.6)	2671 (166.7)

(b)

[1] the density equals to the product of specific gravity and the unit weight of water at room temperature (997.5 kg/m^3 or 62.27 lb/ft^3)

Table 3.9 Specific gravity and density of concrete cylinders from tests performed at Lehigh University: (c) cored cylinders-HB-Series.

Specimen	Bulk sp. gr. (dry)	Bulk sp. gr. (SSD)	Apparent sp. gr.	Bulk Density[1] (dry) kg/m^3 (lb/ft^3)	Bulk Density (SSD) kg/m^3 (lb/ft^3)	Apparent Density kg/m^3 (lb/ft^3)
HB-c1	2.21	2.33	2.53	2203 (137.5)	2329 (145.3)	2520 (157.3)
HB-c2	2.31	2.44	2.66	2306 (143.9)	2438 (152.2)	2657 (165.9)
HB-c3	2.33	2.46	2.69	2325 (145.1)	2458 (153.4)	2684 (167.5)
HB-c4	2.24	2.37	2.57	2236 (139.6)	2363 (147.5)	2564 (160.0)
HB-c5	2.34	2.46	2.68	2331 (145.5)	2458 (153.4)	2671 (166.7)
HB-c6	2.24	2.36	2.55	2239 (139.7)	2357 (147.1)	2540 (158.5)
HB-c7	2.29	2.41	2.61	2281 (142.4)	2405 (150.1)	2604 (162.6)
HB-c8	2.25	2.37	2.58	2240 (139.8)	2368 (147.8)	2569 (160.4)
HB-c9	2.21	2.34	2.55	2200 (137.4)	2336 (145.8)	2545 (158.9)
HB-c10	2.18	2.33	2.55	2179 (136.0)	2322 (144.9)	2542 (158.7)

(c)

[1] the density equals to the product of specific gravity and the unit weight of water at room temperature (997.5 kg/m^3 or 62.27 lb/ft^3)

Table 3.9 Specific gravity and density of concrete cylinders from tests performed at Lehigh University: (d) field-cured cylinders[2].

Specimen	Bulk sp. gr. (dry)	Bulk sp. gr. (SSD)	Apparent sp. gr.	Bulk Density[1] (dry) kg/m^3 (lb/ft^3)	Bulk Density (SSD) kg/m^3 (lb/ft^3)	Apparent Density kg/m^3 (lb/ft^3)
L-Series	2.13	2.26	2.44	2122 (132.5)	2251 (140.5)	2437 (152.1)
HA-Series	2.28	2.41	2.61	2272 (141.8)	2400 (149.8)	2608 (162.8)
HB-Series	2.37	2.37	2.67	2366 (147.7)	2366 (147.7)	2668 (166.6)

[1] the density equals to the product of specific gravity and the unit weight of water at room temperature (997.5 kg/m^3 or 62.27 lb/ft^3)

[2] the specific gravity of field-cured cylinders was the weighted average of 6 tests

Table 3.10 Compressive strength and bulk density (SSD): (a) cored cylinders-L-Series.

Specimen	Bulk Density[1] (dry) kg/m^3 (lb/ft^3)	Compressive Strength MPa (ksi)
L-c1	2244 (140.1)	N/A
L-c2	2254 (140.7)	34.2 (4.97)
L-c3	2265 (141.4)	35.0 (5.07)
L-c4	2241 (139.9)	36.1 (5.24)
L-c5	2266 (141.4)	37.0 (5.37)
L-c6	2283 (142.5)	34.9 (5.06)
L-c7	2302 (143.7)	N/A

(a)

[1] the density equals to the product of specific gravity and the unit weight of water at room temperature (997.5 kg/m^3 or 62.27 lb/ft^3)

Table 3.10 Compressive strength and bulk density (SSD): (b) cored cylinders-HA-Series.

Specimen	Bulk Density[1] (dry) kg/m^3 (lb/ft^3)	Compressive Strength MPa (ksi)
HA-c1	2411 (150.5)	59.7 (8.66)
HA-c2	2403 (150.0)	60.4 (8.76)
HA-c3	2407 (150.2)	62.8 (9.11)
HA-c4	2436 (152.1)	61.5 (8.93)
HA-c5	2408 (150.3)	61.2 (8.88)
HA-c6	2411 (150.5)	61.5 (8.92)
HA-c7	2429 (151.6)	58.1 (8.43)

(b)

[1] the density equals to the product of specific gravity and the unit weight of water at room temperature (997.5 kg/m^3 or 62.27 lb/ft^3)

Table 3.10 Compressive strength and bulk density (SSD): (c) cored cylinders-HB-Series.

Specimen	Bulk Density[1] (dry) kg/m^3 (lb/ft^3)	Compressive Strength MPa (ksi)
HB-c1	2329 (145.3)	67.0 (9.72)
HB-c2	2438 (152.2)	N/A
HB-c3	2458 (153.4)	64.4 (9.34)
HB-c4[2]	2363 (147.5)	65.4 (9.49)
HB-c5	2458 (153.4)	N/A
HB-c6	2357 (147.1)	63.8 (9.25)
HB-c7	2405 (150.1)	N/A
HB-c8[2]	2368 (147.8)	62.3 (9.03)
HB-c9	2336 (145.8)	68.2 (9.89)
HB-c10[2]	2322 (144.9)	57.4 (8.33)

(c)

[1] the density equals to the product of specific gravity and the unit weight of water at room temperature (997.5 kg/m^3 or 62.27 lb/ft^3)
[2] results from tests performed at CTL

Table 3.10 Compressive strength and bulk density (SSD): (d) field-cured cylinders[1].

Specimen	Bulk Density[2] (dry) kg/m^3 (lb/ft^3)	Compressive Strength MPa (ksi)
L-Series	2251 (140.5)	24.0 (3.48)
HA-Series	2400 (149.8)	85.3 (12.37)
HB-Series	2366 (147.7)	72.1 (10.46)

(d)

[1]the specific gravity of field-cured cylinders was the weighted average of 6 tests
[2]the density equals to the product of specific gravity and the unit weight of water at room temperature (997.5 kg/m^3 or 62.27 lb/ft^3)

Table 3.11 Test results from CTL.

Series	Specimen	Dimension mm (in)	[1]f_c MPa (ksi)	[2]σ MPa (ksi)
L	cores	100 x 200 (4 x 8)	40.8 (5.92)	4.6 (0.66)
HA	cores	100 x 200 (4 x 8)	73.1 (10.60)	14.9 (2.16)
HB	cores	100 x 200 (4 x 8)	74.3 (10.78)	9.9 (1.43)
	cores	150 x 250 (6 x 10)	61.7 (8.95)	8.0 (1.16)
	field-cured cylinders	150 x 300 (6 x 12)	81.1 (11.77)	3.2 (0.47)

[1] average compressive strength
[2] one standard deviation of the compressive strengths

Table 3.12 Comparison of test results from CTL and Lehigh University.

Series	Specimen	Dimension mm (in)	[1]f_c MPa (ksi)	CTL / LU[2]
L	cores	100 x 200 (4 x 8)	40.8 (5.92)	1.15
HA	cores	100 x 200 (4 x 8)	73.1 (10.60)	1.20
HB	cores	100 x 200 (4 x 8)	74.3 (10.78)	1.13
	cores	150 x 250 (6 x 10)	61.7 (8.95)	0.94
-	field-cured cylinders	150 x 300 (6 x 12)	81.1 (11.77)	1.13

[1] average compressive strength obtained from CTL

[2] see Table 3.8 for the average compressive strength obtained from Lehigh University, and it should be noted that all specimens tested at Lehigh University are either larger or equal in size of the specimens tested at CTL

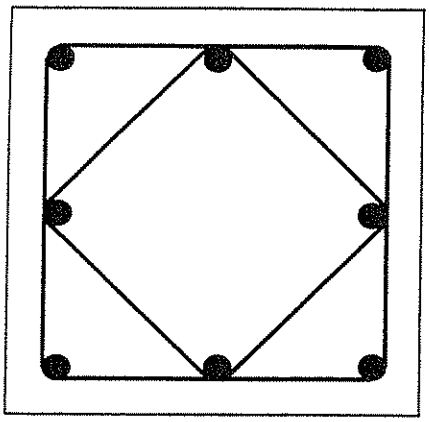

Section A-A

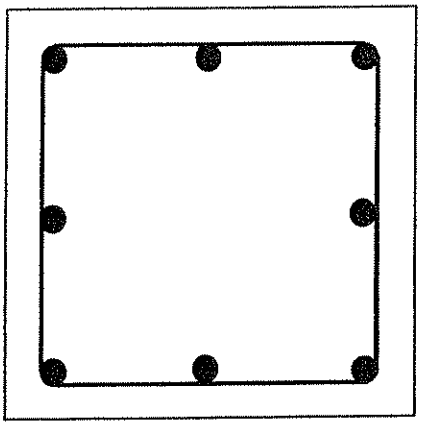

Section B-B

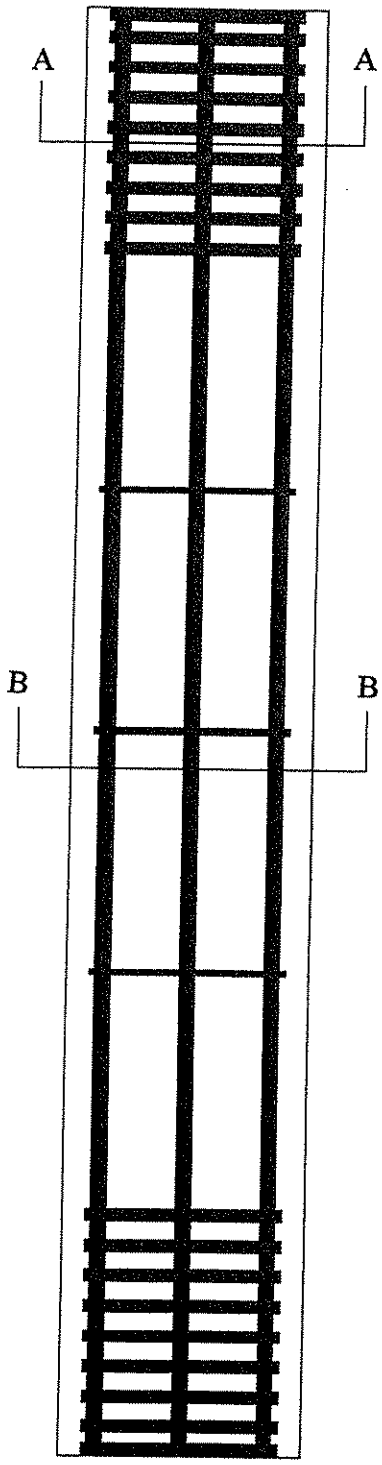

Elevation view

Figure 3.1: Elevation and section views of column specimens.

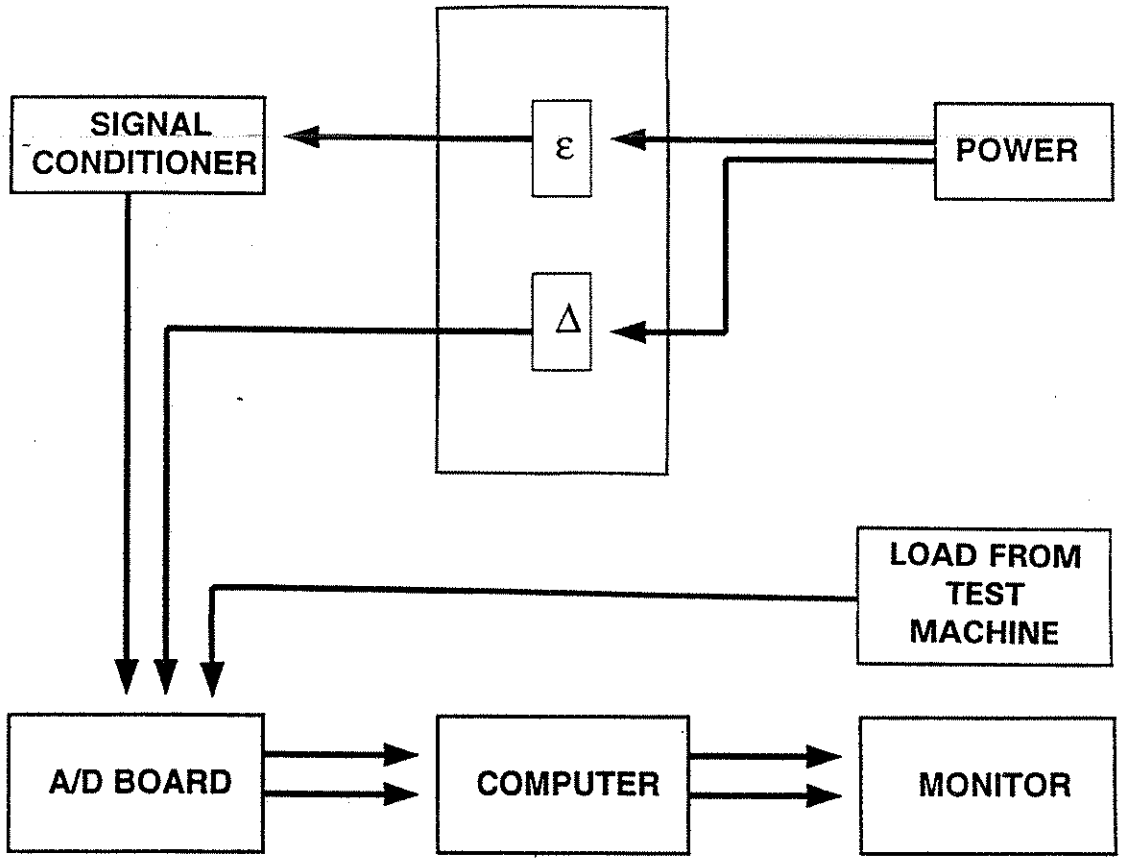

Figure 3.2 Schematic of data acquisition system.

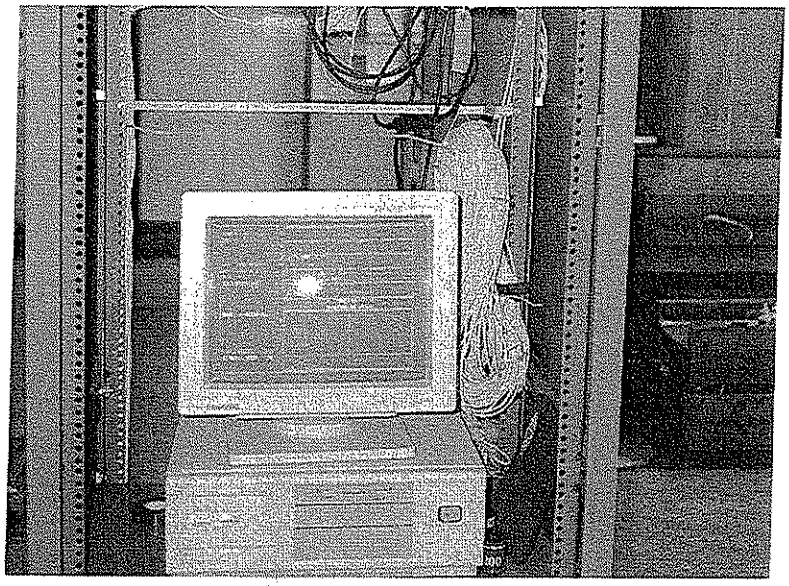

Figure 3.3 Computer monitor during testing.

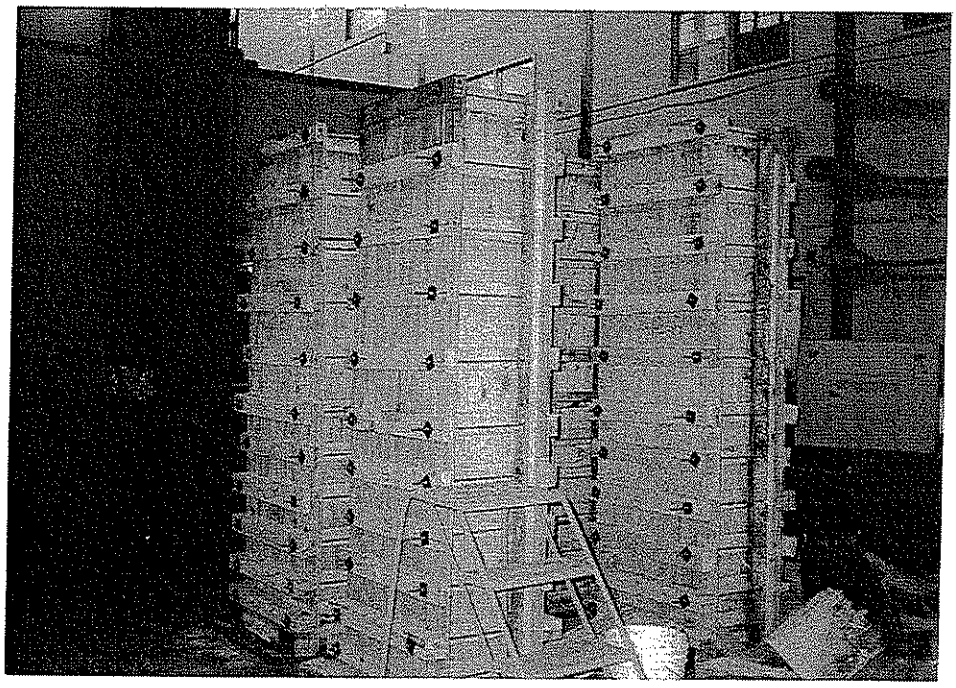

Figure 3.4 Column formwork.

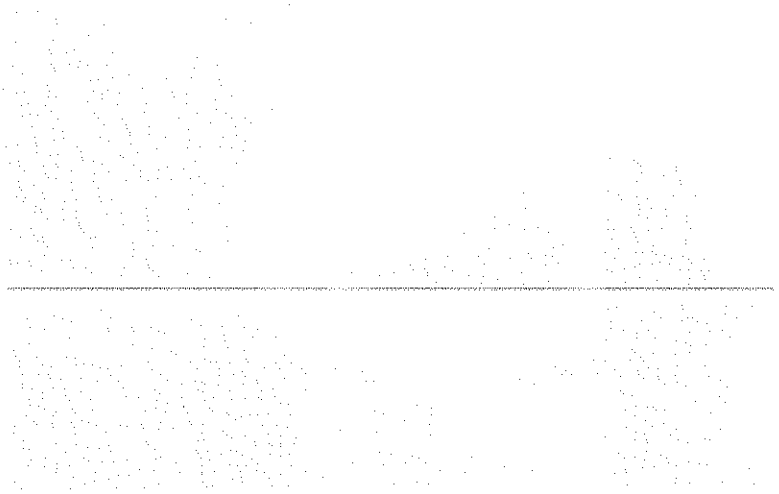

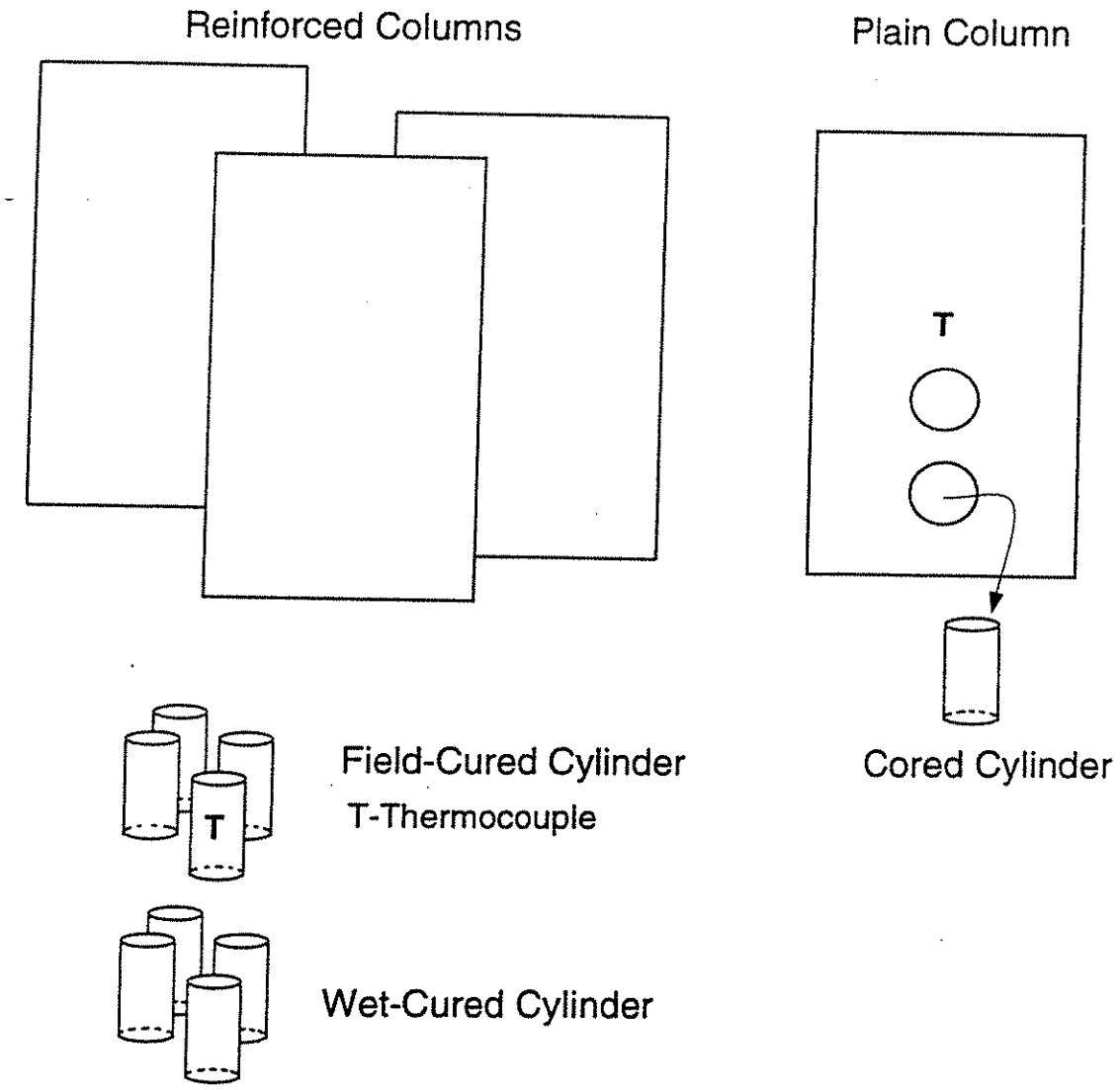

Figure 3.5 Illustration of the different cylindrical specimens used to determine concrete compressive strength.

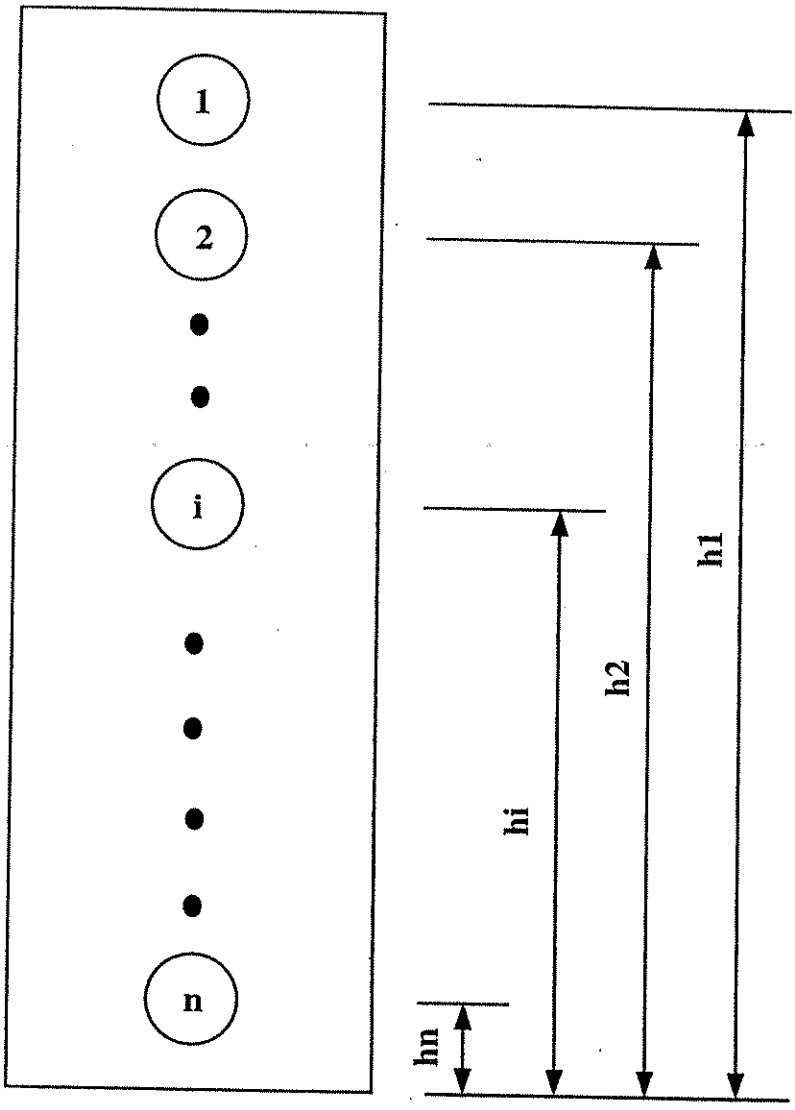

Series	n	h1 mm	h2 mm	h3 mm	h4 mm	h5 mm	h6 mm	h7 mm	h8 mm	h9 mm	h10 mm
L	7	2134	1930	1740	762	533	330	140	---	---	---
HA	7	2121	1918	1715	914	711	508	318	---	---	---
HB	10	2184	1676	1473	1270	1067	876	699	508	318	140

Figure 3.6 Locations at which cores were extracted.

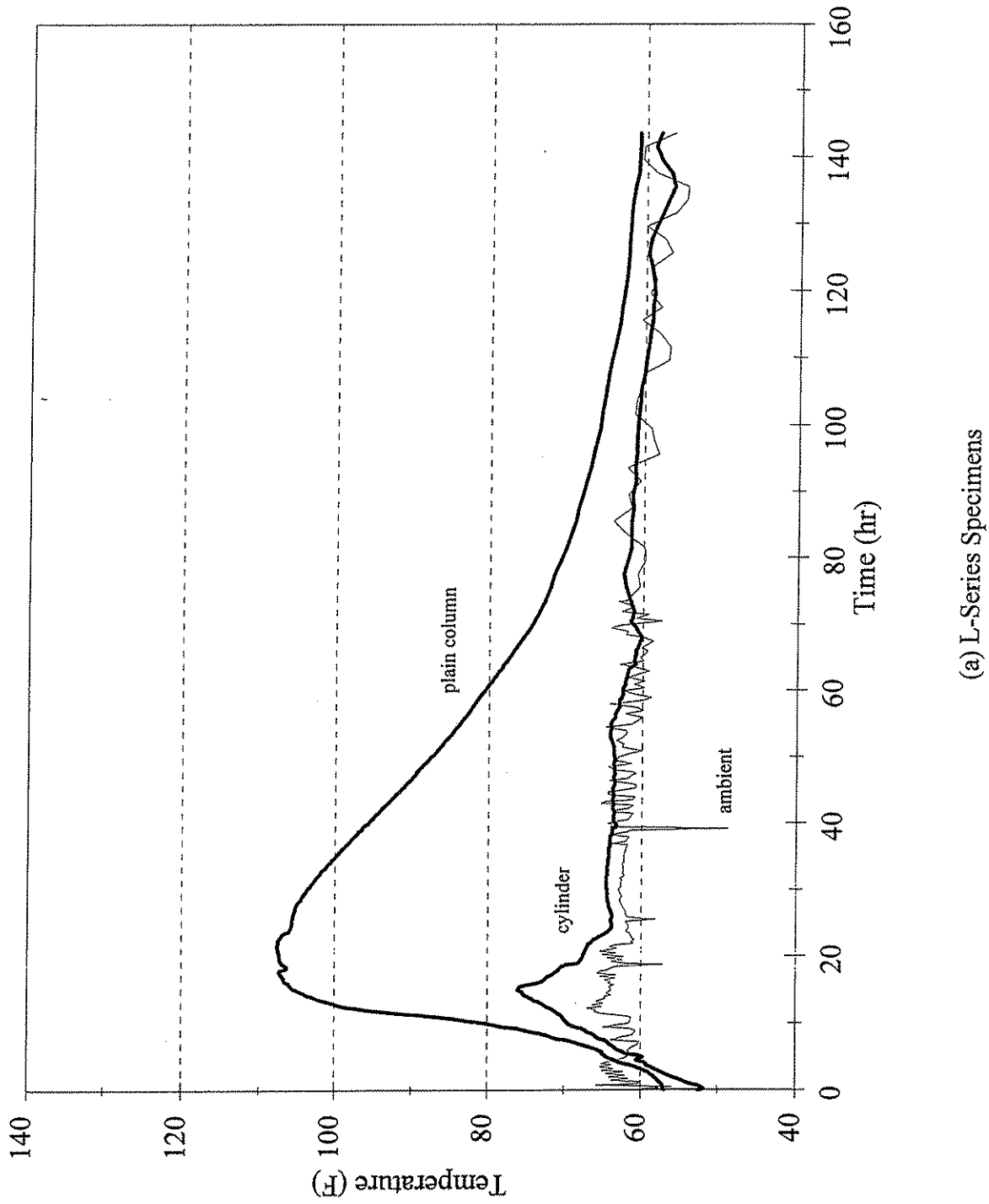

Figure 3.7 Temperature variations of: (a) L-Series specimens.

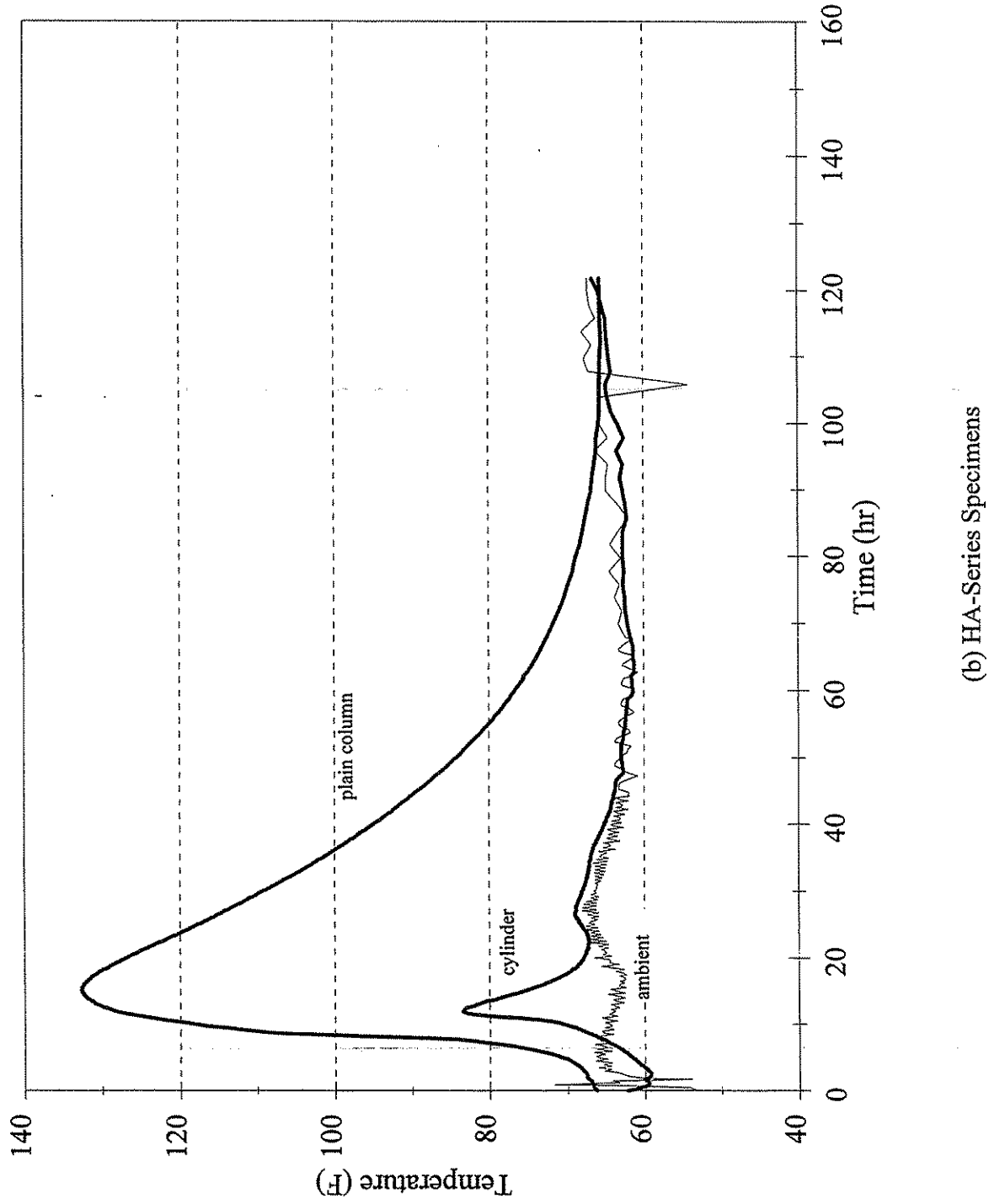

Figure 3.7 Temperature variations of: (b) HA-Series specimens.

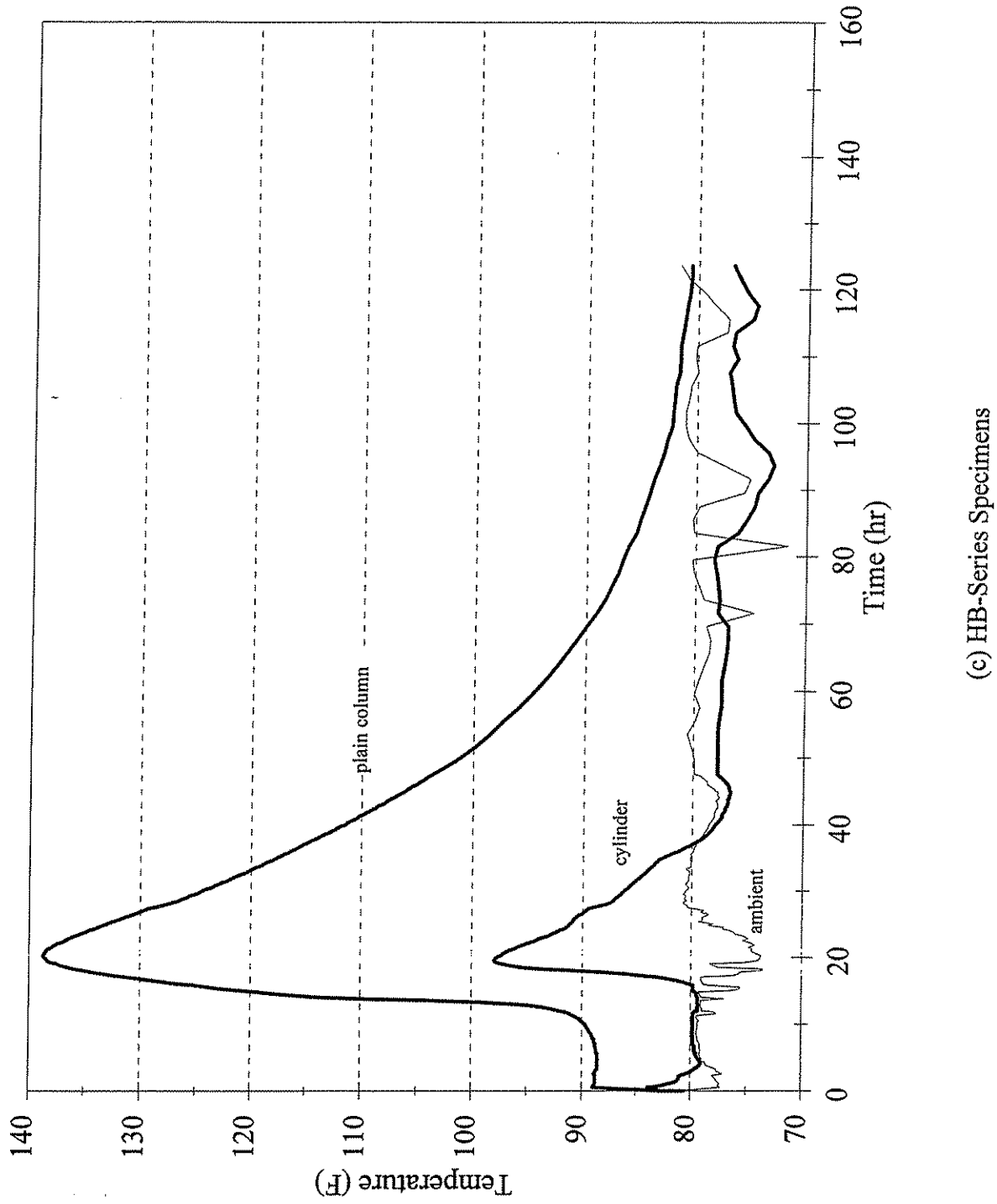

Figure 3.7 Temperature variations of: (c) HB-Series specimens.

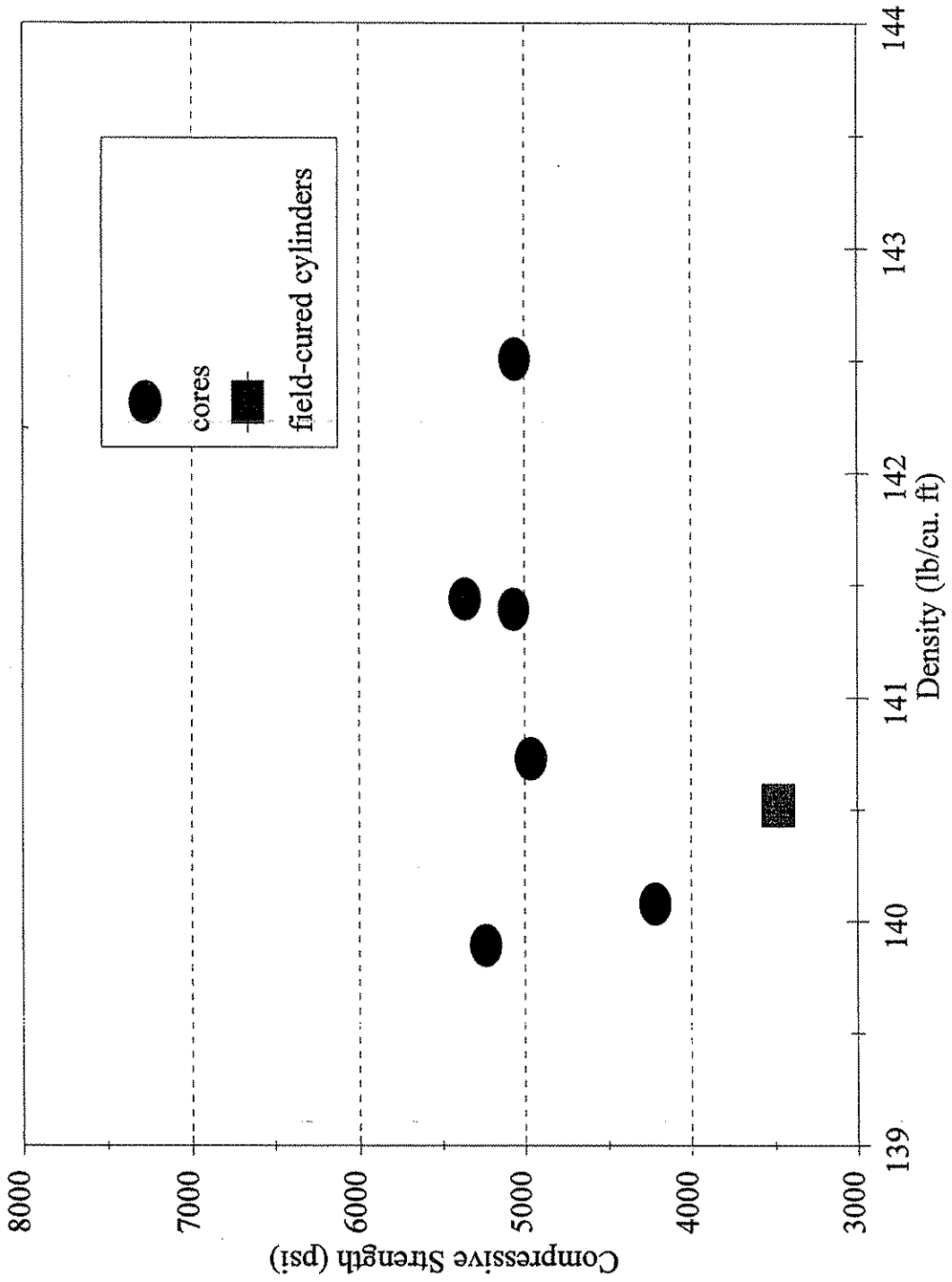

Figure 3.8 Strength versus bulk density (SSD) for L-Series cylinders.

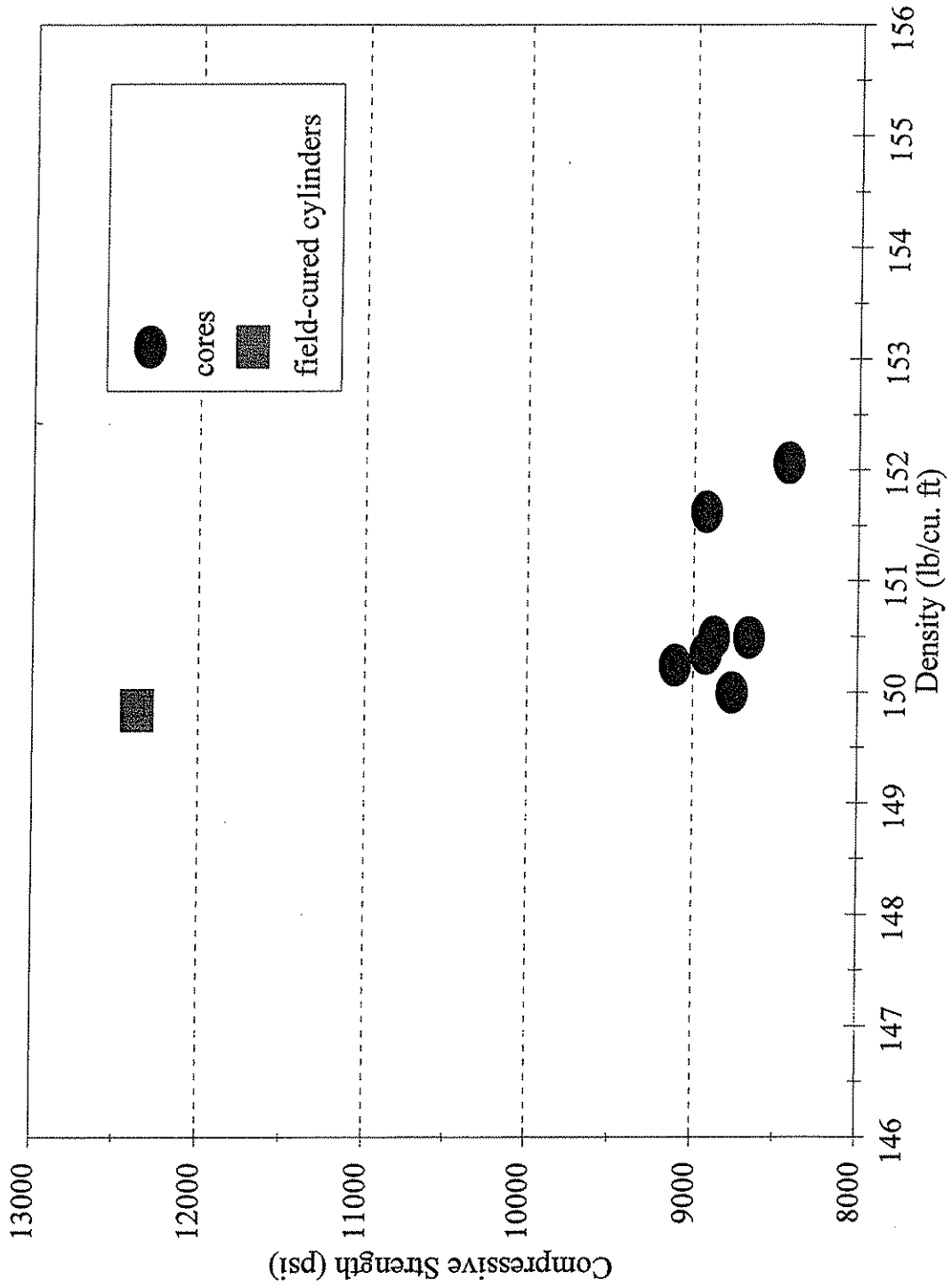

Figure 3.9 Strength versus bulk density (SSD) for HA-Series cylinders.

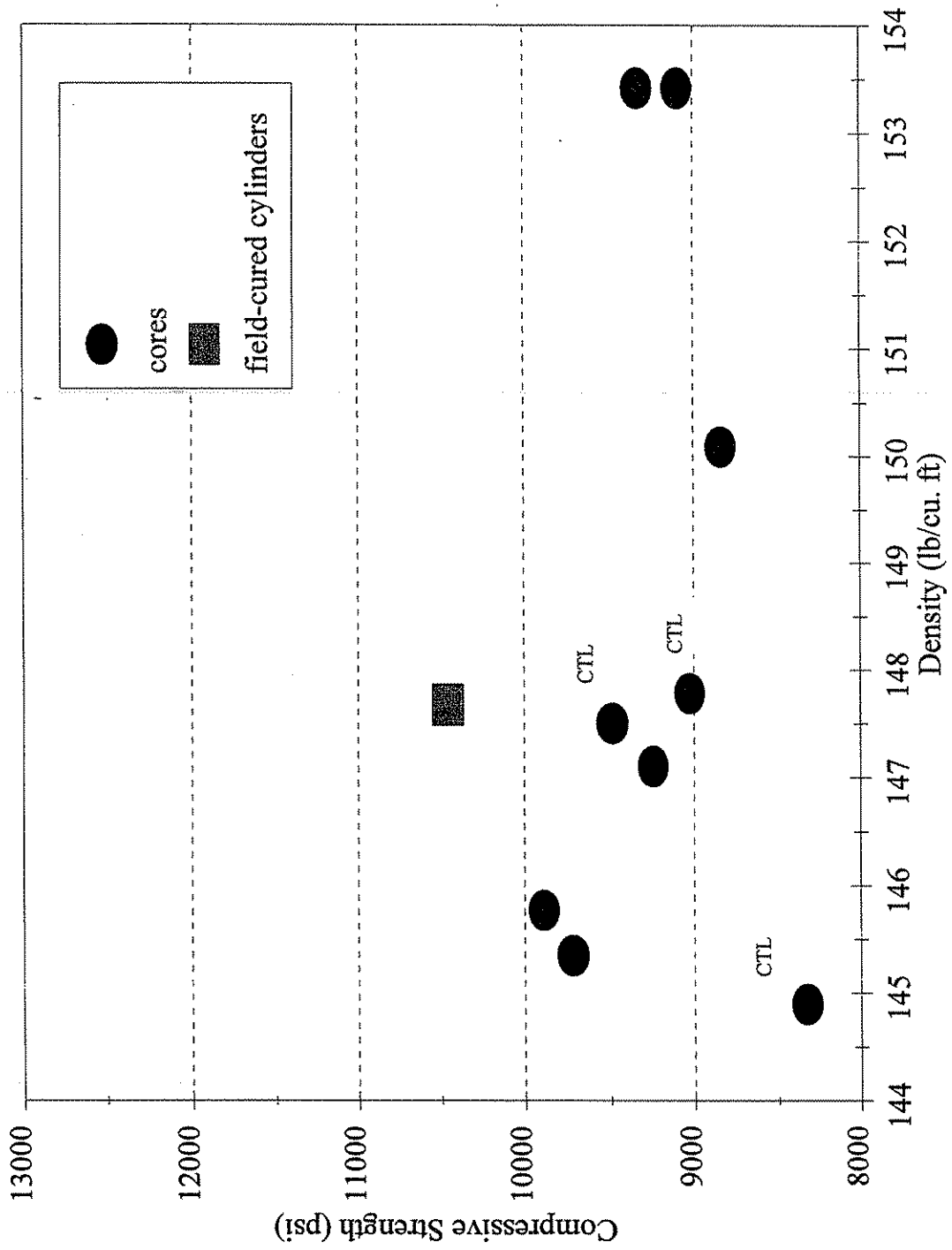

Figure 3.10 Strength versus bulk density (SSD) for HB-Series cylinders.

CHAPTER 4
INDIVIDUAL TEST SUMMARIES

4.1 INTRODUCTION

This chapter provides a detailed description of the results of each individual column test. Section 4.2 explains the general loading procedure used for each test, and Section 4.3 describes in detail the observations made during each test. A comparison and discussion of these results are presented in Chapter 5.

4.2 GENERAL LOADING PROCEDURE

Each column was tested in concentric compression in a 22.2 MN (5000 kip) capacity universal test machine. The test machine operator monitored the applied load, the load rate, and displacement rate (rate of head travel). Testing of each column began at a load rate of about 133 kN/min (30 kips/min). For each column in the L-Series, the initial load rate corresponded to a displacement rate between 0.18 mm/min (0.007 in/min) and 0.20 mm/min (0.008 in/min). For each column in the HA- and HB-Series, the initial load rate corresponded to a displacement rate between 0.10 mm/min (0.004 in/min) to 0.13 mm/min (0.005 in/min). As each column became damaged and decreased in stiffness, this load rate would decrease. Continued testing of each column was then performed at a desired displacement rate of about 0.13 mm/min (0.005 in/min).

4.3 INDIVIDUAL TEST SUMMARIES

This section summarizes the observations made during each test. All the individual test summaries are presented in the same general format which includes the following:

1. A summary of the reinforcement in the specimen and concrete strengths.

2. A detailed description of the observations made during testing.

3. One table that summarizes the experimentally observed and the predicted axial strengths of the column. The table presents predicted column axial strength values based on the concrete compressive strength of the day of test field cured cylinders ($f_{c\text{-field}}$), and the concrete compressive strength of the cored cylinders ($f_{c\text{-core}}$). Both equations assume that the longitudinal reinforcement is at yield when the column reaches its peak strength. The following equations are used to compute the predicted strength values:

$$P_{ofield} = 0.85 f_{c\text{-}field} A_c + A_s f_{yl} \tag{4.1}$$

$$P_{ocore} = 0.85 f_{c\text{-}core} A_c + A_s f_{yl} \tag{4.2}$$

P_{ofield} -The predicted axial strength of the column based on the actual material properties, using $f_{c\text{-}field}$ as the concrete compressive strength.

P_{ocore} -The predicted axial strength of the column based on the actual material properties, using $f_{c\text{-}core}$ as the concrete compressive strength.

4. A graph of axial load versus axial displacement. Several key points are indicated on this graph with the following symbols.

S#Y -S#Y indicates yielding of the longitudinal reinforcement at the location of strain gage number #.

P_{max} -Maximum load sustained by the column.

FCR -First observed cracking of cover concrete.

Δ_1 -Axial displacement corresponding to the intersection of the maximum load (P_{max}) and a line drawn parallel to the initial linear elastic portion of the load-displacement curve. This point is discussed further in Chapter 5 in a discussion of column ductility.

F -Failure of the column. In this research program, failure is defined as the point at which a column experienced a large, often sudden decrease in axial resistance.

Δ_F -Axial displacement at the failure of the column.

E -End of the test. This point was the very next data point recorded immediately after the failure of the column. It indicated the reduction in column strength after the failure. While the load value is considered accurate, the exact shape of the load-displacement curve is not known due to the sudden, explosive nature of several of the failures.

5. Graphs of axial load versus longitudinal reinforcement strains.

6. A set of photographs taken during and after the experiment.

Note that all of the graphs are plotted to the same scale which was determined by the columns that experienced the largest axial load, axial displacement, and reinforcement strain.

4.3.1 Specimen L1

-#3 ties at 406 mm (16 in) spacing
-8-#8 longitudinal bars
-$f_{c\text{-field}}$ = 24.0 MPa (3.48 ksi)
-$f_{c\text{-core}}$ = 35.4 MPa (5.14 ksi)

The load-displacement response of the column is shown in Figure 4.1. This figure shows that the column exhibited an approximately linear load-displacement response from the beginning of the test up to an axial load of about 4.00 MN (899 kips), and that the column exhibited a decrease in stiffness with continued loading beyond this point.

The peak resistance of the column was 6.88 MN (1547 kips) and the corresponding axial displacement was 5.3 mm (0.209 in).

No cracking was observed in the concrete cover before the peak load was reached. As soon as the load started to decrease from the peak load, a series of cracks formed and immediately widened in the concrete cover all around the top 1/3 region of the column which initiated column failure. The column failed shortly after the load on the column further decreased to 6.80 MN (1528 kips) (about 99% of the maximum load) with a corresponding displacement of 5.5 mm (0.217 in). At failure, the resistance of the column decreased dramatically from 6.80 MN (1528 kips) to 1.17 MN (263 kips), and the axial displacement increased dramatically by 74% (from 5.5 mm to 9.6 mm). At this point (marked by a letter E in Figure 4.1) the load on the column was 17% of the peak load. The failure of the column was characterized by buckling of a series of longitudinal bars, and the failure was located within the top 1/3 region of the column.

Figure 4.2 presents the axial load versus longitudinal reinforcement strain curves. Longitudinal reinforcement strains were measured from two strain gages, S1 and S2. Strain gage S2 was located in the region at which the column failed and strain gage S1 was located at the mid-height of the column. First yielding of the longitudinal bars was recorded on strain gage S2 (S2Y on Figure 4.1) prior to peak resistance at an axial load of 6.79 MN (1527 kips) and an axial displacement of 5.1 mm (0.119 in). At this point strain gage S1 was about 83% of the yield strain. Strain gage S1 was about 87% and 88% of the yield strain at the peak load and column failure, respectively.

Figure 4.3 presents a series of photographs taken during and after the column test. At the end of the test the column was completely unloaded, and the separated regions of concrete cover were carefully removed (often this cover remained loosely attached to the column through the tie wire steel used to fabricate the reinforcement cages) to expose the core and tie reinforcement (Figure 4.3(a)-(e)). Figure 4.3(d)-(e) show the inclined failure region at the top 1/3 region of the column.

Table 4.1 Specimen L1-experimentally observed and predicted axial strengths.

Experimental Axial Capacity	Predicted Axial Capacity	
P_{max} MN (kips)	P_{ofield} MN (kips)	P_{ocore} MN (kips)
6.88 (1547)	5.15 (1158)	6.71 (1509)

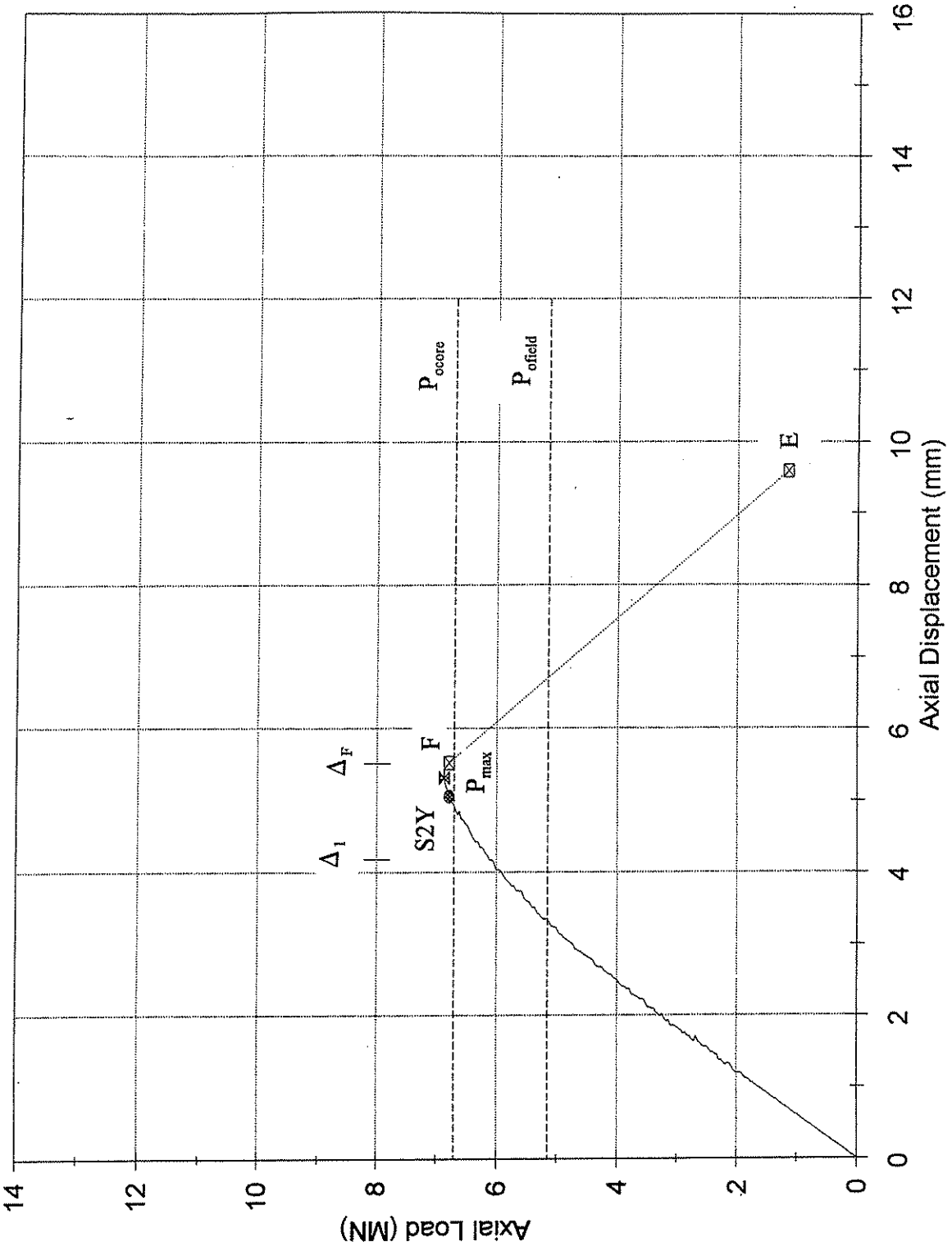

Figure 4.1: Specimen L1-axial load versus axial displacement.

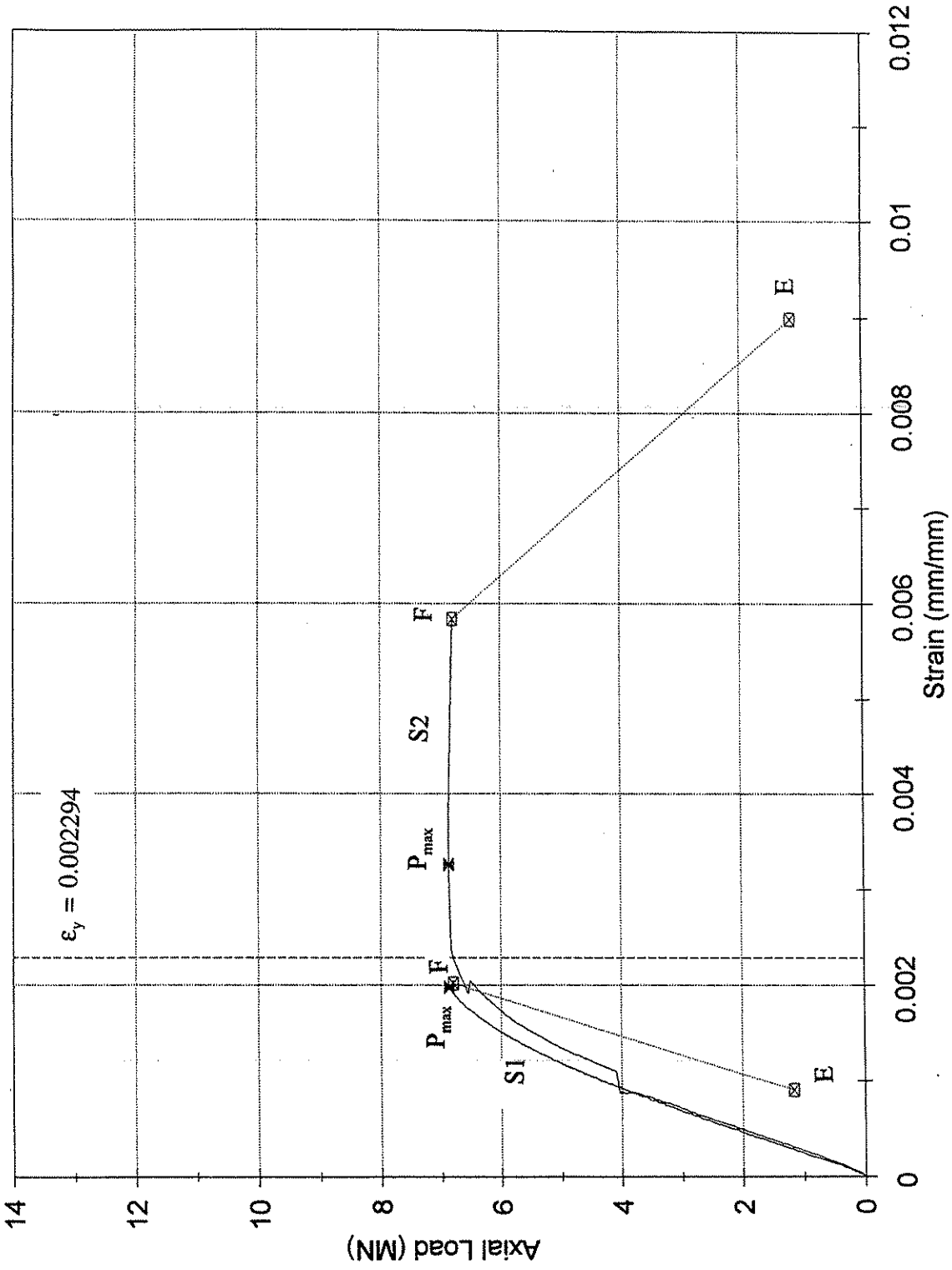

Figure 4.2 Specimen L1-axial load versus longitudinal reinforcement strains, gages S1, S2.

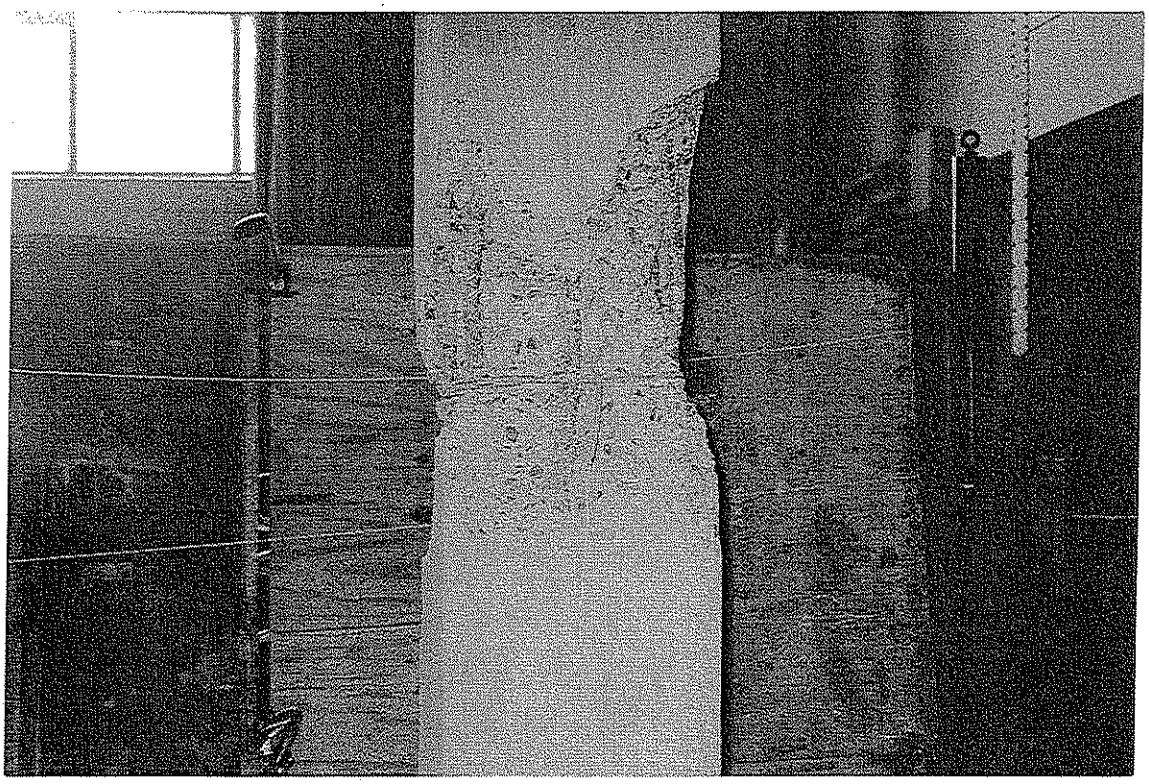

(a)

Figure 4.3 Specimen L1-series of photographs; (a) post-test photograph showing the failure region.

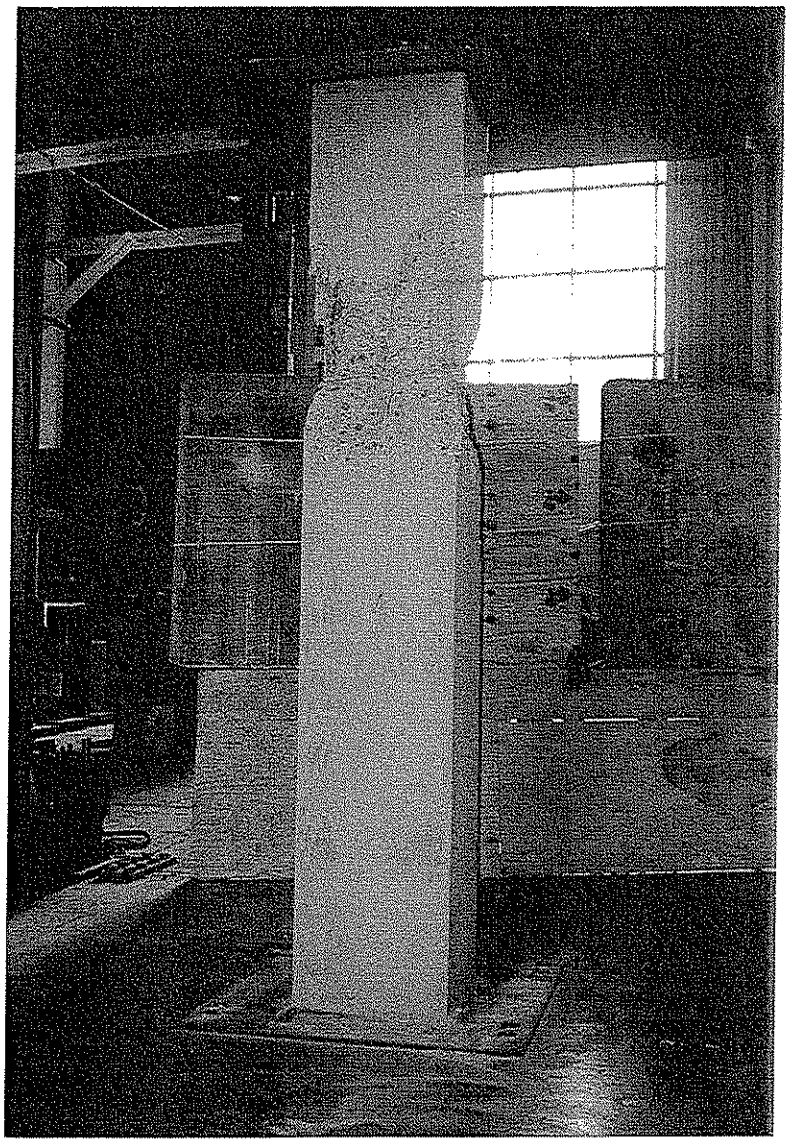

(b)

Figure 4.3 Specimen L1-series of photographs; (b) post-test photograph showing the failure region.

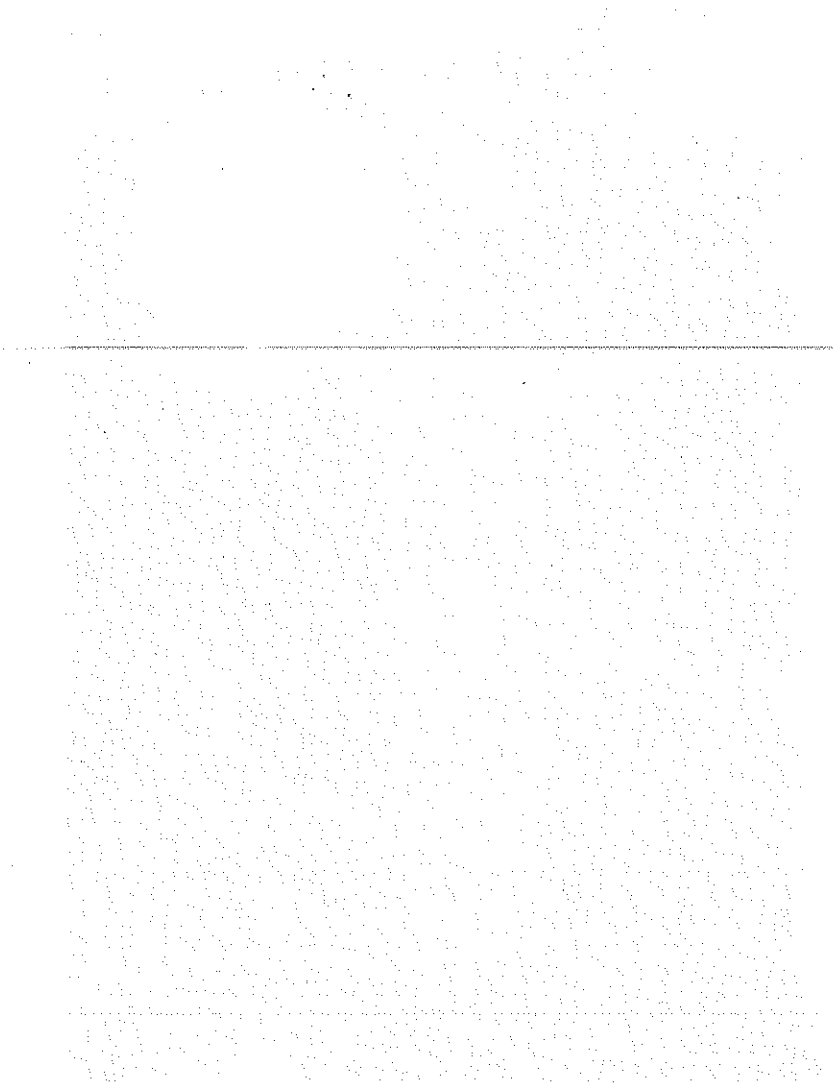

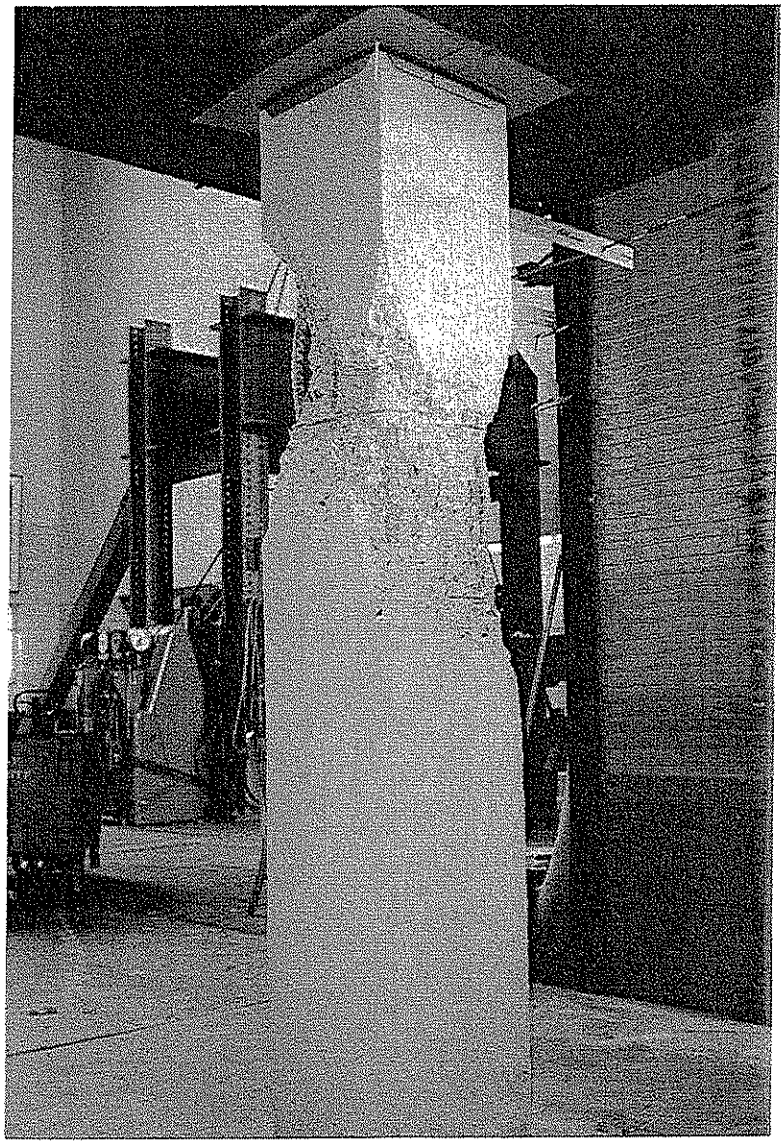

(c)

Figure 4.3 Specimen L1-series of photographs; (c) post-test photograph showing the failure region.

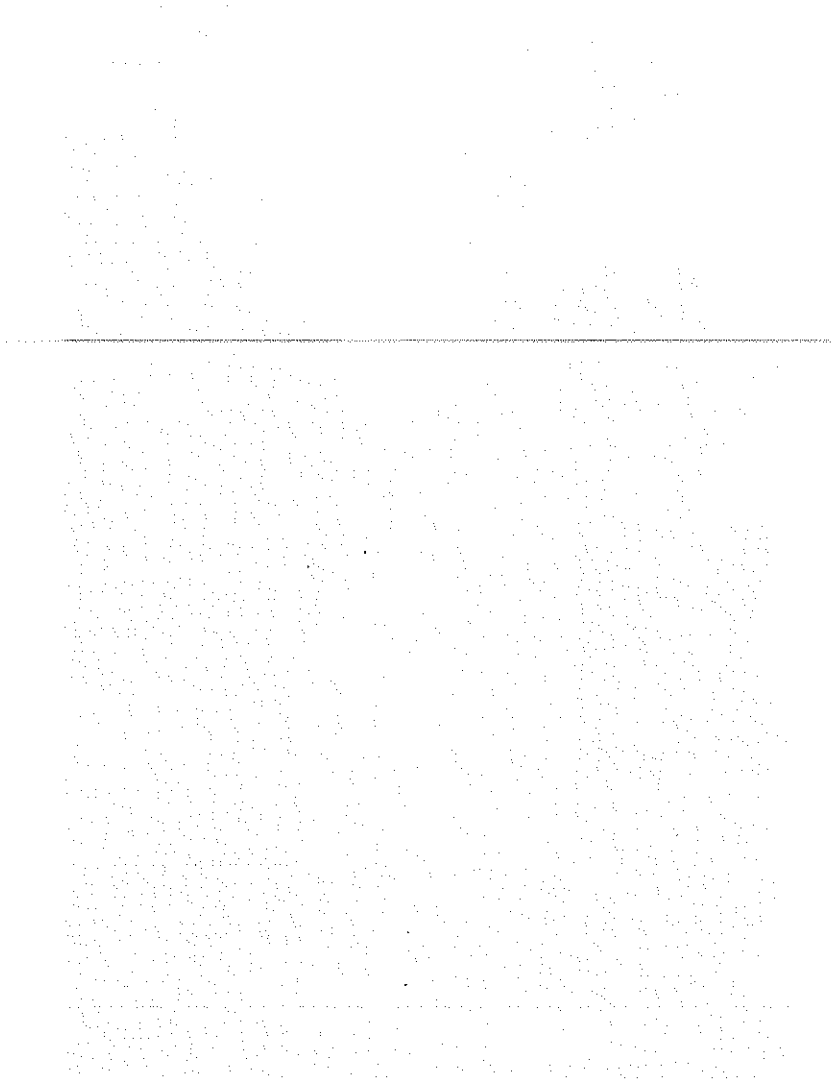

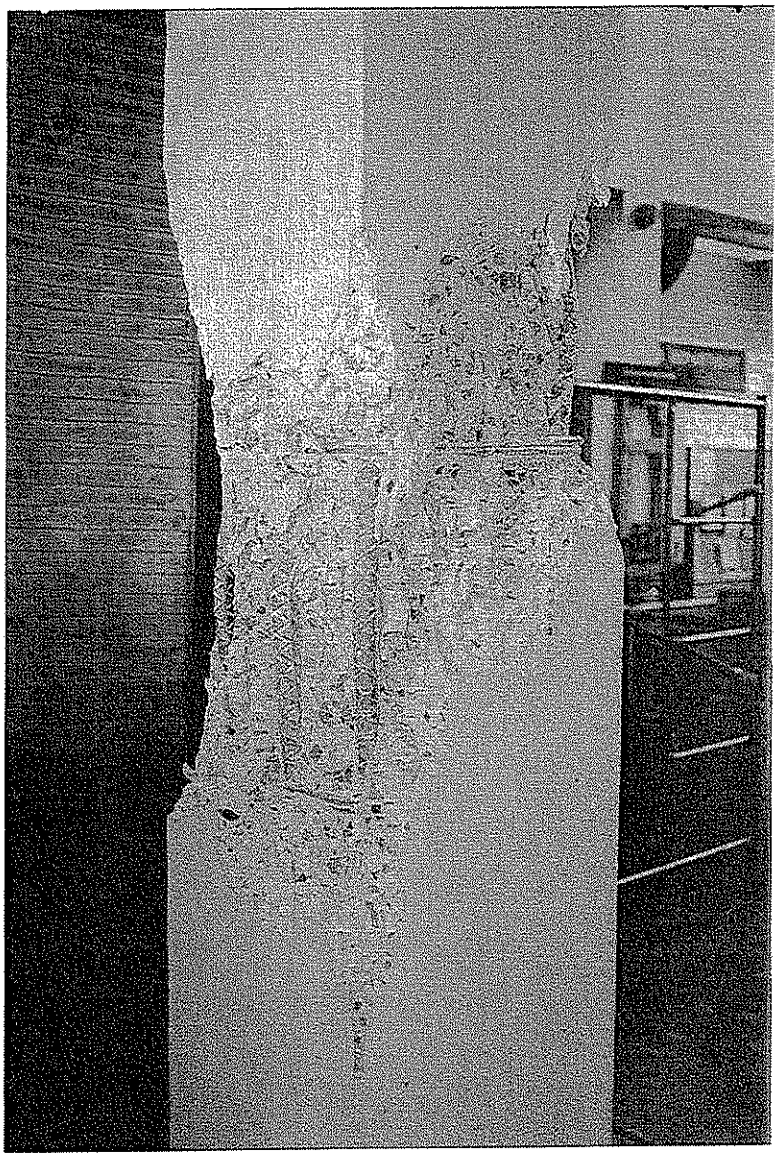

(d)

Figure 4.3 Specimen L1-series of photographs; (d) post-test photograph showing the failure region.

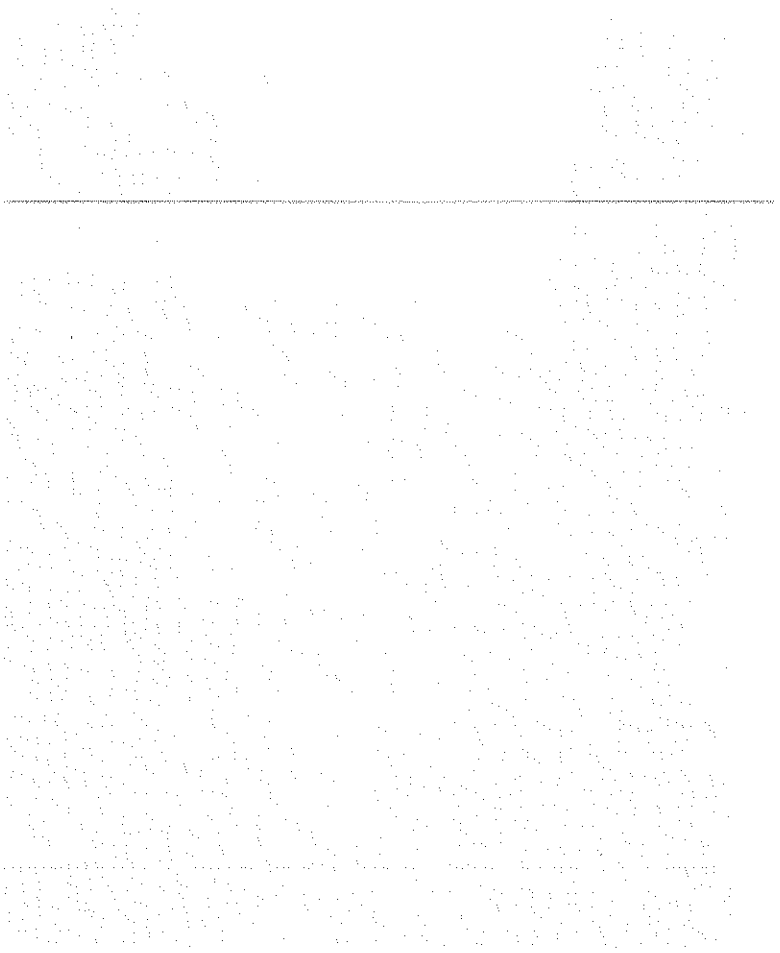

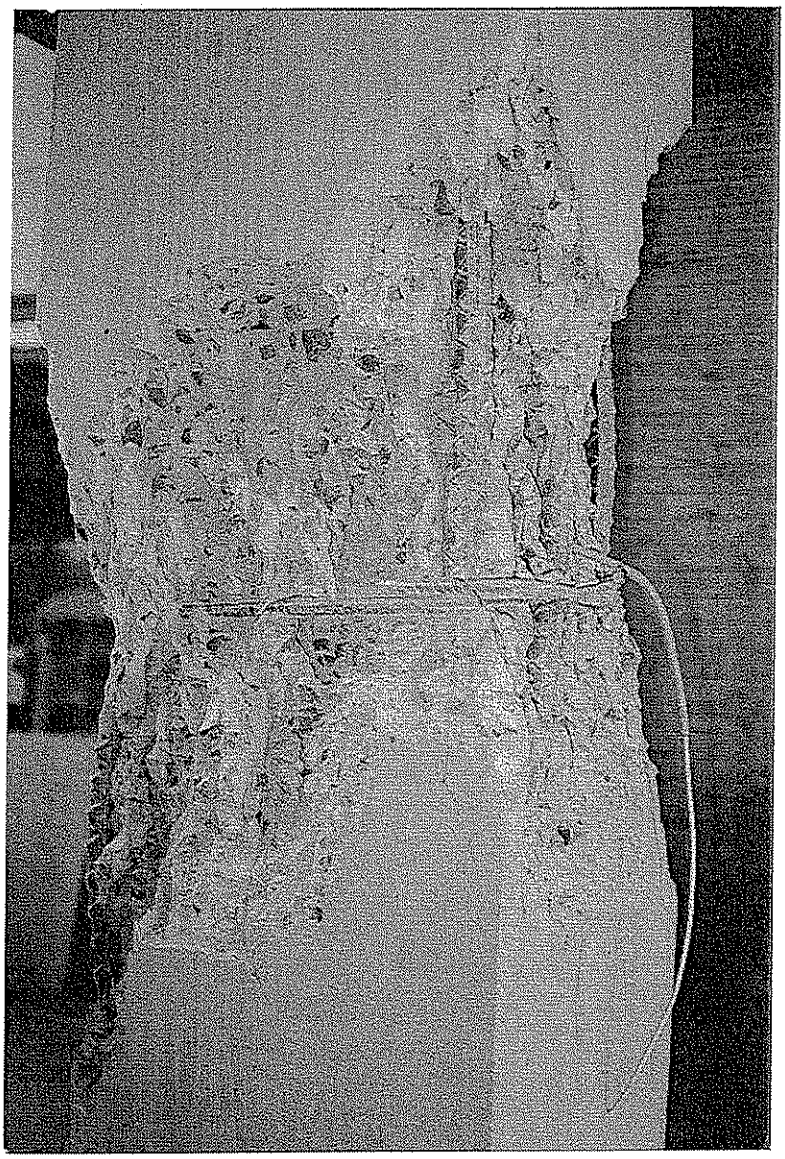

(e)

Figure 4.3 Specimen L1-series of photographs; (e) post-test photograph showing the failure region.

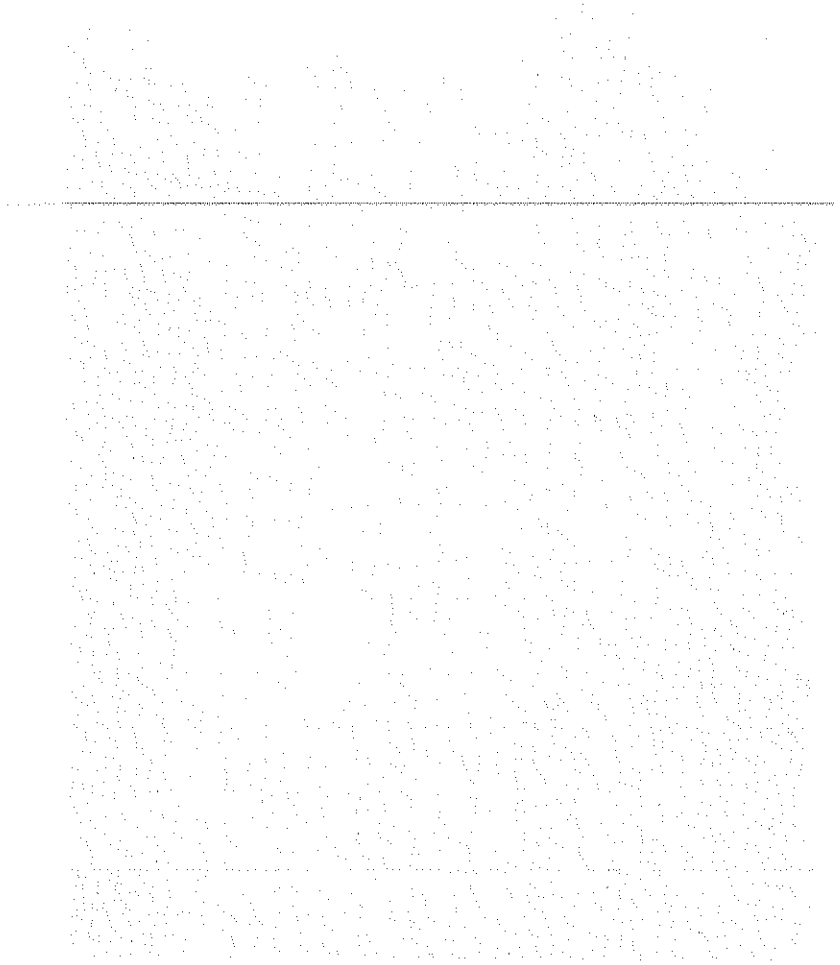

4.3.2 Specimen L2

-#3 ties at 203 mm (8 in) spacing
-8-#8 longitudinal bars
-$f_{c\text{-field}}$ = 24.0 MPa (3.48 ksi)
-$f_{c\text{-core}}$ = 35.4 MPa (5.14 ksi)

The load-displacement response of the column is shown in Figure 4.4. This figure shows that the column exhibited an approximately linear load-displacement response from the beginning of the test up to an axial load of about 4.00 MN (899 kips), and that the column exhibited a decrease in stiffness with continued loading beyond this point.

The peak resistance of the column was 6.79 MN (1527 kips) and the corresponding axial displacement was 5.8 mm (0.230 in).

No cracking was observed in the concrete cover before the peak load was reached. First cracking (FCR) was observed in the concrete cover shortly beyond peak resistance at an axial load of 6.73 MN (1512 kips) and corresponding axial displacement of 6.1 mm (0.239 in). The cracking was comprised of a series of small cracks extending from the northwest corner at about three quarters of the height of the column. These cracks continued to grow and widen as the load on the column was further decreased, and shortly after the load decreased to 6.52 MN (1467 kips), additional cracks formed and the column failed simultaneously. Figure 4.6(a) shows these cracks in the concrete cover just before the column failure.

The column failed at the load of 6.52 MN (1467 kips) (about 96% of the maximum load) with a corresponding displacement of 6.1 mm (0.241 in). At failure, the resistance of the column decreased dramatically from 6.52 MN (1467 kips) to 3.35 MN (753 kips), and the axial displacement increased by 28% (from 6.1 mm to 7.8 mm). At this point (marked by a letter E in Figure 4.4) the load on the column was 49% of the peak load. The failure of the column was characterized by buckling of a series of longitudinal bars, and the failure was located within the top 1/3 region of the column.

Figure 4.5 presents the axial load versus longitudinal strain curve. Longitudinal strain was measured from two strain gages, S1 and S2. Strain gage S2 was located in the region at which the column failed and strain gage S1 was located at the mid-height of the column. First yielding of the longitudinal bars was recorded on strain gage S2 (S2Y on Figure 4.4) prior to peak resistance at an axial load of 6.70 MN (1506 kips) and an axial displacement of 5.5 mm (0.217 in). At this point strain gage S1 was about 85% of the yield strain. Strain gage S1 reached about 93% of the yield strain at the failure of the column, and started to decrease afterward.

Figure 4.6 presents a series of photographs taken during and after the column test. At the end of the test the column was completely unloaded, and the separated regions of concrete cover were carefully removed to expose the core and tie reinforcement (Figure 4.6(b)-(c)). The failure region was characterized by a slightly inclined plane of failure and a bulging of the column at the top 1/3 region.

These failure modes may be seen, however, with some difficulties in Figure 4.6(d) and (e), respectively.

Table 4.2 Specimen L2-experimentally observed and predicted axial strengths.

Experimental Axial Capacity	Predicted Axial Capacity	
P_{max} MN (kips)	P_{ofield} MN (kips)	P_{ocore} MN (kips)
6.79 (1527)	5.15 (1158)	6.71 (1509)

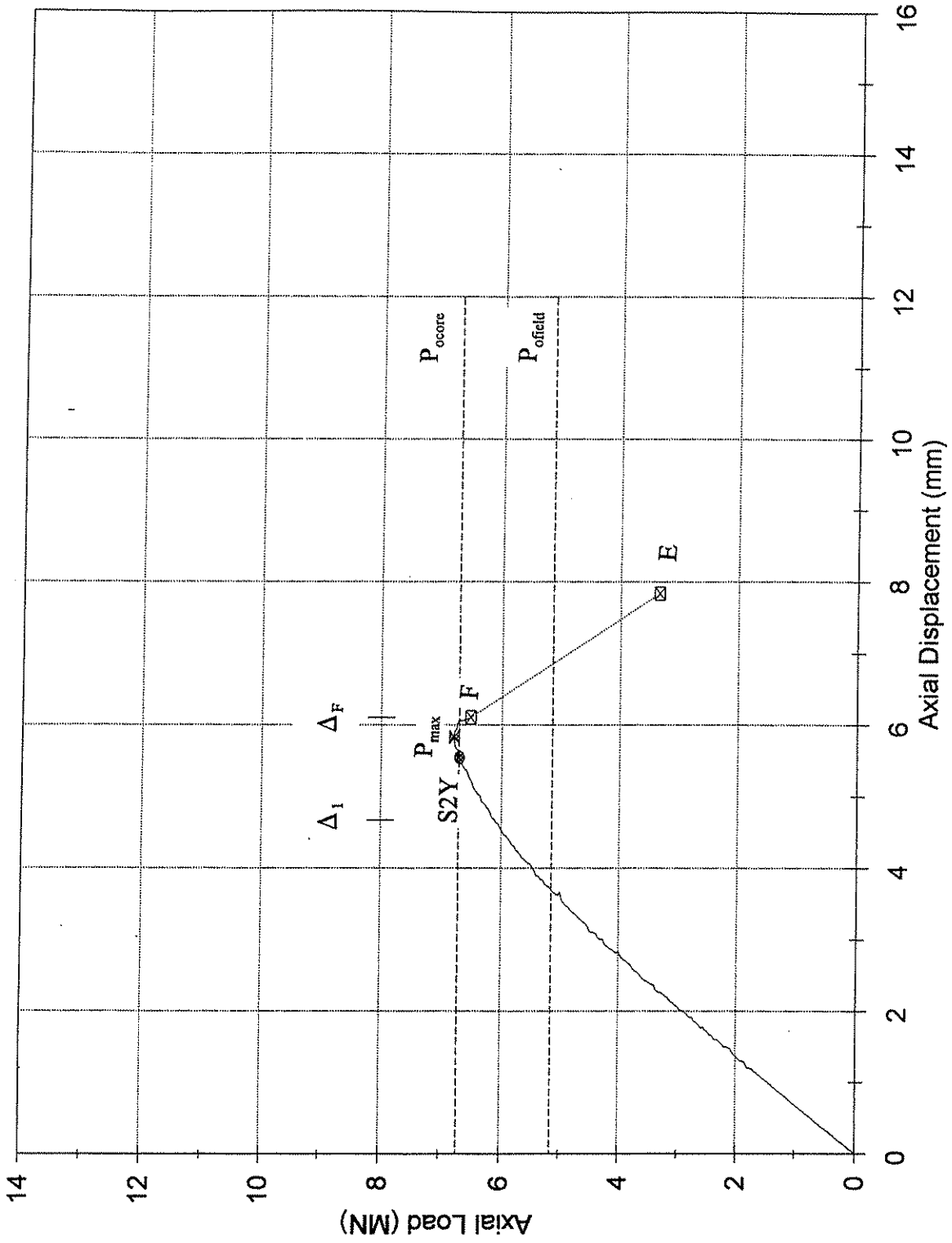

Figure 4.4: Specimen L2-axial load versus axial displacement.

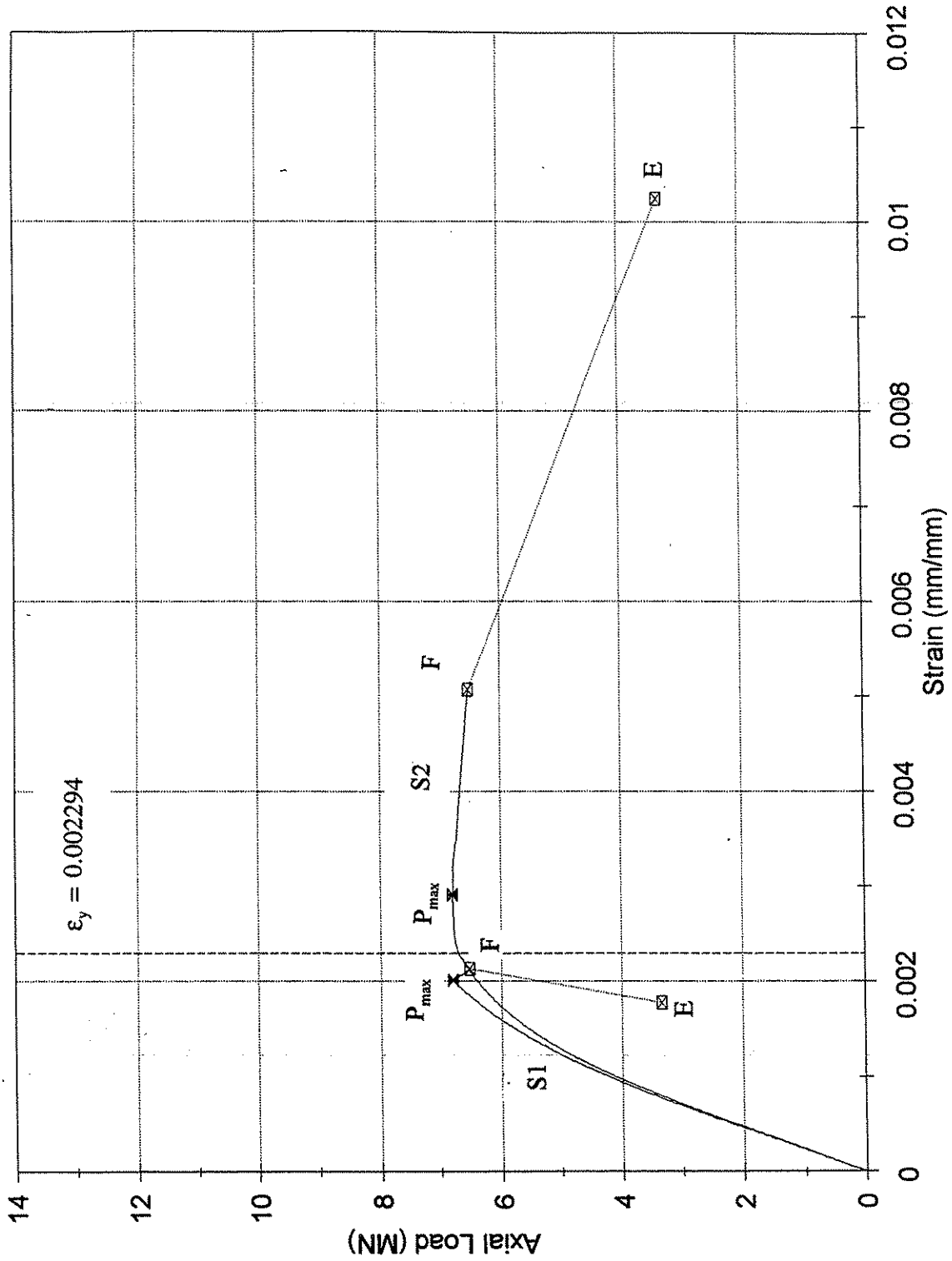

Figure 4.5 Specimen L2-axial load versus longitudinal reinforcement strains, gages S1, S2.

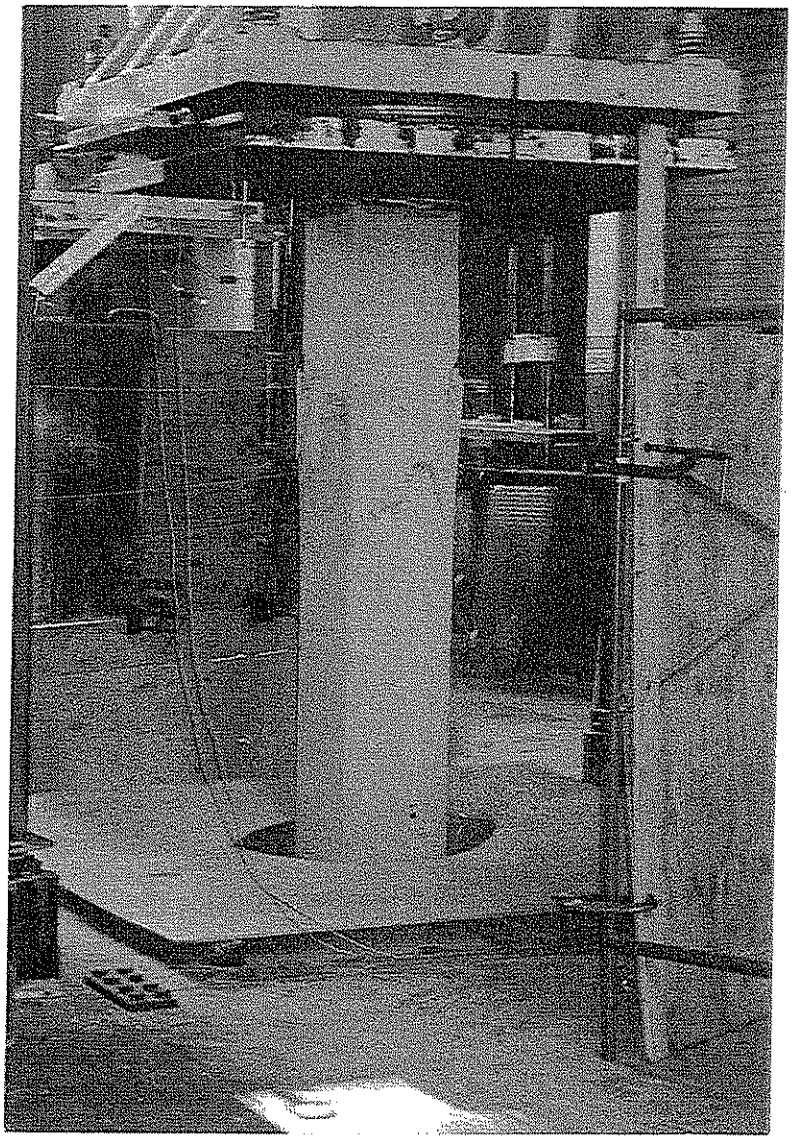

(a)

Figure 4.6 Specimen L2-series of photographs; (a) state of cracking in concrete cover just prior to column failure.

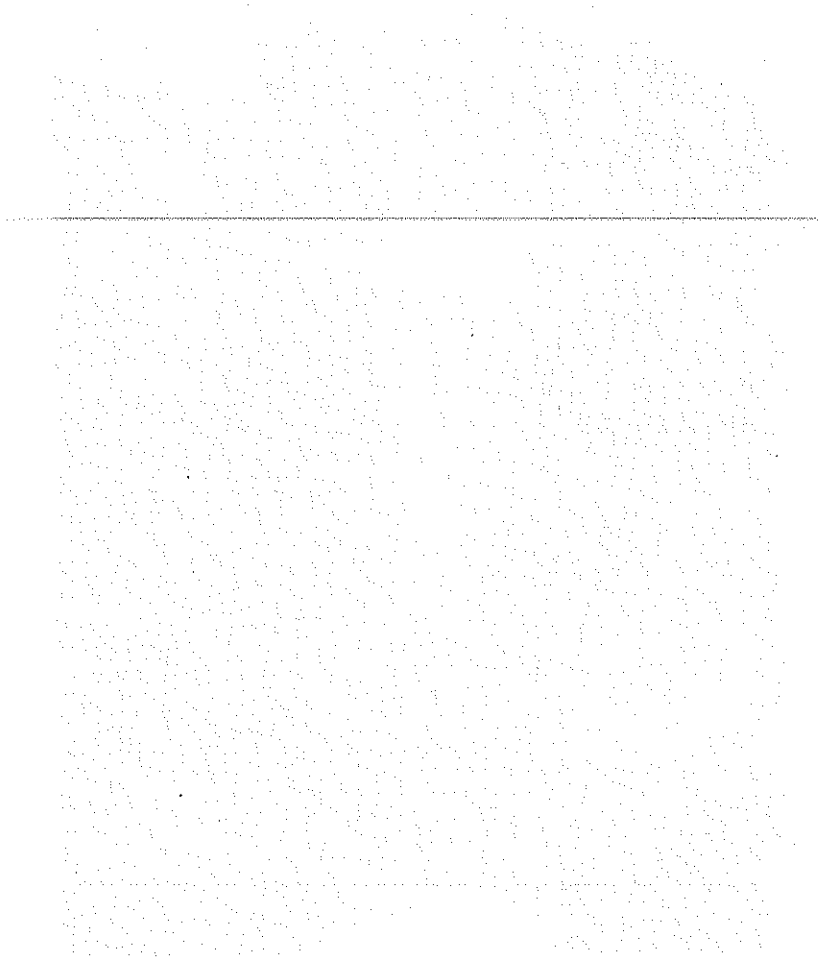

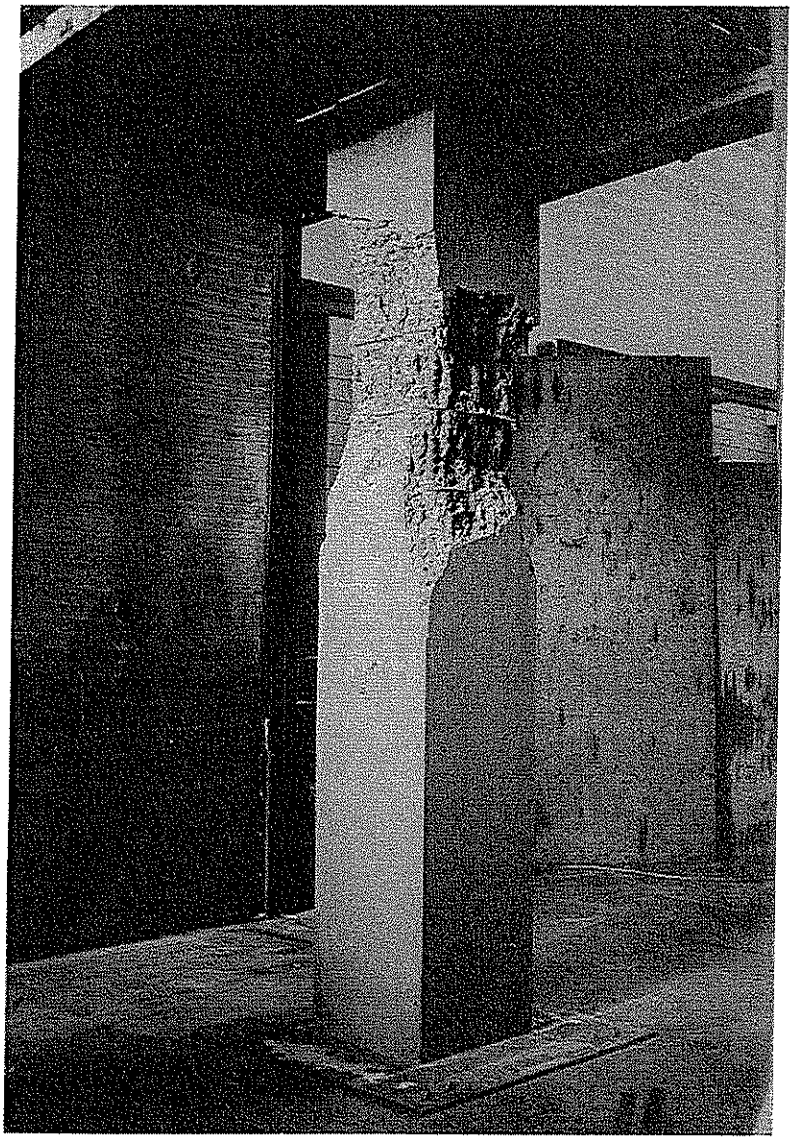

(b)

Figure 4.6 Specimen L2-series of photographs; (b) post-test photograph showing the core and tie reinforcement.

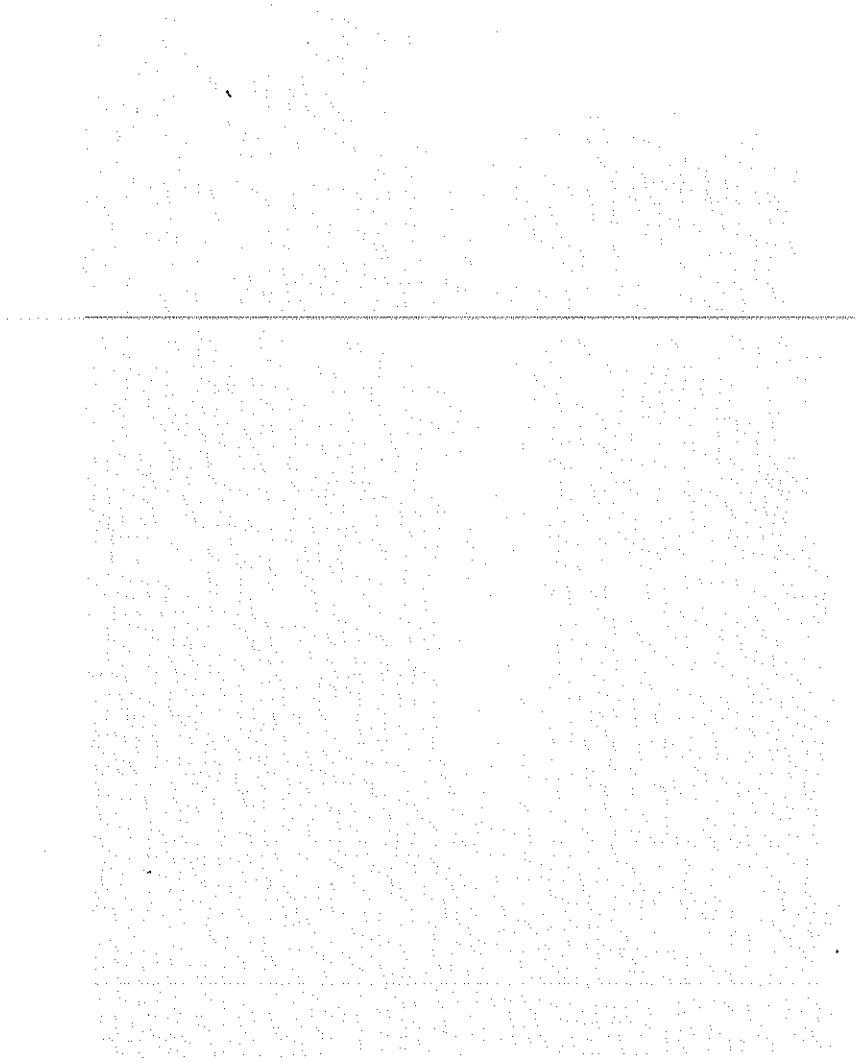

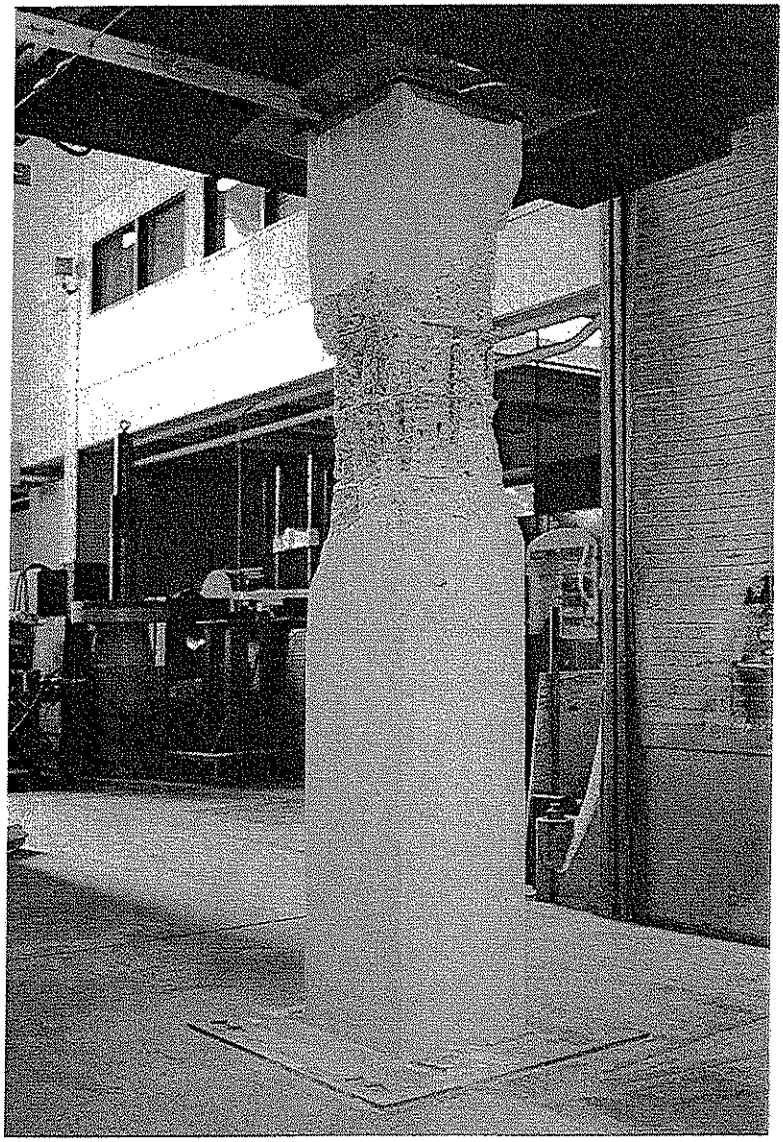

(c)

Figure 4.6 Specimen L2-series of photographs; (c) post-test photograph showing the core and tie reinforcement.

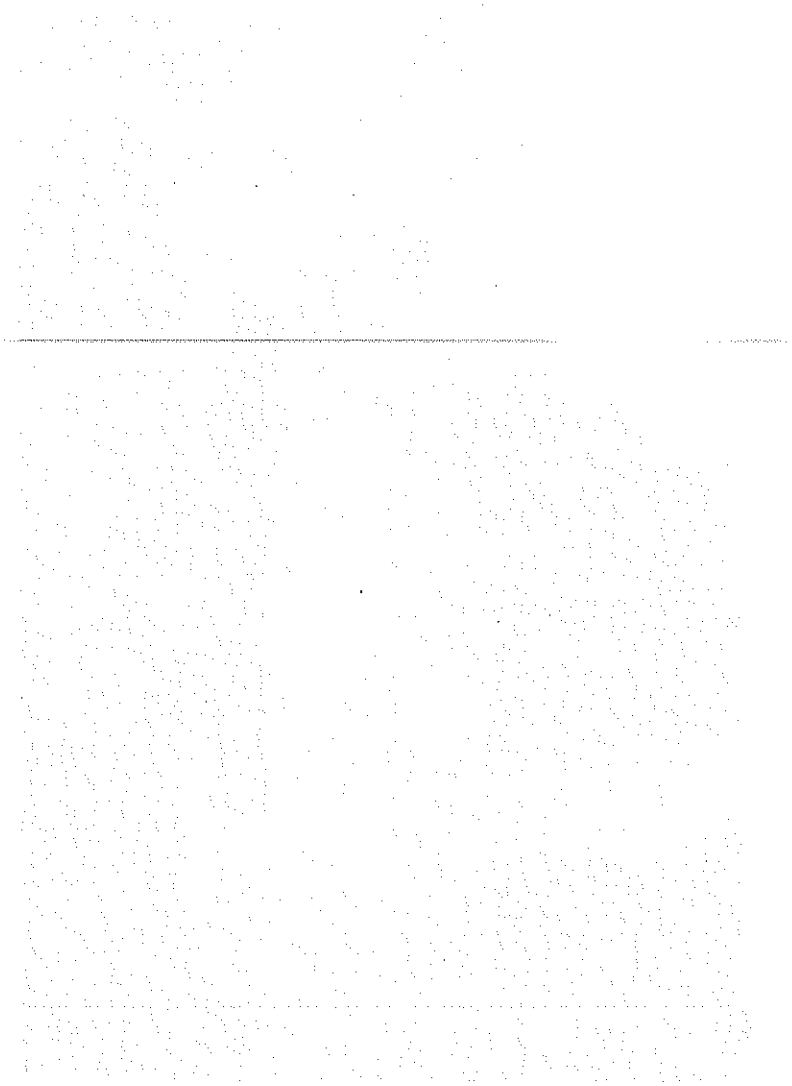

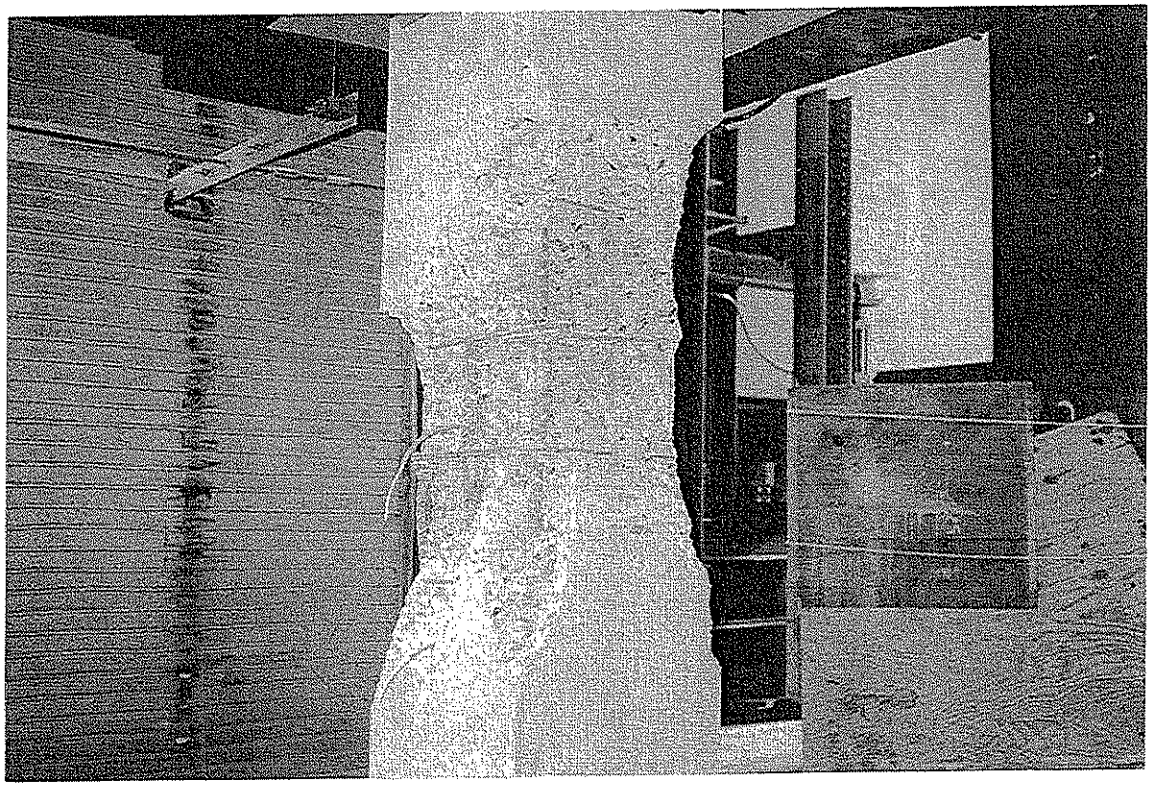

(d)

Figure 4.6 Specimen L2-series of photographs; (d) post-test photograph showing the incline failure plane.

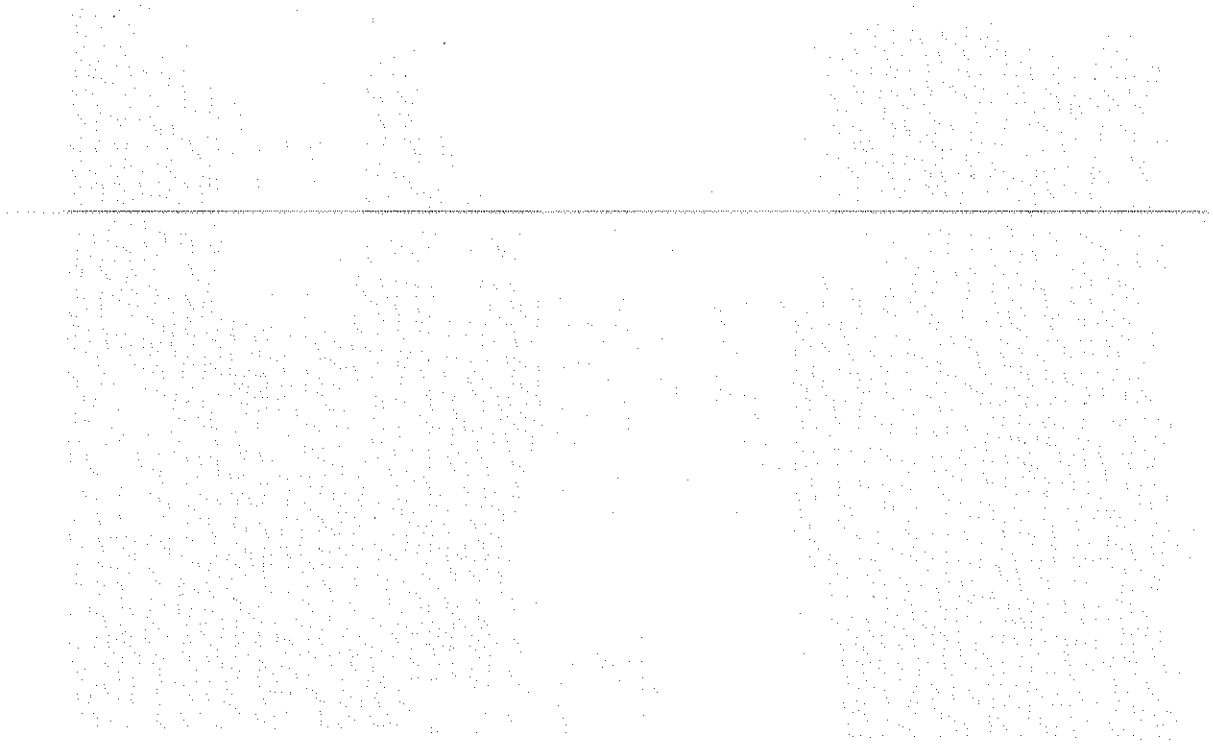

(e)
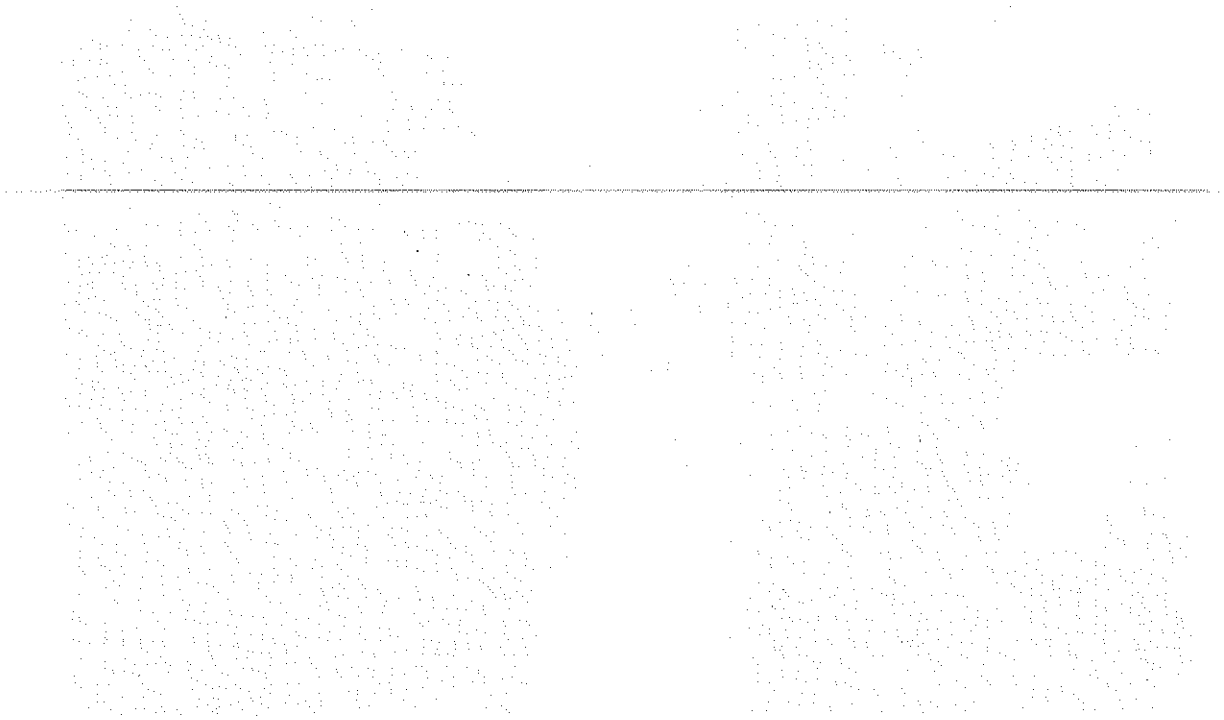
Figure 4.6 Specimen L2-series of photographs; (e) post-test photograph showing the bulged failure region.